Aalto-yliopisto
Aalto-universitetet
Aalto University

Master's Programme in Advanced Energy Solutions

Simulation of the combined oxy-fuel combustion and electrolyte alkaline electrolysis for production of hydrogen

Matthias Re

Master's Thesis
2021

Author Matthias Re

Title of thesis Simulation of the combined oxy-fuel combustion and electrolyte alkaline electrolysis for production of hydrogen

Programme Advanced energy solutions

Major Sustainable energy conversion processes

Thesis supervisor Prof. Mika Järvinen

Thesis advisor Shouzhuang Li, MSc

Date 23.7.2021 **Number of pages** 76+12 **Language** English

Abstract

Carbon dioxide emissions and municipal solid waste are globally increasing, affecting the thin balance on Earth. Oxy-fuel combustion thermal power plants effectively reduce carbon dioxide emissions in the energy sector. However, carbon capture processes have a low overall efficiency, which is a common disadvantage of this strategy.

This thesis investigates the modelling using Aspen Plus of the Vantaan Energia waste-to-energy thermal power plant, taken as a reference case, to its retrofitting into a municipal solid waste oxy-fuel combustion thermal power plant with alkaline electrolysis cells.

The simulation results report that the proposed design is not electrically self-sustainable, which requires an additional supply of 365.5 MW_{el}. The electrical demand might be fulfilled by involving wind park design, which should have a nominal installed power of 1100 MW in order to smooth wind production fluctuations. The wind park installation could result in a higher cost of the system. Nevertheless, the simulation indicates the economic feasibility of the proposed municipal solid waste oxy-fuel combustion system owing to a massive production of thermal power for district heating purpose equal to 191.1 MW. The alkaline electrolysis cells produce 278 MW of hydrogen fuel power. The oxy-fuel combustion system has an overall efficiency of 26.21%. The simulated retrofitted thermal power plant produces hydrogen with a levelized cost of 0.851 EUR/kg. The simulated thermal power plant produces hydrogen and carbon dioxide with a ratio of 2.48:1 (H_2-CO_2), close to methanol production stoichiometric reaction. The reduction in hydrogen cost consecutively results in the economic feasibility of a methanol power plant, which would have a methanol selling price break-even cost of 0.221 EUR/kg. The exploitation of municipal solid waste effectively reduces the cost of hydrogen.

The proposed design is a promising strategy to cope with climate changes, by achieving carbon neutrality, as well as to produce cheap and clean hydrogen.

Keywords oxy-fuel combustion, municipal solid waste, electrolysis, hydrogen, carbon capture and utilisation, Aspen Plus

Table of contents

Preface

I would like to thank my supervisor at Aalto University Professor Mika Järvinen, for supporting my work and for providing helpful expertise in this thesis as well as his constant guidance during the overall thesis process. I would also to thank my advisor at Aalto University Shouzhuang Li, who always makes himself available during the thesis work to provide helpful feedbacks, suggestions and expertise on this project. I would also to thank my supervisor at Politecnico di Torino Professor Massimo Santarelli for his guidance and support. I am really thankful to these people for the time and effort they put into this project, which without them would not have been possible.

I would like to acknowledge the financial support from Politecnico di Torino and the European Union under the Erasmus+ programme, which together with Aalto University gave me the opportunity to work on this project.

I am really thankful to all friends and family, who have accompanied me during this long academic journey, sharing always the best and toughest moments.

Special sincere thanks go to my parents, who have supported me financially and above all emotionally along my whole student career. Many thanks go to my mother, who always encouraged me to be ambitious and taught me the importance of hardly-working. Many thanks go to my father, who taught me working ethics. This work is dedicated to them.

Espoo, 23 July 2021
Matthias Re

Symbols and abbreviations

Symbols

E_{DH}	thermal energy produced for district heating [GWh]
E_{elec}	net electrical energy produced by the steam cycle [GWh]
$E_{fuel\ input}$	energy obtained through fuel input and its combustion [GWh]
$E_{electrolyser}$	energy demand for the electrolyser [GWh]
E_{prod}	energy produced through wind energy in Finland [GWh]
E_s	specific electrolysis cell energy consumption [kWh/Nm^3]
η_F	Faraday's efficiency [-]
η_{HHV}	hydrogen higher heating electrolysis cell efficiency [-]
η_{LHV}	hydrogen lower heating electrolysis cell efficiency [-]
η_{OFC}	energy efficiency of the oxy-fuel combustion system [%]
$\eta_{OFC,overall}$	energy efficiency of the oxy-fuel combustion system including the wind park efficiency through the capacity factor [%]
$\eta_{steam\ cycle}$	energy efficiency of the steam cycle [%]
F	Faraday's constant [C/mol]
f_{av}	availability factor for wind energy in Finland [-]
f_C	capacity factor of the thermal power plant [-]
G	molar specific electrical energy electrolysis demand [kJ/mol]
H	molar specific heat of formation for electrolysis [kJ/mol]
HHV_{daf}	higher heating value of the dry ash-free fuel [MJ/kg]
HHV_{dry}	higher heating value of the dry fuel [MJ/kg]
HHV_{HCOMB}	higher heating value of fuel for HCOMB design [MJ/kg]
I	electrolysis cell current [A]
M_{MSW}	municipal solid waste yearly mass combustion [kg/y]
$\dot{m}_{MSW}$	municipal solid waste fuel input [kg/s]
n_c	number of cell involved in the electrolysis [-]
P_{DH}	thermal power produced for district heating [MW]
P_{el}	electrical power demand to the electrolysis cells [MW]
P_{el,H_2}	specific electrical power demand to the electrolysis cells regarding to hydrogen [MW/(kg/s)]
P_{el,O_2}	specific electrical power demand to the electrolysis cells regarding to oxygen [MW/(kg/s)]
P_{H_2}	power produced as hydrogen [MW]
P_{MSW}	power fuel input for municipal solid waste [MW]
$P_{wind,elec}$	electrical power produced the wind park [MW]
$P_{wind,energy}$	installed nominal power for the wind park [MW]
Q	molar specific heat electrolysis demand [kJ/mol]
t	time [s]
U_{act}	activation overvoltage [V]
U_c	electrolysis cell voltage [V]
U_{con}	concentration overvoltage [V]
U_{ohm}	ohmic resistance overvoltage [V]
U_{rev}	reversible thermal voltage [V]

U_{tn}	thermoneutral cell voltage [V]
$\dot{V}$	volume flow rate produced by electrolysis cell [Nm^3/h]
$W_{electrolyser}$	power demand for the electrolyser [MW]
W_{nom}	nominal installed wind power in Finland [MW]
$W_{nom,park}$	nominal installed power for the wind park [MW]
z	number of electrons involved in electrolysis [-]

Operators

Δ	finite difference
$\sum$	finite sum of specified elements

Abbreviations

AEL	alkaline electrolytic cell
ASU	air separator unit
BOP	balance of plant
CAPEX	capital cost
CAS	cryogenic air separation
CFB	circulating fluidized bed
CCS	carbon capture and storage
CLOU	chemical-looping with O_2 uncoupling
DH	district heating
ETS	emission trading scheme
EU-27	27 member countries belonging to European Union
FC	fixed carbon fraction of the fuel after combustion
FGD	fluidized gas desulphurisation
GHGs	greenhouse gases
HHV	higher heating value
HPT	high pressure turbine
HSY	Helsinki environmental region services consortium - Helsingin seudun ympäristöpalvelut
ITM	ion transport membrane
LCOH	levelized cost of hydrogen
LHV	lower heating value
LPT	low pressure turbine
MEOH	methanol
MPT	medium pressure turbine
MSW	municipal solid waste
NO_xs	nitrogen oxides compounds
OEC	oxygen enriched combustion
OFC	oxy-fuel combustion
OPEX	operating and management cost
PEM	polymer electrolyte membrane
PSA	pressure swiping adsorption

P2X	power-to-X
SDG	sustainable development goal
SOEL	solid oxide electrolysis
SRF	solid recovered fuel
TEG	triethyleneglycol
TSA	temperature swiping adsorption
VM	volatile matter fraction of the fuel after combustion

1 Introduction

Today, thanks to technological progress, our society has experienced a level of wealth higher than seen ever before. However, this condition has a hidden cost that has dramatically emerging over the last twenty years. Through the exploitation of easily extractable resources, such as fossil fuel, society has boosted its economy by ignoring the consequences of this progress. The combustion of fossil fuels produces compounds and CO_2, which are dangerous to humans and the environment [8]. Higher wealth requested a deeper permeation of technology in the society, which forced a higher energy demand as a side effect [44]. Higher energy consumption needs a higher exploitation of energy resources, which now are based mainly on fossil fuels, in particular coal and oil, impacting globally on earth.

To fight climate change, requested by the public opinion, new policies are introduced. For example, after Conference of Parties, held in Paris in 2016, 17 sustainable development goals (SDG) are set for 2030 [18][86]. Affordable and sustainable energy is one of the key concepts of SDG. Net-zero emission is one of the required characteristics for a sustainable energy resource [13][19]. Various improvements have been proposed to reduce the emission of CO_2 and increase efficiency of previous processes, such as supercritical thermal power plants, as well as capture and carbon storage facilities.

Combustion always involves a fuel, resulting in the emission of CO_2 and H_2O, though other products can be generated depending on the presence of other elements or the temperature of the combustion in the chamber. Apart from CO_2, fossil fuels produce other toxic compounds, including SO_2, SO_3, NO, NO_2 and CO. To eliminate these secondary products, the combustion process can be modified to obtain pure CO2 and H_2O flue gas. Nitrogen oxide compounds (NO_xs) are formed in the combustion chamber as a result of the high temperatures from combustion of oxygen and nitrogen. The two precursors N_2 and O_2 of these compounds are found mainly in the comburent air (78% N_2, 21% O_2) and in small quantities in the fuel. The concentration of NO_xs in the flue gas is influenced by the temperature of the combustion and the concentration of the N_2 and O_2 [10].

Oxy-fuel combustion (OFC) thermal power plants use only oxygen to oxidize the fuel. Therefore, since the fuel is the only source of nitrogen inside the combustion chamber and its quantity is negligible, nitrogen oxides are not produced through oxy-fuel combustion. This type of combustion produces flue gas consisting of carbon dioxide and water vapour. After condensation of the water in the flue gas, pure CO_2 can be stored and used to produce methanol or methane, following a power-to-X (P2X) process, instead of being freely emitted. Many technologies have used an air separator unit (ASU) to achieve oxy-fuel combustion [12][36][78]. ASU can produce an almost pure flow rate of oxygen from air due to its many compression and separation stages. However, because of the high energy requirements of the ASU, most of the electricity generated by the power plant would be consumed by the ASU, leading to low efficiency of the whole system [12]. One possible strategy for addressing this challenge would be to adopt an electrolysis unit for providing oxygen to the combustion process. An electrolysis unit would have the advantage that it would produce not only oxygen but also hydrogen, a valuable by-product [24]. The thermal power generated by the combustion cycle is converted into electricity owing to a Rankine steam cycle, which could then be directly supplied to the electrolyser. In this thesis, municipal solid waste (MSW) is adopted as the fuel, thus satisfying the circular economic policies specified by the EU. Similar strategies have been considered by Vantaan Energia together with Wärtsilä as well as by Siemens.

Vantaan Energia and Wärtsilä are currently developing MSW OFC, whose clean carbon dioxide should feed a power-to-methane facility in order to produce biogas for district heating [93]. Siemens patented an OFC system, whose electrolysis is completely fed by renewables with no MSW incineration [36].

1.1 Objectives of the work

The case study aims to reduce the impact of combustion products from thermal power plants and decrease the amount of municipal solid waste, fitting in carbon neutrality and circular economy scenario [13][19][86]. In recent years, EU-27 increased its generation of MSW per capita, demanding for a higher waste management capacity, as it presented in Figure 1. Although the population growth in EU-27 is slowing down, total waste production is strongly increasing [21]. The goal of this research is to evaluate the feasibility of an oxy-fuel waste combustion, whose generated electric power is partially used in an electrolysis unit to provide oxygen for the combustion of MSW and produce hydrogen at a competitive market price. Thanks to this system, the resulting flue gas, after adequate treatment, is composed only by water vapour and carbon dioxide. CO_2 can be used together with H_2 from the electrolysis unit to produce methanol or methane through a methanization facility [12][35][42]. H_2O can be used in the electrolysis unit as feed water, if it is pure enough. The concept to develop is a system that actually can cope with new targeted policies, such as net zero emission and circular economy. The products from the plant are completely exploitable as second energy resources to the grid or stored. The fossil fuel's market is shrinking, which can be further replaced by hydrogen above all in transportation sector [41]. The system can be the starting point of a P2X supplier, where instantly available fuel is produced, which can cope with the increasingly frequent energy demand ramps, caused by the permeation of renewables worldwide in the energy mix. Vantaan Energia waste to energy plant, situated in Uusimaa Province, is studied as a reference case.

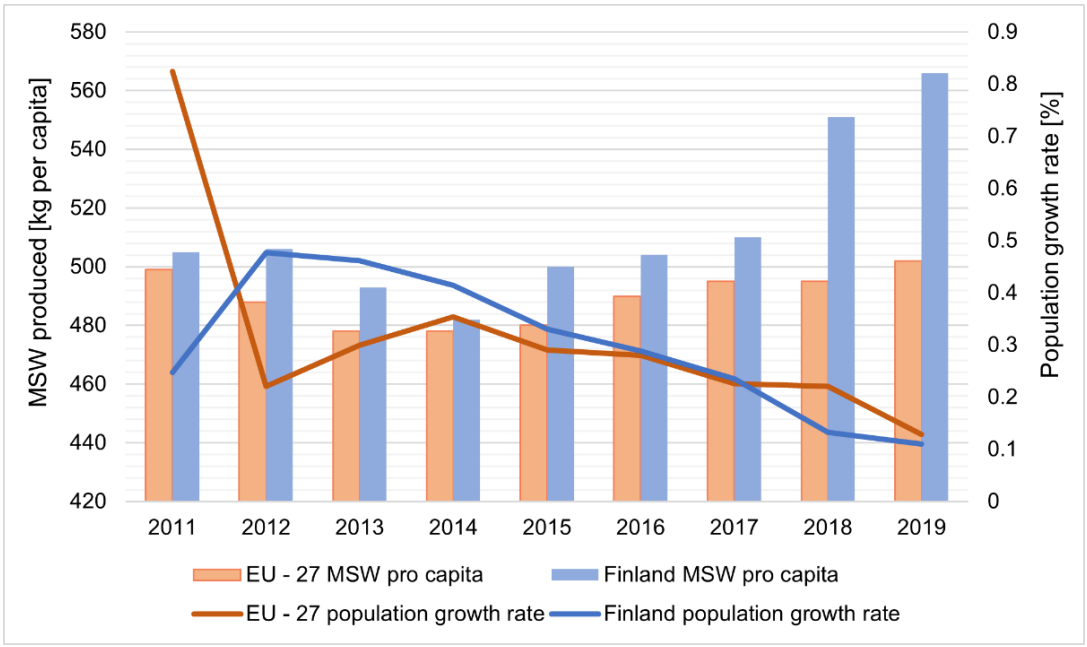

Figure 1: MSW production with respect to the population growth. Data obtained from iea.org [41].

1.2 Thesis structure

The remainder of this thesis is structured as follows. Chapter 2 reviews the literature on municipal solid waste combustion, oxy-fuel combustion, power-to-X, the alkaline electrolysis cell, as well as the hydrogen and carbon dioxide market. Chapter 3 presents the simulation modelling the reference retrofitting cases. Chapter 4 introduces the simulation results for the electrical power output and the cost of produced hydrogen, as well as in comparison to these previous research and conventional technologies. Chapter 5 summarizes key findings and suggests future work.

2 Literature review

In the case study, literature review on key topics is presented, underlining the most important features. Municipal solid waste combustion is discussed in Section 2.1, analysing from the entry point to the end of the combustion process. Oxy-fuel combustion's review follows in Section 2.2, which focuses on the main features which compose the system. The subsequent section is dedicated to the alkaline electrolyser. The highlights of the H_2 and CO_2 present and future market concludes the review in Section 2.5.

2.1 Municipal solid waste combustion

Every living being has an effect in their ecosystem. Humans shaped and carved Earth's surface more than ever, becoming the most impacting species on our world. For instance, it is sufficient to think on how fossil fuel technologies are resulting in global climate change. Moreover, our society was established as a disposable or linear economy, thus emerging the need to cope with waste issue.

Every year human population and its wealth are growing, resulting in a significant production of waste [78]. Municipal solid waste (MSW) by definition is what is discarded by households, collected by municipal authorities and disposed through the municipal waste management system [13]. EU-27 produced a total waste hazardous and non-hazardous of 1.950 billion tonnes in 2008 and 2.149 billion tonnes in 2018 [23], of which only 0.222 billion tonnes were MSW [21]. There are four main processes to cope with waste issues: recycling, composting, landfilling and incineration. In 2018 the most used procedure to treat MSW was recycling (30.8%), followed by energy recovery (waste-to-energy) (26.7%), landfilling (24.6%), composting (17.4%), and incineration (without waste-to-energy) (0.52%) [21], as it is illustrated in Figure 2. With respect to the EU-27, in Finland landfilling procedure is almost completely substituted by energy recovery.

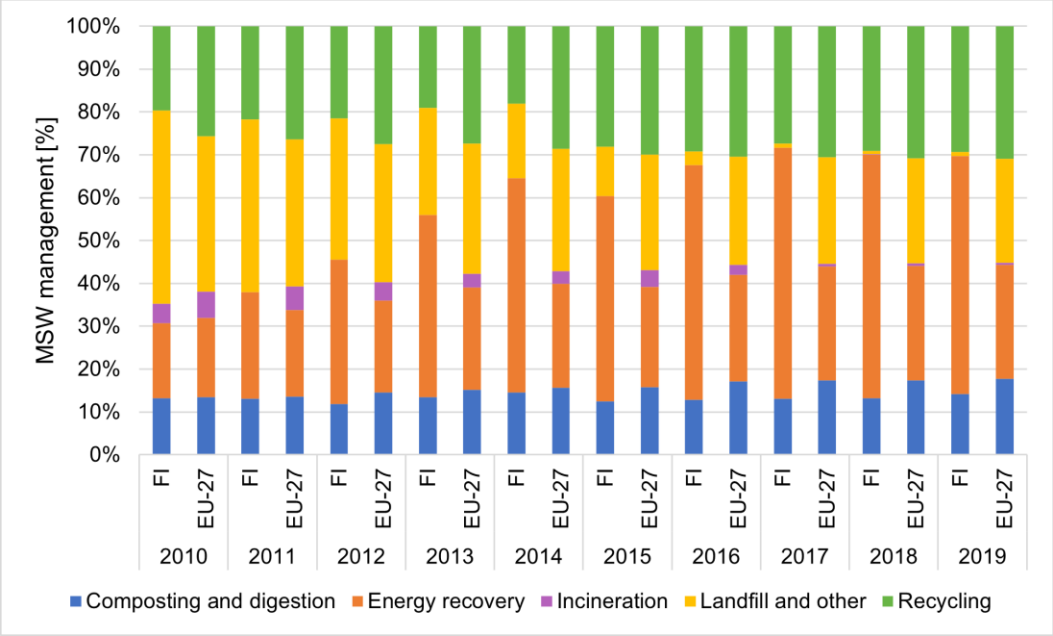

Figure 2: MSW management divided by method for EU-27 and Finland. Data obtained from ec.europa.eu [23].

Landfilling was the traditional way to cope with MSW, involving high-risk environmental issues. In the last twenty years, Europe has been establishing policy limiting landfilling method, in favour of recycling and composting [13][73]. Landfilling is the procedure, where a selected land is deeply excavated into the ground, filled with waste and then covered with soil. In this case, MSW throughout a long period is naturally decomposed and methane is produced, which can be used for energetic purpose. The main issue with landfilling is that the decomposition of MSW's organic part leads to the formation of acid leachate, which can pollute the ground and infiltrate into ground water, thus contaminating the potable water system. If methane is not extract from the site, it leaks to the environment, resulting in air pollution because of its high carbon dioxide equivalent factor and spontaneous combustion [13].

Incineration is a useful procedure to reduce the amount of waste. The first waste incinerator was introduced in Germany in 1896 [10]. Only recently the thermal heat released by the combustion of MSW was used to produce electrical energy. Therefore, waste-to-energy incineration has the two advantages to reduce high volumes of waste and meanwhile extract the energy from it. Compared to landfilling, waste-to-energy incineration releases less pollutants [40]. MSW LHV has a wide range because it is affected by regionality, so China' (4–10 MJ/kg$_{MSW}$), Brazil' (7–10 MJ/kg$_{MSW}$), and Europe's MSW (10–14 MJ/kg$_{MSW}$) have completely different values of LHV [40][52][57][59]. Therefore, because of its aleatory characteristics, MSW LHV is hardly predictable. The energy inside MSW is released thanks to combustion, where the main elements, such as carbon, sulphur and hydrogen, are oxidized thanks to the presence of O_2 in the comburent air. The main combustion reactions are expressed by the following equations:

$$C + O_2 \rightleftharpoons CO_2, \quad (1)$$

$$H_2 + \frac{1}{2}O_2 \rightleftharpoons H_2O, \quad (2)$$

$$\text{and } S + O_2 \rightleftharpoons SO_2. \quad (3)$$

MSW LHV is not as high as fossil fuels, because it has low carbon and high oxygen contents as well as there is a component that does not oxidize through combustion, which is called moisture. Moisture content affects strongly MSW's LHV, which in studies is suggested to be between 20–60% of the total waste [31][40][52] [57][59]. If the moisture content increases in MSW, its LHV will be lower due to the reduction of combustible content in it. In MSW all sort of materials are collected, such as kitchen waste, yard biowaste, plastic or paper packaging, glass, metals, and many others. Metals and glasses are not suitable for combustion, belonging to the moisture fraction of this kind of waste and lowering the LHV of MSW. Some procedures can be adopted before the combustion to reduce the amount of moisture and increase the efficiency of the combustion. For instance, since MSW contains a huge portion of water, it is possible to keep the waste at 105 °C for 24 hours. This pre-treatment allows MSW to get rid of the wet portion, which during combustion will absorb heat through water evaporation, reducing the thermal power to the heat exchangers [1][31][67]. Furthermore, non-combustible part, such as metals and glass, can be retrieved and recycled before the combustion. Thus, in the combustion chamber the MSW, which in this case is defined as solid recovered fuel (SRF), will be made mostly by combustible matter and the ash amount reduced. With this procedure LHV can raise up to 19.8 MJ/kg$_{SRF}$ [40].

Through the combustion, which takes place in the incinerator furnace, thermal power is released and thanks to a Rankine's steam cycle is converted into electric power. The whole system is similar to conventional thermal power plants referring to the combustion chamber, the Rankine's cycle and the generators. Three main arrangements can be adopted in the combustion chamber: rotary furnace, grate firing, and fluidized bed. The first one is suited for special waste, whereas for MSW usually grate firing or fluidized bed are set. MSW is collected in a pit, where it is continuously mixed to achieve the uniformity of the fuel, and then it is relocated towards the furnace.

In the case of grate firing, the fuel is arranged on three grates, usually oriented with an angle of 10°–25° [52], which moves from the collecting point to the end of furnace [59], as it is presented in Figure 3. The comburent primary air is blown from below the grates upwards and perpendicular to the movement of the fuel. During the combustion, MSW quantity is reduced and ashes are progressively generated. The combustion consists in three steps: drying, devolatilization and char and volatile combustion. The energy gain during combustion is achieved mainly through volatile and char combustion [52]. Therefore, in MSW's firing the process, which released energy, refers to the combustion of the gaseous phase [54]. To achieve the complete combustion of MSW, secondary air is needed, which is blown upper to the flame in the furnace. After the combustion fly and bottom ashes are produced. Bottom ashes because of gravity falls and are collected below the grates, whereas fly ashes due to their mass are transported together with the flue gas in the upper furnace section.

On the other hand, fluidized bed differs from grate firing in the combustion strategy. Regarding to fluidized bed, MSW needs to be finely grinded and placed continuously on a bed of silica. Research suggests the possibility to adopt ilmenite rather than silica, to reduce the impact of pollutants in the flue gases [52]. The primary comburent air is blown from below

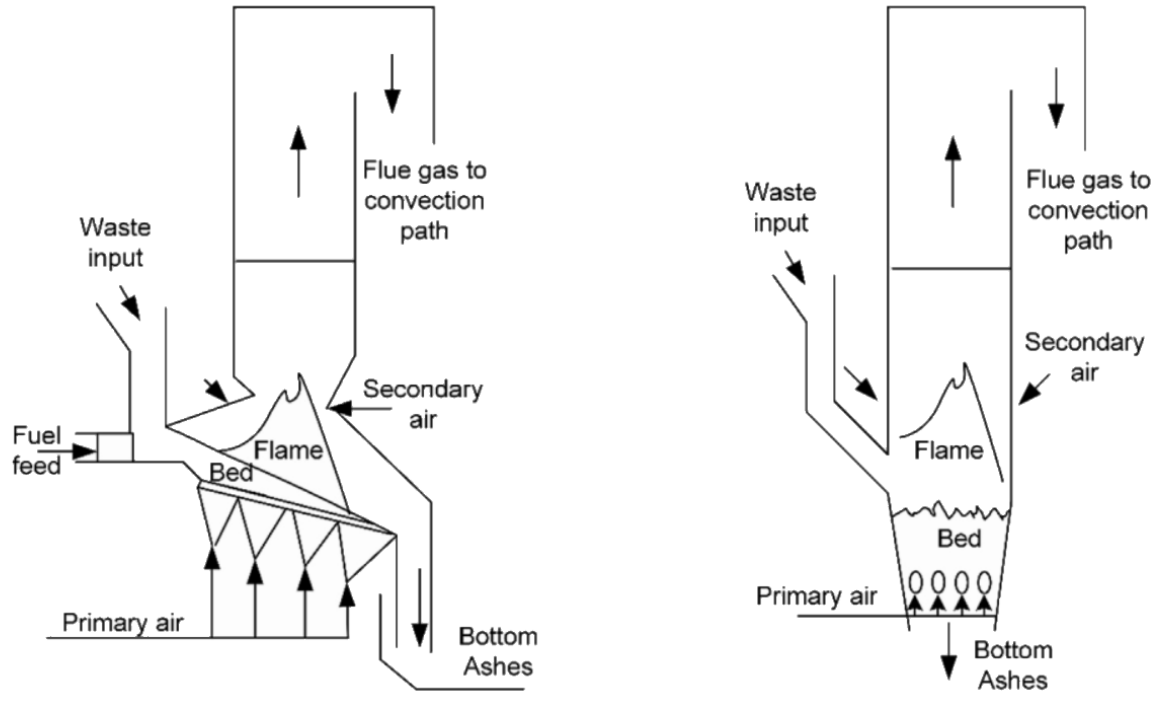

Figure 3: Furnace's scheme of GF (a) and FBC (b). Figure obtained from [52].

upwards, whereas the secondary one is blown upper the flame. Furthermore, two technologies can be used in fluidized bed combustion: bubbling fluidized bed or circulating fluidized bed (CFB). Bubbling fluidized bed is suited for small incineration operation (<10 t/h) [52]. MSW mixture can be highly aleatory without a constant LHV, leading to high fluctuations in the combustion, the temperature, and the thermodynamic performance of the system. The advantage of fluidized bed consists in silica bed, which has a very high heat capacity, thus keeping the combustion temperature around 900 °C, smoothing out any fluctuations [52]. These fluctuations can happen instead in grate firing due to the combustion strategy. In the case of fluidized bed, the primary air flows throughout the silica bed and it must oxidize the fuel without any obstacle, requiring a compulsory pre-treatment of MSW. By comparing the two strategies, it seems that there is no clear winner in benefit vs. cost analysis [52]. Nevertheless, when pre-treatment and recycling take place, as in the case of fluidized bed, the emissions and amount of ashes are reduced [40].

Combustion feedback is mandatory to achieve the wanted generated electrical power output. In the case of grate firing, the feedback procedure is more complicated because it needs the regulation of grates' speed motion in the furnace. It is not possible to put sensors inside the furnace because they cannot withstand temperature such high as the one developed by the combustion, as they would directly face the flame. Thus, temperature sensors are set in a colder region, situated at the ceiling of the incinerator before the flue gas treatment [34][52]. Through analytical calculations is possible to compute the temperature inside the furnace and regulate the introduction of the fuel. Another regulations consists in the cooling of the grates, which is achieved through air, or when the cooling is not sufficient, it is operated through steam water [52]. Furnace cameras are used to measure and monitor combustion.

The conventional incineration with waste-to-energy purpose consists in the MSW combustion in the furnace with comburent air supplied from environment. There are many possible combinations and application to exploit the energy contained in MSW through the incineration. For instance, as already cited, it is possible to raise the LHV by collecting all the incombustibles, such as metals and glasses, thus obtaining the SRF [40]. Gasification process can be set before the combustion, which leads to a cleaner flue gas [57]. Other strategies analyse the behaviour of oxygen in the combustion and how to make it more efficient. Oxygen enriched combustion (OEC) consists in an increase in the oxygen content in air supply. When OEC is set in incineration, it increases the efficiency and stability of the combustion while decreasing pollutants emission [59]. It is possible to use as the oxidizing agent also fully oxygen supply, i.e. oxy-fuel combustion (OFC). OFC leads to an almost pure CO_2 flue gas but with a very low efficiency of the whole system, as the oxygen fully separation demands for most of the electrical power produced by the system [12]. In addition, fuel can be mixed with other resources, consisting in co-combustion. MSW can be mixed with coal, to achieve an equilibrium between the higher coal LHV and the better emission performances of MSW combustion [1][31][99]. Oil refining waste can be added in the mixture to increase the total LHV of the fuel and avoid polluting the environment with its uncontrolled disposal [31]. Furthermore, sewage sludge together with MSW can be burnt to avoid its polluting effect if it is disposed into the environment without any treatment [10].

Fuel combustion involves the oxidation of several hydrocarbons, contained in the fuel. When the reaction happens, products are H_2O and CO_2. However, there are other process products, which come from the oxidation of the comburent air or from the fuel itself. The concentration of those products depends on the concentration of their precursors and the

reaction temperature, which favours one or the other side of the chemical kinetics balance. In a conventional thermal power plant, the oxidizing agent for the fuel's combustion is air, which contains 21mol% of O_2, required by the carbon-oxidizing reaction. In addition, air contains 78mol% of N_2 and because of the high temperature in the furnace and its high concentration in the supplied air, it produces NO_xs as shown in the following equations [72]:

$$N_2 + O_2 \rightleftharpoons 2NO \quad (4)$$

$$\text{and } 2NO + O_2 \rightleftharpoons 2NO_2. \quad (5)$$

Regarding to nitrogen oxides generated through comburent air, they can be thermal or prompt type. Thermal NO_xs are produced from N_2 and O_2 in high temperature environment (1200–1300 °C), following these three reactions according to Zeldovich's mechanism [38]:

$$O + N_2 \rightleftharpoons NO + N, \quad (6)$$

$$N + O_2 \rightleftharpoons NO + O, \quad (7)$$

$$\text{and } N + OH \rightleftharpoons NO + H. \quad (8)$$

The concentration of oxygen, nitrogen and the temperature affect the production of the resulting compound in Equations 6–8. The production rate of NO is directly proportional to the concentration of N_2 and directly squared proportional to the oxygen reactants content. Therefore, if an excess of air is supplied to the furnace, thermal oxides will increase. In addition, if temperature increases, the concentration of NO_x increases. Prompt oxides are related to the presence of radical hydrocarbons in the combustion chamber near the flame, producing HCN and N, which can oxide, becoming NO. From N contained in the fuel, species such as HCN and NH_3 are produced and then can oxidize, obtaining NO [38][72]. In the case of OEC, the oxygen content is increased in supply air, thus increasing NO_x in flue gas [59]. In co-combustion research suggests that it is possible to find an optimum point to reduce the amount of NOx, when 75% coal and 25% MSW fuel mixture is adopted. If MSW percentage is increased or decreased, the concentration of nitrogen oxides increases. The phenomenon can be explained by the fact that, if MSW is reduced, the LHV of the fuel increases and so the temperature of the combustion. Since N content inside MSW is twice the one in coal, fuel NO_xs increase in the flue gas [99]. To remove nitrogen oxides some technologies are involved in the flue gas treatment, such as catalytic reduction, non-catalytic reduction or the usage of ammonia. The process reactions are expressed through the following equations [12]:

$$4NO + 4NH_3 + O_2 \rightleftharpoons 3N_2 + 6H_2O, \quad (9)$$

$$2NO + 4NH_3 + 2O_2 \rightleftharpoons 3N_2 + 6H_2O, \quad (10)$$

$$\text{and } 6NO_2 + 8NH_3 \rightleftharpoons 7N_2 + 12H_2O. \quad (11)$$

Other products are created from the oxidation of S, which is present in small but not negligible quantities in the fuel. The reaction of the oxidation of S is presented in Equation 3, which can be the precursor of SO_3, as illustrated in the following equation [72]:

$$2SO_2 + O_2 \rightarrow 2SO_3. \quad (12)$$

The main problem with sulphur oxides is the corrosion deriving from its mixture with water and the irritating characteristic to the respiratory system. The main solution to deal with sulphur pollution is to let it react with injected basic absorbent, like $CaCO_3$, $Ca(OH)_2$, $CaCOMgCO_3$, Na_2CO_3, and others either mixed in the silica bed or in a separate stage after the combustion [40][72]. For instance, in order to create calcium-sulphur compound, useful in industrial application, by involving calcium, several possible reactions can be selected, presented by the following equations:

$$CaCO_3 \rightarrow CaO + CO_2, \quad (13)$$

$$Ca(OH)_2 \rightarrow CaO + H_2O, \quad (14)$$

$$CaO + SO_2 \rightarrow CaSO_3, \quad (15)$$

$$\text{and } CaO + SO_2 + \frac{1}{2}O_2 \rightarrow CaSO_4. \quad (16)$$

Desulphurization methods refer to combustion types, such as flue bed combustion and grate firing. The first arrangement requires the reactants in the combustion bed. The second type involves flue gas desulphurization (FGD) after the steam generator. FGD can be dry, semi-dry and wet process, depending on the desulphurization strategy. FGD has an industrial efficiency of 95–99% and a working temperature of 60–80 °C [12][72]. The removal sulphur rate is zeroth dependent from the carbon dioxide concentration. The flue gas humidity higher than 0.08 enables the production of calcium carbonate at low temperatures, which is one precursor of calcium sulphate [55][78].

MSW contains small percentage of chlorine, forming HCl, that can be treated together with sulphur oxides to separate it from the flue gas. The process is described through the following reaction:

$$2HCl + Ca(OH)_2 \rightleftharpoons CaCl_2 + 2H_2O. \quad (17)$$

Flue gas after combustion is treated and then released into the environment. However, non-burnable components are present after combustion as fly or bottom ashes. In the case of fly ashes, due to their mass, particles are transported together with flue gas to the flue gas treatment section. To reduce the amount of fly ashes, i.e. particulate matter, some technologies can be set, such as cyclonic separation, baghouse, electrostatic or wet precipitators [59][72]. Bottom ashes are collected at the bottom of the furnace, falling through the grates or silica bed, in grate firing or fluidized bed, respectively. The wide variety of MSW content from households characterises the bottom ashes with respect to other fuels. Sb, Cu, Pb, Sn, Ti, Zn, and chlorides are typically found in bottom ashes [39][57][99]. When MSW is mixed with other fuels, heavy metals concentration decrease in the ashes. For instance, a reduction of those compound is achieved through sewage sludge co-combustion, but with an increase content in As level. The temperature of the combustion does not influence heavy metals' ash concentration. The only exception consists in Zn, which undergoes on a more stable residual fraction with higher temperatures [10]. The ash percentage is reduced in the case of OEC [59]. The process ends with ash disposal, which should be set as mono-disposal facility to have the possibility for further treatment [67].

2.2 Oxy-fuel combustion

In 2016 EU-27 set high standards for 2050 within the Paris agreement in order to achieve carbon neutrality by following the European Green Deal [13][18][19]. Greenhouse gases (GHGs) atmosphere concentration is constantly increasing, which is rapidly changing the thin balance established on Earth over hundreds thousand years. Renewables are deeply permeating our energy production to decrease GHG's emissions by replacing fossil fuel combustion. However, renewable energy resource because of their aleatory characteristic are not exploitable to fulfil base load demand, which is granted by nuclear or fossil fuel thermal power plants. In addition, combustion is an option to supply thermal power at high temperatures with respect to renewables. Thus, the need to exploit the process of combustion will persist for the next future. In 2018 EU-27's energy sector accounted for 33.4% of total CO_2 emissions and Finland's for 39.1% [41]. Several conventional technologies can be enhanced to reduce or nullify polluting emissions in energy generation in order to achieve carbon neutrality and at the same time to obtain all the advantages from combustion. Among carbon capture and storage (CCS) common technologies are pre-combustion, post-combustion, and oxy-fuel combustion [73].

Pre-combustion comprises the gasification of a carbonaceous fuel to obtain CO, a possible precursor of CO_2. The gasification consists in the production of syngas through high-temperatures and oxidation with semi-stoichiometric oxygen supply. The outflow contains CH_4, CO, CO_2, and H_2. When steam is added to CO in the mixture, CO_2 is obtained by water-shift gas reaction [73][93]. Because of the different chemical properties of CO_2 and H_2, these two compounds are easily separated before the combustion [34][57][73]. Post-combustion procedure affects the after-combustion products, where monoethanolamine (MEA) or sterically hindered amine (KS-1) are used as absorbent to extract CO_2 and N_2 [34][73][76][96]. Literature suggests an efficiency more than 90% with a CO_2 capture of 90% for post-combustion [96].

OFC consists in a conventional fuel combustion, where the supplied comburent is fully oxygen. The main advantages of these strategies are focused on the resulting flue gas and how easily CO_2 is extracted from it. Flue gas in the case of OFC is reduced and is made mostly of CO_2, reducing the cost of flue gas treatment and the possibility to directly supply CO_2 for industrial or energetic purposes. Research suggests that OFC is one of the best solutions in the case of retrofitting of a pre-existent thermal power plant or a new-build one [73].

OFC main system is presented in Figure 4. The fuel together with O_2 and a fraction of recirculated CO_2 is burnt in the furnace. Flue gases are treated and almost pure CO_2 is obtained, then supplied where it is needed, such as sink, storage and P2X facility. The combustion produces mainly CO_2 and H_2O in vapour phase, so water is easily separated from carbon dioxide through condensation [34][36][47][90]. Thermal power is extracted from the combustion and also from the condensation unit. Research results and analyses unspecify and contradict each other about the recirculation source point. Literature proposes that recirculation's source can be directly set after combustion without any flue treatment [93]. However, the recirculation of dust-containing flue gas might lead to the clogging of the furnace because of its increasing content in the flue gas during nominal operations because of the absence of any flying ashes sink. Therefore, another option consists in a one-step treatment before recirculation, which refers to the removal of particulates and fly ashes [76][96]. In the case of coal OFC, a denitrification unit is set before the dust collection unit [34]. Research

suggests that in MSW OFC both recirculation before or after any flue gas treatment can be set [29][93]. In any case the reasons are not provided for selecting one arrangement with respect to another.

OFC system is basically a conventional thermal power plant, except for the ASU presence, which provides pure oxygen to the furnace. Thus, all conventional components are still present, i.e. steam generator within the boiler, compressor and turbine in the Rankine's steam cycle, and the flue gas treatment facility. The major difference consists in the thermodynamic condition of the plant. When comburent air is involved in the combustion, only 21% of the air input supports the combustion and releases energy, i.e. the oxygen. The remaining quantity, such as N2 and Ar, absorbs a non-negligible fraction of that energy, resulting in an increase of temperature of these inert gases and an overall lower average temperature of the flame and the flue gas [30]. This means that if only oxygen is supplied, furnace temperature will increase with respect to air combustion. Temperature has to be limited because of thermal and mechanical stresses as well as ageing of both steam generator and furnace internal wall [34]. The solution is to recirculate a fraction of the produced CO_2 directly into the furnace. Carbon dioxide and water vapour are not involved in the combustion reaction, thus helping to reduce the temperature in the furnace. When high temperatures are involved, the formation of CO is favoured, which is thermodynamically more suitable than CO_2 because of thermal dissociation phenomenon [30]. Research suggests that the pressure can influence the thermodynamic condition of the system. For instance, when very high pressure is obtained in advance ultra-supercritical and hyper supercritical OFC, the temperature decreases. Heat transfer from the combustion to the heat exchangers is not dependent from the pressure. In pressurized combustion, NO has a lower concentration as a consecutive effect of the temperature decrease because of the pressure increase. NO_2 are not affected by the change in pressure [58]. Controlling the recirculated mass flow rate results in the control of the heat transfer in the furnace [34]. 30% O_2 and 70% CO_2 oxidizing mixture is similar to air combustion kinetics and thermodynamics [93].

In MSW 's OFC the products are the same of a conventional waste-to-energy plant, as it is discussed in section 2.1, except for nitrogen oxides. This compound is effectively reduced by the avoidance of the comburent air and so the absence of molecular nitrogen, one of NO_xs

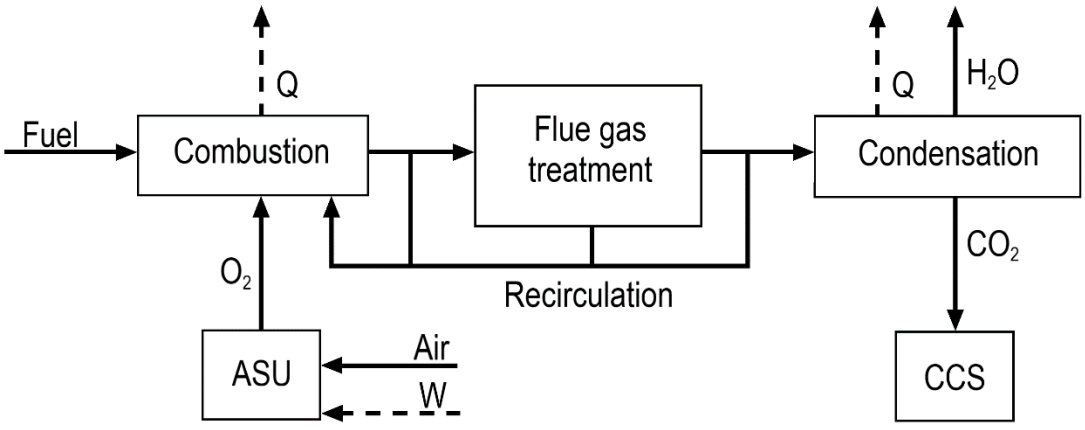

Figure 4: Oxy-fuel combustion's main system.

required precursors. However, a non-negligible fraction has still to be treated. With respect to other fossil fuels, MSW has higher content of N. Thus, MSW combustion produces a higher mass flow rate of fuel-nitrogen oxides [99].

The basic idea of OFC is to provide only oxygen to the furnace together with fuel to achieve the combustion. The resulting flue gas is treated and almost pure CO_2 stream is obtained. Several technologies are adopted to provide the required oxygen to the boiler, whose main characteristics are summed up in Table 1, such as cryogenic air separation (CAS), ion transport membrane (ITM), pressure or temperature swiping adsorption (PSA and TSA), chemical-looping with O_2 uncoupling (CLOU) and electrolysis.

CAS is one of the most common and commercialized technology to separate oxygen from air. The main principle exploits the liquefaction temperature of gases. At low pressure and temperatures through fraction distillation is possible to separate to oxygen form other gases in the ASU. The process requires a huge amount of energy to obtain cryogenic thermodynamic conditions, which strongly decreases the overall efficiency of the power plant [96]. Nevertheless, it is one of the most suitable for large scale production together with PSA [29].

ITM consists in the ionization of O_2. The resulting O^- is absorbed by an electrically conductive coated crystal lattice structure, separated from air by a physical membrane. A driving force is established through an electric voltage or partial pressure. This technology focuses on the diffusion process of the ionized oxygen, calculated by Fick's 1st law, where three different separation can occur: mean free path separation (based on Knudsen number), molecular sieving (size exclusion), or solubility diffusion (solubility in the matrix of the compound to separate). The main disadvantage refers to the membrane, which has to withstand both mechanical and thermal stresses. Suitable candidates for membrane consist in zeolite and carbon based molecular sieves, which give sieving property, thermal resistance, and chemical stability. With doping, fluorite nano particles, or cations with a single dominant oxide state, it is possible to enhance O_2 output flux. Typical thermodynamic conditions refer to 700°C (600–1100 °C) and 0.2–3 bar [73]. Thoroughly, the technology is expensive and difficult to realize, since it still has some issues regarding to the material instability at high temperatures [96].

Table 1: Oxygen production technologies main characteristics.

	AEL	**CAS**	**CLOU**	**ITM**	**PSA/TSA**
Purity [%]	99.98–99.999	97.85	-	-	30–66
Recovery ratio [%]	-	99.5	-	99.8	90–99.9
T [°C]	60–90	$T_{liquefaction}$	800–1000	600–1100	1–7
p [bar]	10–30	$p_{liquefaction}$	1	0.2–3	25
Phenomenon	electrolysis	liquefaction	oxidation and reduction (bulk)	membrane selectivity	adsorbance (polarization, surface)
Material	KOH solution	-	CuO, Co_3O_4, Mn_2O_3	zeolites, carbon based molecular sieving	zeolites

PSA and TSA are available only on small scale. The process exploits the different chemical characteristics of the involved gases. For instance, N_2 is more polarizable than O_2, so when nitrogen is polarized, it can interact with the electric field and it can be easily separated. Adsorption is the adhesion of a molecule on a surface, so the properties are referred to the surface of the medium and not to the bulk ones, like in diffusion. The adsorption is selective to a specific gas at a certain temperature (TSA) or pressure (PSA). Zeolites are set as the adsorbent material because of their charge imbalance properties, attracting the more polarizable N_2. More stages or beds can be set to increase adsorbent recovery rate. Temperature more than 150 °C allows the separation of N_2 and Ar. Literature reports that PSA is the cheapest way to supply oxygen because of lower initial investment, shorter construction cycle and smaller floor area [29].

CLOU involves two chemical reactions: one oxidation and one reduction. During the oxidation, oxygen contained in air reacts with typically Cu, Co, or Mn to form CuO, Co_3O_4, and Mn_2O_3, respectively. These elements are suitable candidates because they form oxygen-compound through exothermic reactions. This means that if the temperature is increased, the release rate of oxygen will also increase. These new compounds are then transferred into the fuel reactor where a reduction reaction takes place, which breaks the compounds again into O_2 and the precursors. The precursor for the oxidation starts again the process in a loop way. The optimal temperature for the process is 800–1000°C [96].

All these oxygen separation processes extract oxygen from air. Thus, the resulting flows from the ASU are O_2 and a mixture of N_2, Ar and other gases, normally present in air. Consequently, if pure nitrogen is needed, it has to be purified in a further process. Another technology to obtain pure oxygen consists in the electrolysis. Electrolysis breaks water molecules, obtaining H_2 and O_2 separately. Both products do not require further processes and can be exploit in OFC thermal power plant combined with a P2X process [35][36][42][90]. Thus, OFC, achieved through electrolysis, results in completely exploitable products from the process.

Every oxygen separation method needs electrical power and thermal power to achieve their function. Air comburent for combustion is almost zero-cost choice. Only fans to supply air to the furnace are needed. Antithetical to conventional combustion, OFC requests a huge amount of energy in separating the oxygen from air, strongly affecting the overall efficiency with a drop of 8–12 % [29][93]. Because of lack in literature further research is needed to understand and compare efficiencies and oxygen production energy cost per unit of mass, to select the best theoretical candidate.

The gaseous combustion products require flue gas treatment in order to extract CO_2. The treatment consists in several processes, such as particulates removal, desulphurisation, denitrification and dehydration. Except for dehydration, all the other processes are similar to a conventional thermal power plant treatment, as discussed in Section 2.1. The dehydration system extracts the high water content in the flue gas by condensation. The flue gas has water content in vapour phase. Therefore, the flue gas needs to be cooled down below the dew point in order to condense the vapour water. The dew point is proportional to the water content in a gas and so to its partial pressure. Depending on the required water content after the dehydration, several stages of condensation and compression can take place. For instance, the flue gas is cooled down to a suitable temperature, then compressed and cooled down again. Typically, the dehydration system involves 4–5 condensation stages. The system comprises a compression stage every two condensation units. For example, literature proposes a system with three-stage compression with pressures of 3.13 bar, 9 bar and 30 bar

involving inter-cooling [12]. Furthermore, chemical dehydration can be used to completely extract the water content using triethyleneglycol (TEG) adsorbent [12].

2.3 P2X

The exploitation of renewables sources, such as solar and wind, seems to be a promising way to reduce GHGs from energy production sector. However, the deep permeation of renewables results in an instability in dispatching the electrical grid, since with respect to conventional power plant, ran by coal for example, renewables power experiences lack of reliability and flexibility [24]. EU-27 has a permeation of solar and wind renewables in electricity production of 16.3%, whereas Finland has 8.4% [42]. The aleatory, intermittent and seasonal renewables resources characteristics involve market issues balancing, leading to congestion management [53][82][97]. The Transmission System Operators are reliable to balance the grid all time, decided in market day-ahead and intra-day power auctions. The first resource to be used is renewables, to avoid its waste, then the energy from the lowest levelized cost resource. Because of high ramping in renewables, the system might expect a sudden increase or decrease in the production with respect to forecasts, thus resulting in an over-powered or under-balanced electrical grid. To avoid this phenomenon, base-load power resources might be reduced or increased, and renewables cut out from the grid. Base-load power plant, such as nuclear or coal, have slow ramping transients, which means the impossibility to follow the behaviour of the grid balance fluctuations. Thus, a suitable option consist in stopping the production of power from renewables, thus wasting energy and decreasing its revenue [46].

Literature suggests that P2X can be a suitable option to cope with renewables grid issues and to avoid any waste of energy. P2X comprises a system, where electrical power is converted to an energy resource, which are typically hydrogen, methane, and methanol (MEOH) as well as heat (power-to-heat). As fuels, those products are burnt to supply again electrical power and work, whenever they are needed. Methane and hydrogen can also be directly injected in gas grid, depending on the gas feed regulations [11][53]. If methane or methanol are the final products, the process involves also chemical reactors. In the case of methane, the methanation can be biological or chemical. The advantage with respect to electrical storages, such as batteries, consists in the energy storage, which is used as a combustion precursor, thus avoiding any energy time degradation.

The process begins with the supply of electrical power to an electrolyser unit, typically alkaline electrolytic cell (AEL) because of market availability [11][46][90]. Polymer electrolyte membrane (PEM) and solid oxide electrolysis (SOEL) usage are also under investigation [66][90]. O_2 and H_2 are obtained from electrolysis, as presented in Figure 5. Many studies do not involve the usage of the produced oxygen, which is released to the environment, resulting in a loss of profit [24]. Hydrogen is a ready-burnable fuel. Methane output choice is more suitable than hydrogen because H_2 has higher permeation, lighter density, flammability and explosivity. Oxygen can be supplied to other facilities, such as an oxy-fuel combustion prior to the P2X system, which can feed the methanation unit with the required CO_2.

P2X is involved following the fluctuations of the market. The electrical power input can be everything, but for the sake of balancing the grid, it is considered from renewable resources. When renewables parks generate electrical power, if the grid is balanced, P2X is not

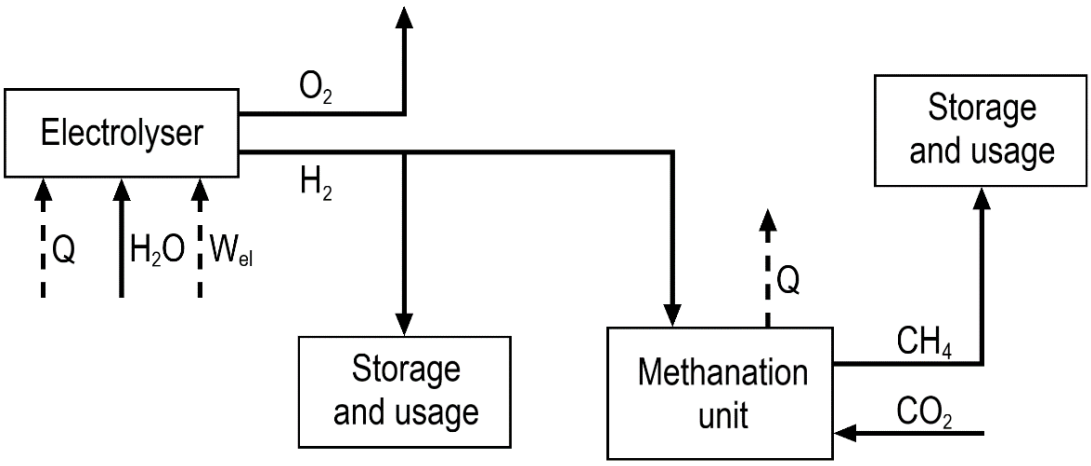

Figure 5: P2X main system's scheme in case of methanation.

involved. However, if Transmission System Operators experience a higher power supplied into the grid, in order to avoid over-powering and wasting, the over-power from renewables is supplied to the P2X facility. The system produces fuel. On the contrary, when the grid is under-balanced after a sudden drop in renewables generation, the previously produced and stored fuel can be burnt again to fulfil the demand. Thus, the P2X works to smooth the ramping steepness and the peaks caused by renewables, ensuring a less aleatory supply into the grid and reduction in demand for power plants reserves [46][97]. Furthermore, P2X products can be used in the transportation sector.

CO_2 is fundamental in the methanation process. High exploitation of power-to-gas process, involving methane, demands for even higher CO_2 flow rate into the system. Nowadays, when carbon dioxide is produced, it is freely emitted into the environment, resulting in GHGs emission. Instead, the usage of CO_2 in P2X processes and other industrial ones, opens a new CO_2 market, which might lead to the construction of CO_2 pipeline grid, where any kind of producers emission (sewage, thermal power plants, brewing industries…) is directly linked with the consumers [11][24][60]. Thus, renewables, together with CO_2 emissions and methane are coupled to fulfil the electrical demand, with the advantage to produce locally standalone fuels [24][60].

In the case of chemical methanation following the Sabatier process, CO_2 together with H_2 is transformed into CH_4. There are three reactions, which describe the phenomenon: global reforming, water gas shift, and steam methane reforming [28][60]. The reactions are the following ones:

$$CO_2 + 4H_2 \rightleftharpoons CH_4 + 2H_2O, \quad (18)$$

$$CO_2 + H_2 \rightleftharpoons CO + H_2O, \quad (19)$$

$$\text{and } CO + 3H_2 \rightleftharpoons CH_4 + H_2O. \quad (20)$$

Form stochiometric viewpoint the reaction in Equation 18 is the hydrogen most requesting one, leading to a ratio of reactants H_2-CO_2 as 4:1. The process involves a catalyst, typically Ni based with calcium cementite cement (Ca:Al, 1:5), but also other metals from group VIII–

X of the element periodic table can be used. The exothermic reaction in the packed-bed methanation reactor can cause hot spots at 500–700 °C, leading to the sintering of catalyst's grains and drastically reducing its surface, disabling its main function [11][66]. Moreover, the presence of sulphur in the reactants can reduce the efficiency of the process. Although Ni-catalyst are quite tolerant to sulphur, they undergo catalyst deactivation with sulphur presence [11].

Methanol can be another product of P2X process, whose chemical formation reactions are presented in the following equations [69]:

$$CO + 2H_2 \rightleftharpoons CH_3OH, \quad (21)$$
$$CO_2 + H_2 \rightleftharpoons CO + H_2O, \quad (22)$$
$$\text{and } CO_2 + 3H_2 \rightleftharpoons CH_3OH + H_2O. \quad (23)$$

With respect to methane, methanol formation reaction has a stoichiometric ratio of 3:1 (H_2-CO_2), requiring less hydrogen supply with respect to the carbon dioxide demand.

2.4 Alkaline electrolysis cell

Along the path towards carbon neutrality, suitable options are power-to-gas and oxy-fuel combustion to face renewables permeation and fossil fuel substitution, as discussed in section 2.2 and 2.3. These two processes respectively demand for hydrogen and oxygen as inputs. Electrolysis technology can be adopted to fulfil the supply [24][35][46][60][90].

Electrolysis consists in the reaction where a direct current flows between two electrodes, immersed in an electrolyte, which causes the liquid water to split into hydrogen and oxygen, expressed in the following equation:

$$H_2O \rightarrow H_2 + \frac{1}{2}O_2. \quad (24)$$

Equation 24 states the stoichiometric balance between reactant and products. Every mole of water produces theoretically one mole of molecular hydrogen and half of molecular oxygen. Enthalpy of formation ($\Delta H_f^\circ = +\ 286$ kJ/mol at 298 K and 1 bar) of Equation 25 is almost constant with respect to temperature and pressure. This quantity is proportional to the contribution of Gibbs free energy, supplied electrically, and to a contribution supplied thermally to the system [90]. It is possible to decrease the electrical supply by raising the temperature and so providing more thermal supply. For instance, the supply of the reactant can be steam instead of liquid water. The formation heat ΔH is obtained as

$$\Delta H = \Delta G + \Delta Q, \quad (25)$$

where ΔG and ΔQ are respectively the electrical and heat supplied for the electrolysis. Electrolysis is a threshold reaction, whose limit is the reversible thermal voltage U_{rev}, which denotes the theoretical minimum cell voltage, which allows electrolysis to occur, calculated in the following equation:

$$U_{rev} = \frac{\Delta G}{zF} \quad . \quad (26)$$

In Equation 26, z denotes the number of electrons involved in the process, 2 in this reaction, and F refers to the Faraday's constant equal to 96485 C/mol. Another characteristic parameter for the process consist in the thermoneutral cell voltage U_{tn}, which refers to the voltage needed by the cell without providing any heat supply, expressed by the following equation:

$$U_{tn} = \frac{\Delta H}{zF} \quad . \tag{27}$$

The functioning of the electrolyser, like efficiency and hydrogen flow rate production, depends strongly on the cell voltage, which is presented in Figure 6. Cell voltage is calculated through the summation of reversible cell voltage U_{rev}, ohmic resistance U_{ohm}, activation U_{act} and U_{con} concentration overvoltages, presented in the following equation [7][47]:

$$U_c = U_{rev} + U_{ohm} + U_{act} + U_{con}. \tag{28}$$

Two configurations are possible regarding to electrolysis cell: monopolar and bipolar. The main difference consists in the fact that the single units are connected in parallel for monopolar cells, requiring the same voltage. Besides for bipolar cells, only two electrodes are connected to the grid, sharing the same current and thus obtaining the total cell voltage as the sum of single modules voltages. In the case of bipolar cell, the volume flow rate produced by the cell $\dot{V}_{H_2}$ is calculated as

$$\dot{V}_{H_2} = \eta_F \frac{n_c \cdot I}{2F} \left(22.414 \cdot 3.6 \frac{\frac{Nm^3}{h}}{\frac{mol}{s}} \right) \quad , \tag{29}$$

where n_c denotes the number of connected cells, operating at current I and at the Faraday's efficiency η_F [7][49]. It is possible to obtain the efficiency of the electrolysis unit referring to the hydrogen higher heating value (HHV) or lower heating value, depending on whether it

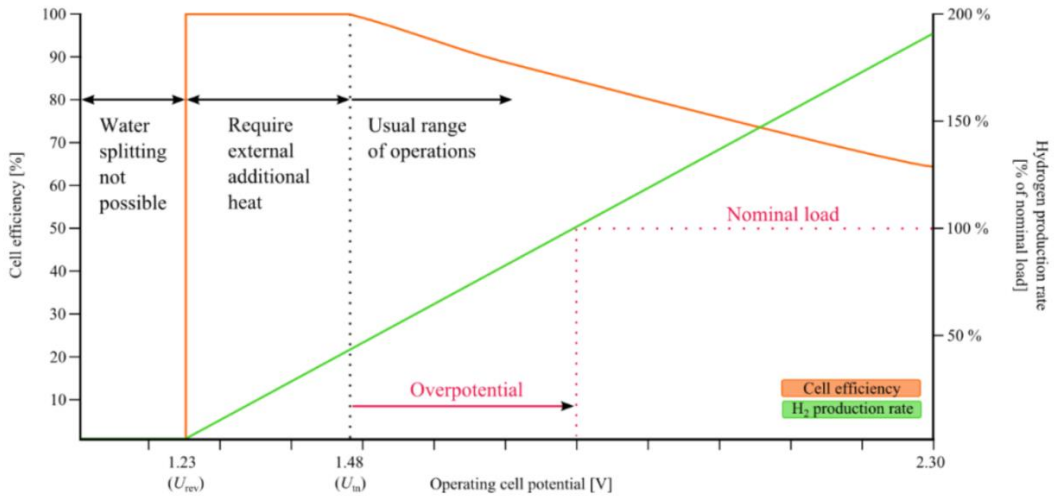

Figure 6: Efficiency and hydrogen production rate as a function of the cell voltage. Figure obtained from [47].

refers to a high temperatures electrolyser (HHV) or a low one (LHV) [7][47], calculated in the following equations:

$$\eta_{HHV} = \frac{\dot{V}_{H_2} \cdot HHV_{H_2}}{P_{el}} = \frac{1.48V}{U_c}\eta_F \quad \text{and} \tag{30}$$

$$\eta_{LHV} = \frac{\dot{V}_{H_2} \cdot LHV_{H_2}}{P_{el}} = \frac{3.00}{3.54}\eta_{HHV} = \frac{1.25V}{U_c}\eta_F \quad . \tag{31}$$

In Equation 30, U_c refers to the voltage cell, which is inversely proportional to the efficiency, as presented in Figure 6. Regarding to normal condition for gases, the relation, which links produced molecular hydrogen to molecular oxygen, is conserved also in Nm^3/s, that is 1:0.5 (H_2-O_2) by following the stoichiometric balance in Equation 24. Thus, it is possible to obtain the volume flow rate for oxygen [49], calculated in the following equation:

$$\dot{V}_{O_2} = 0.5 \cdot \dot{V}_{H_2} = 0.5 \cdot \eta_F \frac{n_c \cdot I}{2F}\left(22.414 \cdot 3.6 \frac{\frac{Nm^3}{h}}{\frac{mol}{s}}\right) \quad . \tag{32}$$

Equation 29 and 32 neglect the purity of the O_2 and H_2 outflow, which depends on the involved technology. Specific cell energy consumption is calculated through the following equation:

$$E_s = \frac{LHV_{H_2}}{\eta_{LHV}} = \frac{2.4}{\eta_F}\frac{U_c}{V} \quad . \tag{33}$$

There are several suitable technologies regarding to the electrolysis process, such as PEM, SOEL, and AEL. PEM technology consists in the usage of a proton conducting membrane to achieve the separation of hydrogen and oxygen molecules, produced through electrolysis. Typical involved materials are Ir and Pt as catalysts and Nafion® for the membrane. Through PEM is possible to obtain a H_2's purity more than 99.99%. Nominal temperature is below 100 °C and pressure is up to 200 [47] – 350 [7] bar.

High temperatures electrolysis can be achieved with SOEL technology. Working temperatures refers to 700–1000 °C, enhancing the kinetics and thermodynamic of reactions and thus resulting in a higher efficiency of the system thanks to ionic conduction and diffusion of reactants through the electrolyte [54]. However, higher temperature affects strongly the stresses applied to the involved materials, which might lead to deterioration, such as the delamination of the oxygen electrode [65]. Reversible operation into fuel cell is also possible with this technology [7][47].

In the case of AEL, electrodes are immersed into a liquid solution, typically 30 wt.% KOH, and separated from each other by a diaphragm, as illustrated in Figure 7. Regarding to the chemical reactions, at the cathode hydrogen is formed (Equation 34) and at the anode oxygen (Equation 35) [7][47][90], by following these equations:

$$2H_2O + 2e^- \rightarrow H_2 + 2OH^- \tag{34}$$

$$\text{and } 2OH^- \rightarrow \frac{1}{2}O_2 + H_2O + 2e^-. \tag{35}$$

The mixture of hydrogen and oxygen with KOH solution flows towards a gas separator device, where the wanted products are dried and sent to the demanding facilities. KOH solution from gas separator encounters pumps and heat exchangers and then it flows back into the electrolyser, thus achieving temperature as well as pressure control.

AEL nominal commercial values refer to 5–1400 Nm^3/h as H_2 flow rate, 0.03–6.0 MW for power, and 1–60 bar as the maximum pressure [7][47]. An excessive working pressure results in a lower efficiency of the cell [76]. AEL has a working temperature of 60–90 °C [7][47]. In addition, increasing the temperature results in a higher efficiency. AEL experiences an increase in temperature of 1–3 °C during the electrolysis process [76]. The technology has an average oxygen production purity of 99–99.8%, enhanced up to 99.999% by catalytic gas purification, whereas AEL has an hydrogen purity of 99.5–99.9% [7][47]. Considering the purity, the actual volume flow rates for hydrogen and oxygen are obtained from Equation 29 and 32, respectively, multiplied by the purity coefficient.

The AEL electrical power requested by the system to provide 1 kg/s of hydrogen and oxygen consists of a key parameter to evaluate the performance of the electrolyser. This value is obtained starting from the energy specific consumption of the cell. Literature suggests the hydrogen has a specific energy consumption E_{s,H_2} of around 4.2–4.8 kWh/Nm^3 by considering 56–70% LHV efficiency [7]. Electrical power per unit of mass flow rate is obtained with a molar mass equal to 2 kg/kmol and 32 kg/kmol for hydrogen and oxygen respectively as well as 4.5 kWh/Nm^3 as the average specific energy consumption, in the following equations:

$$P_{el,H_2} = \frac{E_{s,H_2}}{MM_{H_2}} 22.413 \frac{Nm^3}{kmol} \cdot 3600 \frac{s}{h} = 181.5 \frac{MW_{el}}{kg_{H_2}/s} \quad \text{and} \tag{36}$$

$$P_{el,O_2} = \frac{\dot{n}_{O_2}}{MM_{O_2}} E_{s,O_2} = 2 \frac{E_{s,H_2}}{MM_{O_2}} \cdot 22.413 \frac{Nm^3}{kmol} \cdot 3600 \frac{s}{h} = 22.69 \frac{MW_{el}}{kg_{O_2}/s} \quad . \tag{37}$$

Regarding to oxygen in Equation 37, the calculation takes into account also the stoichiometric balance for the molar flow rate, which consists in multiplying by 2 the energy con-

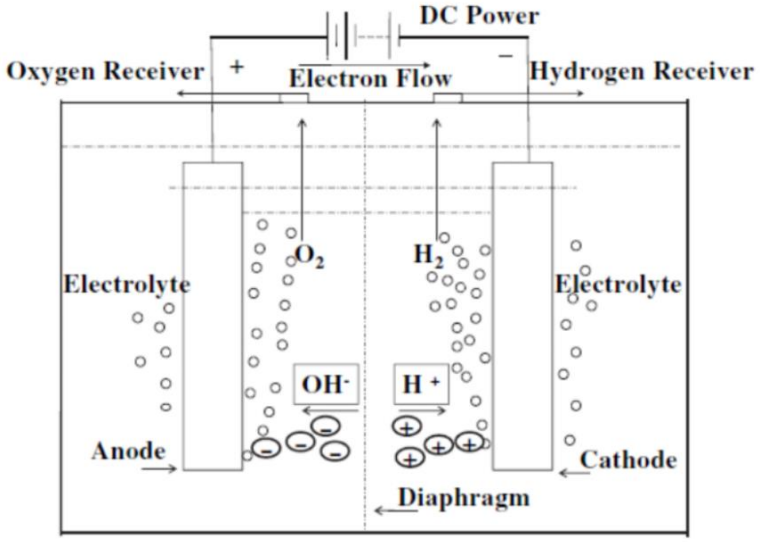

Figure 7: AEL schematic functioning. Figure obtained from [90].

sumption for hydrogen. Other resource reports 141.8 $MW_{el}/(kg_{H2}/s)$ [47] and 163.6$MW_{el}/(kg_{H2}/s)$ [76] of typical requested power to produce hydrogen. AEL has a power specific capital cost (CAPEX) of 700 EUR/kg [24] and operating and management (OPEX) equal to 3% of the CAPEX one [60].

With respect to other electrolysers, AEL is a mature, commercially available, cheaper and less energy consuming technology [7].

2.5 H_2 market and CO_2 tax

Hydrogen is a key resource in the carbon neutrality European 2050-scenario , which can substitute intensive-carbon fossil fuels [15]. As it is discussed in Section 2.3, hydrogen can be used to produce electrical and thermal energy in P2X process, and it is needed in many other sectors, such as in the chemical industry for producing of ammonia and for refining oil [43][47]. The usage of hydrogen is not narrowed only to the energy sector, which makes wider its market.

H_2 is typically produced with steam methane reforming process or through electrolysis, as it is presented in Section 2.4. In the first case, methane together with water reacts into carbon monoxide and hydrogen [11][53]. As the main inputs are different for these two processes, the related cost of hydrogen will be non-identical. For instance, regarding to steam methane reforming reaction, methane is supplied to a reactor unit, which means that in this case the hydrogen cost is related to the methane market. In addition, the main reaction produces carbon monoxide, resulting in a correlation with carbon policies and a higher cost of hydrogen. Therefore, CO_2 and CH_4 market affects hydrogen's producing cost in case of steam methane reforming process.

Instead, referring to electrolysis, as discussed in Section 2.4, the input is electricity. Therefore, H_2 cost is influenced by the cost of electricity. Fluctuations in electricity market have an effect on the hydrogen cost production. With respect to steam methane reforming process, the by-product of electrolysis is oxygen, which is a valuable resource in the market. P2X may use hydrogen, whether the grid experiences an underload, thus increasing the revenue for using hydrogen, as discussed in Section 2.3. Vice versa an overload in the grid results in a depreciation of the electricity cost, consequently decreasing the cost of hydrogen in that particular situation.

In order to compare production prices for different technologies, an annual average cost is considered. Literature reports several values for hydrogen production cost, which are presented in Table 2. The cost of hydrogen in currencies different from EUR/kg are calculated by multiplying the value by the market exchange rate [95]. To sum up the literature review, a suitable value for hydrogen cost should be around 2–5 EUR/kg, with some exceptions on bad conditioned market evaluation [62] and renewables photovoltaic park cost [63]. Steam reforming gas process leads to a cheaper cost of hydrogen, with respect to electrolysis. Nevertheless, if it is also considered the valuable oxygen production from the electrolyser, it can be more competitive [51].

Hydrogen market is indirectly linked with the carbon dioxide one [51]. As it was discussed previously, steam gas reforming produces carbon monoxide, whereas electrolysis results in oxygen second production. Thus, with a strict carbon neutral policy the cost of hydrogen from steam gas reforming could be higher than from electrolysis. However, whether P2X is involved after hydrogen production, in a carbon trading scheme scenario, the overall cost of

hydrogen should decrease thanks to the carbon absorption of P2X with both technologies. For instance, the price of hydrogen can decrease from 4.4 to 0.73 EUR/kg , if oxygen selling and carbon absorption rewarding are considered [98].

Hydrogen's policies are established for the next future in Finland and Europe, but no financial strategy has been planned yet to achieve their targets. According to European Commission's hydrogen roadmap report, hydrogen can be a suitable solution to decarbonise challenging sectors, such as transportation. It is estimated that in 2020 hydrogen price in EU-27 is 1.5 EUR/kg from steam methane reforming, 2 EUR/kg with carbon capture, and 2.5–5.5 EUR/kg from electrolysis. According to previsions, in 2030 steam methane reforming will have a hydrogen price of 2-2.5 EUR/kg because of fossil fuel taxation and carbon policies, whereas electrolysis will produce hydrogen with a price of 1.1–2.4 EUR/kg owing to a decrease in the price of this technology [7][15]. Regarding to Finland, hydrogen is a key resource to achieve carbon neutrality, targeted in 2035, but no hydrogen strategy has been set yet. Hydrogen together with biofuels should lead to the phase-out fossil fuels exploitation [24].

CO_2 is an unwanted by-product compound, which is freely released into the environment. Recently, carbon capture utilisation processes have been exploiting carbon dioxide to produce fossil fuels, as discussed in Section 2.3. However, CO_2 market is still controversial because in some sectors it is needed, such as in metallurgic and P2X industry, resulting in an actual cost of this resource. Literature reports an average cost of 0.025 EUR/kg [69][68] and 0.0153–0.0674 EUR/kg [98]. From 2005, emission trading scheme (ETS) with 'cape and trade' system has been established in EU-27, allowing to flourish carbon dioxide market and economically rewarding sectors with low carbon emissions [16][24]. ETS involves industrial, chemical and carbon storage facilities. Electricity production is not eligible for ETS rewards [16].

2.6 Summary

This chapter has introduced the pre-requisites to understand the physics and the technology of the proposed case study, thus providing insight about typical industrial values. Literature reports some previous analysis of municipal solid waste oxy-fuel combustion with air separation unit with low efficiencies. In order to achieve future carbon neutrality and circular economy targets, a system, which comprises MSW combustion and electrolysis unit, is designed. This strategy might produce hydrogen with a cheaper cost than the current one. The next chapter will explain step by step the modelling process for obtaining a MSW oxy-fuel combustion through electrolysis simulation.

Table 2: Literature review about hydrogen cost.

Reference	Process (primary resource)	Country	Resource cost [EUR/MWh]	Hydrogen cost [EUR/kg]	Year of publication
[33]	Electrolysis (smart grid)	DE	27.52	2–3[a]	2018
[47]	Electrolysis (smart grid)	DE, FIN	51 (DE)	3.2–4.1 (DE) 4.2–5.0 (FIN)	2015 (2012)
[47]	Steam methane reforming	DE, FIN	n.a.	1.8 (DE,FIN)	2015 (2012)
[62]	Electrolysis (smart grid)	US	0–88.5	2.25–106.48	2020
[63]	Steam methane reforming	IT	n.a.	2.08	2020
[63]	Electrolysis (photovoltaic)	IT	-	23.33	2020
[69]	Electrolysis	n.a	30	3.09–4.10	2020
[71]	Electrolysis (mix renewables)	CHI	-	2.71–3.52	2020
[83]	Steam methane reforming	FR	n.a.	5.1[b]	2020
[98]	Electrolysis	US	62	0.73–4.4	2021

[a] optimal result with secondary reserve market strategy and participation

[b] overall analysis cost including taxes and transportation

3 Research material and methods

This chapter will explain in detail the model developed in this thesis for an MSW oxy-fuel combustion thermal power plant with electrolysis. The model is obtained through the programme Aspen Plus V11. The model consists of Vantaan Energia waste-to-energy thermal power plant retrofitting, taken as a reference case. Firstly, the model comprises the design of the reference case into Aspen Plus, from which is possible to validate the simulation. Then, the validated model integrates the recirculation system, the electrolysis unit, and the flue gas treatment.

This chapter is structured as follows. Fuel analysis is discussed in Section 3.1 by presenting the chemical local characterisation of Helsinki region and its material partition. Vantaan Energia reference case analysis and data collection are outlined in Section 3.2. Section 3.3 investigates step by step the design process in Aspen Plus from the waste-to-energy reference case model to its retrofitting into oxy-fuel combustion with electrolysis.

3.1 Fuel analysis

The case study involves municipal solid waste as the fuel for the combustion in the thermal power plant. The characterisation of MSW provides the heating values and the chemical composition. Through this preliminary analysis of the fuel, it is possible to achieve the thermal power during the combustion, depending on the mass flow rate input to the boiler.

Because of the choice to retrofit a pre-existent thermal power plant, such as Vantaan Energia waste-to-energy power plant, the model should follow as much as possible its characteristic, such as the fuel input. Thus, data is collected from the Helsinki environmental region services consortium (Helsingin seudun ympäristöpalvelut, HSY) about the MSW composition and from literature the chemical analysis. HSY data is used for the case study because it was not possible to retrieve data directly from Vantaan Energia thermal power plant.

MSW depends consistently on the location, as previously discussed in Section 2.1. Moreover, MSW sorting determines the chemical composition of the fuel and consequently the LHV. The HSY analyses MSW partition, collected in Helsinki area [37]. The HSY reports that the majority of MSW is composed of kitchen waste, plastic, garden waste and wood, as well as paper origin waste, presented in Figure 8. Above all, plastic materials have the highest LHV [68]. The lowest percentages consist in metals and glasses. As discussed in Section 2.1, metals and glasses are non-combustible material, thus absorbing the energy released by the combustion. The HSY favours the presence of high calorific materials and the reduction of non-combustibles with recycling policy, thus resulting in a high net calorific value.

Fuel chemical composition was not provided by Vantaan Energia. Therefore, data is collected from local analysis. Chemical composition and net calorific values from literature are summed up in Table 3 [68]. Helsinki region's MSW has a HHV of 19.6 MJ/kg. The fuel has carbon content as the highest fraction, followed by oxygen and hydrogen. Other elements have a fraction lower than 1wt%. MSW has an ash content calculated at 550°C of 22.4wt%.

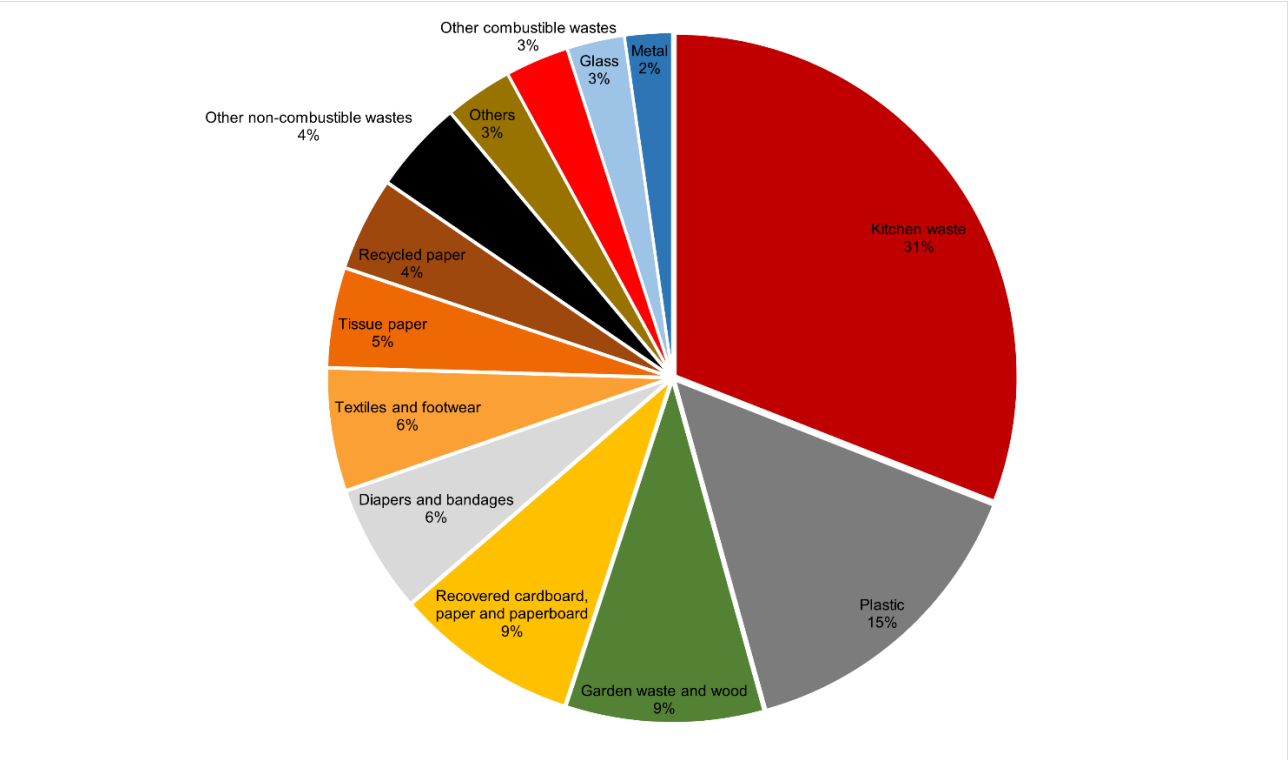

Figure 8: MSW sorting fraction analysis. Data obtained from [37].

Table 3: Helsinki's region MSW chemical characterization. Data obtained from [68].

Analysed parameter	**MSW**
Moisture content [wt%]	13.5
Ash 550°C [wt%]	22.4
Volatile matter [wt%]	79.4
Carbon content (dry) [wt%]	47.0
Hydrogen content (dry) [wt%]	6.2
Nitrogen content (dry) [wt%]	0.5
O calculated content (dry) [wt%]	0.2
Sulphur content (dry) [wt%]	19.6
HHV (as received) [MJ/kg]	16.7
HHV (dry) [MJ/kg]	19.6

Vantaan Energia reports an annual combustion of 374000 t of MSW [88]. Therefore, with some further assumptions it is possible to obtain the total MSW mass flow rate. The assumption consists in evaluating the capacity factor equals to 0.9 for a base load thermal power plant, such as Vantaan Energia waste-to-energy plant. The MSW input stream $\dot{m}_{MSW}$ is calculated as

$$\dot{m}_{MSW} = \frac{M_{MSW}}{\Delta t} \cdot f_C = \frac{374 \cdot 10^6}{365 \cdot 24 \cdot 3600}\ 0.9 = 13 \frac{kg}{s} \quad , \tag{38}$$

where M_{MSW} [kg] refers to the total MSW annual combustion, Δt [s] denotes the time in one year, and f_C [-] designates the capacity factor of the thermal power plant. The reference power plant is assumed to have a mass flow rate of 13 kg/s, calculated from Equation 38.

3.2 Vantaan Energia waste-to-energy plant system

Vantaan Energia waste-to-energy plant, which is shown in Figure 9, is analysed as the reference case for this case study. The system consists in a conventional thermal power plant configuration with four sub-sections: pre-treatment of fuel, furnace, steam cycle, and flue gas treatment. The combustion of MSW releases energy, which is exploited by the steam cycle coolant to achieve higher enthalpy, thus producing electric power. In addition, the Vantaan Energia power plant comprises a gas turbine, which can be used to produce additional 31 MW_{el} to the grid. Gas turbine flue gas is exploited like a thermal power source for the steam cycle because of its high temperature.

Vantaan Energia reports the system structure and functioning of this MSW thermal power plant [88]. Firstly, MSW is pre-treated. It is collected in a waste pit, where the fuel is continuously mixed to achieve a uniform LHV as well as stored for one week to diminish the water content. Vantaan Energia MSW combustion involves two furnaces. These furnaces are grate firing type, whose grates together with the combustion flame reach the temperature of 1100 °C. Through radiation, the flame heats up the saturated liquid water in boiling pipes of the evaporation section. The flue gas proceeds forward to the ceiling, thus encountering the superheater and the economizer. The flue gas from the gas turbine heats up the coolant of the steam cycle to the steam turbines. After these two exchangers the flue gas is cooled down and treated. The cooling of the flue gas produces an additional thermal power of 30 MW_{th} for district heating purpose [26].

Figure 9: Vantaan Energia thermal power plant in Vantaan, Finland. Figure obtained from [87].

The treatment consists of removing the main environmentally harmful and toxic compounds before the emission, such as fly ashes, particulates, sulphur dioxide and heavy metals. The latter is typically produced in MSW combustion, as discussed in Section 2.1. Fly ashes are collected in electrostatic precipitator. Particulates removal is accomplished by bag filters. Sulphur dioxide is absorbed by lime and heavy metals are absorbed by activated carbons.

Figure 10 presents the scheme of the waste-to-energy plant provided by Vantaan Energia. The thermal power, released by the MSW combustion, is transferred to the water coolant owing to the boiler. Through the high quantity of heat achieved by the coolant, subcooled water becomes steam. As presented in Figure 10, the steam is exploited in a steam cycle, where it expanses in three turbines: at high (HPT) to 38 bar, medium (MPT) to 5.5 bar, and low pressures (LPT) to 0.85 bar. The Rankine's steam cycle does not comprise a steam reheating before the MPT with respect to a conventional thermal power plant. The turbines produce a net electrical output of 49.5 MW_{el} by considering the balance of plant and mechanical efficiencies. The electricity is supplied to national grid.

After the expansion stage owing to the turbines, the coolant has still a higher vapor fraction close to dry steam condition. Therefore, a condenser unit is set before the pump. The pump experiences a steep increase in compression work, whether vapour fraction is present in the fluid. Thus, the condenser unit cools down the wet steam to the liquid saturation state by extracting thermal power in a heat exchanger. The thermal power discarded by the condenser is used for district heating, thus avoiding the need of residential heating and its high polluting effect. With respect to conventional thermal power plants, if district heating is requested, an option consists in an increase of the condenser working pressure, known as counter-pressure. District heating (DH) network has a typical temperature supply of 65–110 °C and return of 50 °C [24]. Thus, in order to heat up the coolant for district heating network, the steam from turbines has to condense at a higher temperature than the hot inlet, so more than 90–110 °C. It is assumed that the temperature of district heating supply is 90 °C. The pressure of a bi-phase fluid is directly linked with its temperature, following Gibbs variance rule [31]. Therefore, only one thermodynamic parameter is needed to determine the system, which in this case is the pressure. In the bi-phase region if the pressure is higher, the temperature consequently increases. Conventional thermal power plants without district heating have typical condenser working pressure of 0.05 bar [72]. The thermodynamic bi-phase state for 0.05 bar corresponds to 32.5 °C, which is not enough to heats up the coolant to 90°C for district heating purpose. Owing to the counter-pressure by increasing the condenser pressure to 0.85 bar, such as in the chosen reference case, the condensing fluid has a temperature of 95 °C [31]. In addition, the condensation process involves a constant-temperature phase change, which releases huge thermal power. Vantaan Energia reference case extracts from the condenser 119.3 MW_{th} to district heating.

In Figure 10 the condenser unit has no hot coolant outlet, which is assumed to be directly connected to a pump (LPP1) and then to a deaerator. The pump compresses the fluid to a pressure of 2.7 bar. The deaerator unit removes the incondensable gaseous fraction contained in the coolant at a pressure of 2.7 bar. This fraction leads to severe chemical corrosion of the piping network [72]. These incondensable gases permeate in the cycle mainly because of infiltration from the low pressure turbine. Vantaan Energia thermal power plant has a condenser pressure of 0.85 bar, which is lower than the room pressure, thus resulting in these pressure-difference infiltrations. In addition, this latter unit typically heats up the

feedwater owing to the bleedings from the steam line. However, because of lack of data for the steam cycle the deaerator connection is not present in the Vantaan original scheme.

Figure 11 shows the steam cycle by combining the original scheme collected from Vantaan Energia in Figure 10 and the assumptions set in this thesis. The scheme should provide a clearer insight of the steam cycle by showing every connection and streams. In this scheme the gas turbine is not shown and so its connection to the boiler. The saturated liquid water flows from the deaerator towards a second low pressure pump (LPP2), where it is compressed to 5.5 bar. The feedwater is split into two streams. The first stream has a mass flow rate of 2.8 kg/s and it is heated by the flue gas from the boiler, thus achieving a temperature of 157 °C. The heated split fraction is then mixed with the steam coming from the medium pressure turbine. The second one proceeds in two further compression stages. After the compression to 38 bar owing to the medium pressure pump (MPP), the feedwater is split again in two streams. With the same strategy of the previous split, one stream is heated up to 400°C and sent to the steam line. This stream has a mass flow rate of 8.1 kg/s and it is mixed with steam coming from the high pressure turbine. The remaining feedwater is compressed in the final stage to a pressure of 91 bar. The last pump is known as HPP. The resulting highly compressed feedwater flows through the boiler, thus increasing its temperature and enthalpy.

The boiler comprises three main section: economizer, evaporator, and superheater. By exploiting the heat transfer from the MSW combustion and the flue gas, the subcooled feed water becomes superheated steam. The economizer heats up the liquid coolant to its saturated state. This saturation state has a pressure of 91 bar and a temperature of 303 °C with zero vapour fraction. The evaporator evaporates the saturated liquid to dry steam state with the same temperature and pressure. The superheater accomplishes the superheating duty of the dry steam to a temperature of 535 °C. In addition, the superheater accounts for the pressure losses of the whole boiler, thus achieving an outlet boiler steam pressure of 86 bar. The steam is sent to the turbines stage, where the cycle starts again.

In Table 4 the thermodynamic characteristics of the steam data are summed up, which are provided by Vantaan Energia in normal operation (without gas turbine).

3.3 Modelling in Aspen Plus

The MSW oxy-fuel thermal power plant model in Aspen Plus comprises four main systems: combustion cycle, steam cycle, oxygen supplier system, and flue gas treatment facility. The combustion cycle combines the MSW fuel and the comburent air for extracting the chemical combustion energy. This energy is given to the steam cycle in order to produce electrical power. In addition, the combustion cycle is coupled with the flue gas treatment facility. The combustion produces flue gas, which is treated in this latter facility, in order to obtain water owing to a dehydration processes, as well as clean CO_2. The resulting water from the flue gas treatment is supplied to the electrolysis, where oxygen is produced and used, thus achieving oxy-fuel combustion.

The oxy-fuel retrofitting is obtained from Vantaan Energia reference case, whose data is summed up in Section 3.2. Sub-sections 3.3.1 describes the combustion cycle and Section 3.3.2 the steam cycle. Firstly, these two cycles will be explained for the Vantaan Energia case. Then, Sub-section 3.3.3 will investigate about the modifications of the original combustion as well as steam cycle into an oxy-fuel system.

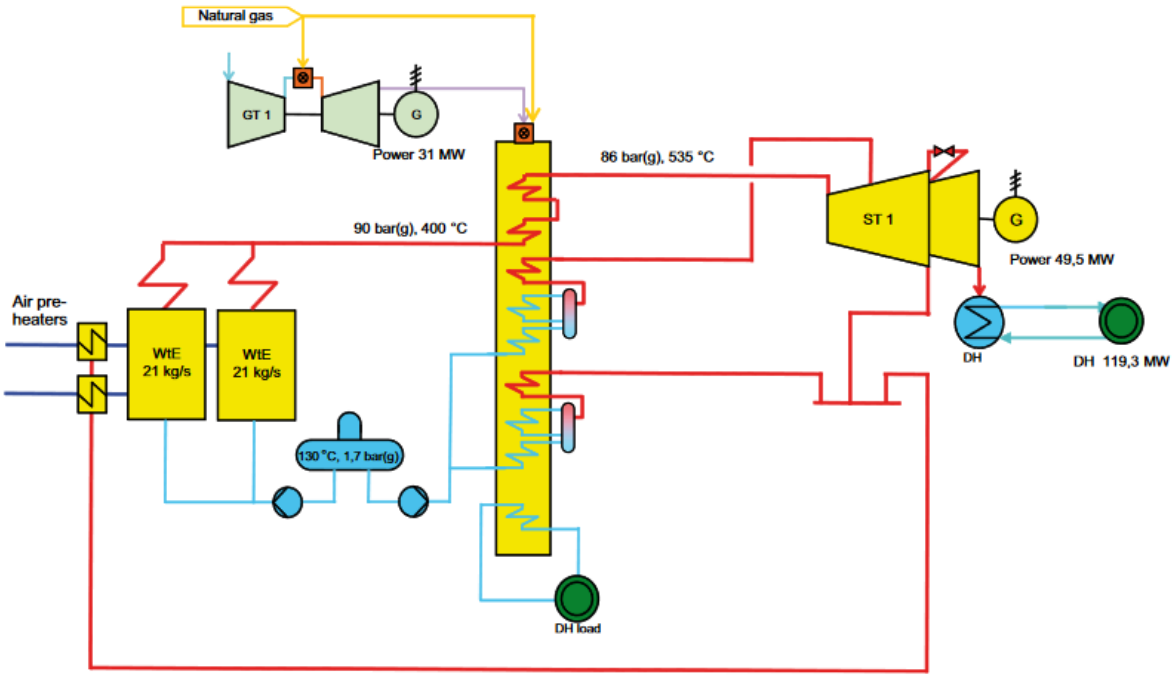

Figure 10: Vantaan Energia waste-to-energy plant scheme. Figure obtained from [74].

Table 4: Thermodynamic characteristics of the main steam Rankine's cycle points.

Components	Pressure [bar]	Temperature [°C]	Mass flow rate [kg/s]
HPT	87→38	535→n.a.	46.1
MPT	38→5.5	n.a.→ n.a.	55.2
LPT	5.5→0.85	n.a.→ 95[a]	57
Bleeding MP	38	400	8.1
Bleeding LP	5.5	157	2.8
Condenser	0.85	n.a.	57
LP1P	0.85→2.7	95[a] →130	57
Deaerator	2.7	130	57
LP2P	2.7→5.5	130→n.a.	57
MPP	5.5→38	n.a	55.2
HPP	38→91	n.a	46.1
Economizer	91	n.a.→303[a]	46.1
Evaporator	91	303[a]	46.1
Superheater	91→87	303[a]→535	46.1

[a] calculated through saturation tables

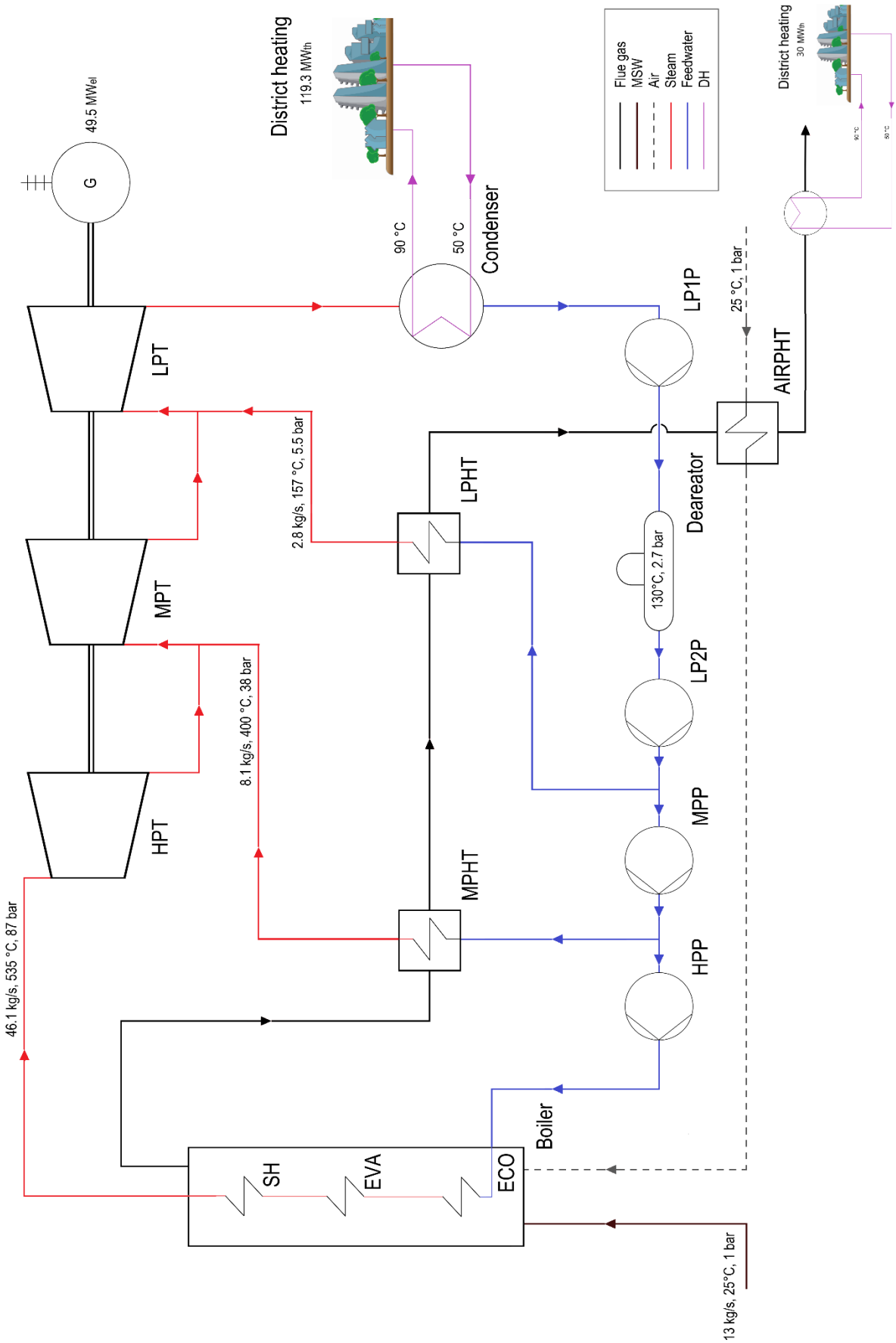

Figure 11: Steam cycle scheme of Vantaan Energia waste-to-energy plant.

3.3.1 Combustion system

The combustion cycle models the actual combustion in the furnace of Vantaan Energia thermal power plant. In the whole combustion cycle, the pressure losses are not considered, thus obtaining a constant pressure from the entry point to the stack. The geometry of the furnace and of other components is not modelled in this thesis. The combustible fuel is MSW, which is a non-conventional compound. In Aspen Plus MSW is not present as a known compound. Therefore, this fuel has to be created in the compound library. All the fuel chemical characteristics are taken from the previous fuel analysis, reported in Section 3.1. Starting from Table 3, it is possible to obtain all the three required analysis for the MSW feed stream: Proxanal, Ultanal, and Sulfanal. Proxanal consists of the moisture content, volatile matter (VM), fixed carbon (FC), and ash on dry basis analysis. Ultanal analysis refers to the chemical composition of the dry fuel including ashes. Sulfunal corresponds to the origin of the specified sulphur content in the Ultanal analysis, which in this case is only organic. MSW non-conventional coefficients are summed up in Table 5. This fuel stream has a mass flow rate of 13 kg/s, as assumed in Section 3.1. MSW is fed at standard conditions (25°C and 1 bar) to the first combustion cycle block. All blocks used in this cycle are summed up in Appendix A in Table A1. The model flowsheet of Vantaan Energia reference case is presented in Figure 12.

In order to obtain the combustion, MSW has to be firstly separated in its basic elements. The decomposition task is accomplished by RYIELD block ("DECOMP"). This block allows to specify the flash type, thus separating MSW into the elements with a known thermodynamic state. DECOMP is set with a pressure of 1 bar and a temperature of 25 °C. The block requires yield coefficients, which are calculated from the ultimate chemical analysis of MSW feed stream (ULT). These coefficients refer to the Ultanal values but calculated on wet basis. Yield decomposition calculation is obtained owing to an algorithm script in Fortran language, which is shown in Appendix A.

The resulting decomposition streams are supplied to RGIBBS block. These streams denotes the decomposed MSW stream and the heat stream requested by RYIELD block for its functioning. The RGIBBS block models the combustion of the fuel. In addition, it is possible to set manually the HHV of the fuel in the properties section by specifying HCOMB value for MSW. In this case, MSW HHV is calculated as

$$HHV_{HCOMB} = HHV_{dry} = HHV_{daf} \cdot (1 - ASH) = 15.21 \frac{MJ}{kg} \quad , \tag{39}$$

where ASH denotes the ash content and HHV_{daf} refers to the dry-ash-free HHV in the chemical analysis, reported in Table 3. In Vantaan Energia, the combustion comburent consists of air taken from the environment. The air has standard conditions as well as an assumed molar fraction of 79mol% of nitrogen and 21mol% of oxygen. Regarding to RGIBBS settings, the specification refers to the phase and the chemical equilibrium with an operating pressure of 1 bar. The air stream is preheated in a heat exchanger (HeatX) by the hot flue gas, after the steam cycle. The possible products from RGIBBS reactor block are identified by Aspen Plus. This block calculates the equilibrium of the process with respect to the specified input components by minimising the Gibbs free energy [2]. The combustion produces a flue gas together with ash stream, which is supplied to an ash separator unit. A flash block is involved

Table 5: MSW non-conventional stream component attribute.

Proxanal	
Moisture	13.5
FC	15.9856
VM	61.6144
Ash	22.4
Sulfanal	
Organic	0.20952

Ultanal	
Ash	22.4
Carbon	49.5942
Hydrogen	6.54944
Nitrogen	0.52768
Chlorine	0
Sulphur	0.20952
Oxygen	20.7192

in the process in order to model the separation process. The solid and unburnt fraction is separated from the main stream at a pressure of 1 bar in adiabatic condition.

The cleaner flue gas proceeds to boiler section of the furnace. In order to simplify the model, the boiler furnace superheater and the heater of the flue gas turbine are combined together in one heat exchanger. Thus, the boiler is modelled in three heat exchangers, owing to HeatX Aspen Plus block. These heat exchangers are known as “EVA” (evaporator), “SH” (superheater), “ECO” (economizer). Furthermore, the flue gas-bleedings heat exchangers are referred as “MPHEAT” (medium pressure heater), and “LPHEAT” (low pressure heater). These heat exchangers are set with shortcut and countercurrent specifications. The flue gas is the hot fluid in all exchangers. In order to follow as much as possible the reference case, the boiler first block refers to the evaporator, where from the coolant side saturated water becomes dry steam. Therefore, the specification of the evaporator block refers to cold stream outlet vapour fraction, which is set equal to 1 as design calculation. The gas proceeds to the superheater. The flue gas exchanges thermal power with the steam cycle coolant, which becomes superheated steam. As designed in the reference case, the superheater has a cold stream outlet temperature of 535°C. The third block functions as the economizer, which specifies the cold stream outlet vapour fraction equal to 0, thus achieving saturated liquid water on the coolant side. Then, the flue gas exchanges thermal power with the coolant in the medium and low pressure heaters. These heaters heat up a fraction of the cold feedwater to a temperature of 400 °C and 157 °C, respectively for medium and low pressure heaters. Thus, these blocks are set with cold stream outlet temperature of 400 °C and 157 °C design specification. The steam cycle exchangers cool down the flue gas. Nevertheless, the flue gas can still have enough temperature to heat up the comburent air. Therefore, another exchanger (HeatX) is set in the model, known as “AIRPRH”. In the block a cold outlet temperature of 250°C is specified as design calculation. After the preheater, the flue gas flows through one last heat exchanger, thus exploiting its hot temperature. The thermal power from the heat exchanger is used for district heating purpose. Therefore, the supply and return pipe are assumed to have a temperature of 50°C and 90 °C, respectively. The flue gas is cooled down to 55 °C. Lastly, the flue gas is emitted in the environment after treatment, thus ending the combustion cycle.

The air mass flow rate was not possible to be retrieved from provided data. Thus, it is assumed that the flue gas has an oxygen molar content of 5mol%. This assumption requires

a design specification, which achieves the targeted 5 mol% oxygen flue gas fraction by varying the air comburent mass flow rate.

3.3.2 Steam cycle

Vantaan Energia steam cycle produces 49.5 MW_{el} and 149.3 MW_{th}. The model tries to follow as much as possible the scheme presented in Figure 10. Model data is retrieved directly from Vantaan Energia, which is summed up in Table 4. The coolant is pure water. The model in Aspen Plus for the steam cycle is shown in Figure 12. All blocks used in this cycle are summed up in Appendix A in Table A2.

The steam cycle receives thermal power from the combustion cycle in the boiler section. Owing to the boiler, the liquid feedwater becomes steam with a temperature of 535 °C and a pressure of 87 bar. The steam has a mass flow rate of 47.1 kg/s. This stream is fed to a three-stage turbines (COMPR): high, medium and pressure. All turbines have an assumed isentropic coefficients of 0.9 and mechanical efficiencies of 0.95, as no outlet thermodynamic expansion state was provided. The first turbine expands the fluid to 38 bar. The resulting stream is mixed with a medium pressure 'bleeding' from the feed water line. The bleeding stream is heated by the flue gas to a temperature of 400 °C in the medium pressure heater, owing to outlet cold steam temperature design heater specification. The medium pressure bleeding stream has a mass flow rate of 8.1 kg/s. Therefore, after mixing the two streams, the new stream has a mass flow rate of 55.2 kg/s. The mixed stream is expanded in the second turbine to 5.5 bar. Like the previous streams mixing, the resulting expansion stream is merged with low pressure bleeding from the feed water line. The low pressure bleeding is heated up to 157 °C by the flue gas, owing to a outlet cold temperature design specification. The bleeding has mass flow rate of 2.8 kg/s. The last turbine expands the steam to 0.85 bar. Then, the wet steam is supplied to the condenser (HeatX), which condenses the coolant into saturated liquid water by 0 hot stream outlet vapour fraction design.

The condenser provides thermal power to the district heating network. It is assumed that district heating network has a return pipe temperature of 50°C, typically 40–60 °C and supply pipe temperature of 90°C, typically 65–115°C [24]. Thus, a design specification is required to achieve the desired hot supply temperature by varying the mass flow rate of district heating coolant. The district heating coolant is assumed to have a pressure of 4 bar.

The condenser supplies the cold feed water to the pumps stage. The pumps have an assumed isentropic efficiency of 0.95 and a driver of 0.99. In order to be mixed with the steam line, the total feed water line is pumped to 5.5 bar and it is split to feed the low pressure heater. The same strategy is adopted for the medium pressure flow rate to a pressure of 38 bar. After the two splits, the feed water line has a pressure of 38 bar and a mass flow rate of 47.1 kg/s. The stream is compressed to 91 bar and encounters the boiler, where it becomes superheated steam. This task is accomplished by outlet cold temperature heater design. The superheater (SH) is the only component, which accounts for the pressure losses of the steam cycle equal to 4 bar.

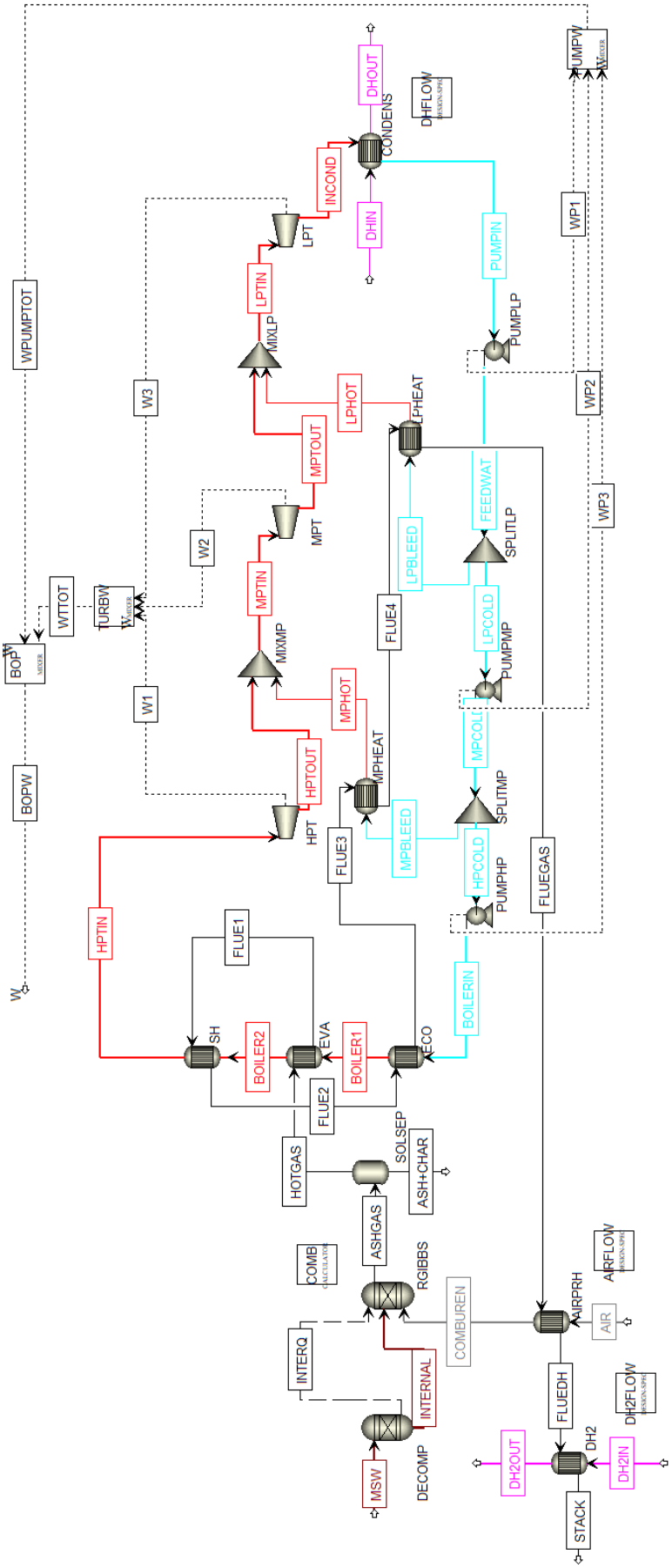

Figure 12: Vantaan reference case model in Aspen Plus.

3.3.3 Oxy-fuel waste combustion system's retrofitting

The oxy-fuel combustion model is designed from the Vantaan Energia thermal power combustion and steam cycle, discussed in the two previous subsections. A pure oxygen supply to the furnace leads to an excessive combustion temperature, as discussed in Section 2.2. Thus, in order to reduce the temperature, the system introduces a recirculation strategy in the combustion cycle. In this model, the recirculation originates from the cold flue gas after the steam cycle exchangers and before the flue gas treatment. The pure oxygen stream substitutes the previous air supply, thus avoiding the need for an air preheater. The oxygen comburent is mixed with the recirculated fraction and supplied to the RGIBBS reactor. In order to achieve the same flame temperature of 1100°C with respect to the reference case, a design specification is set by varying the flue gas recirculated fraction. Therefore, with respect to the conventional MSW thermal power plant, the model comprises one more mixer block between oxygen and recirculation stream as well as one more splitter block after the steam cycle exchangers. With respect to the recirculation strategy, the model does not address the design of particulate and volatile matter removal unit, which should be placed before the recirculation, as discussed in Section 2.2. The oxy-fuel flowsheet model is shown in Figure 13.

Regarding to the steam cycle, the modification of the reference model consists in the coolant mass flow rate. The oxy-fuel combustion results in a higher potential thermal power exchanged to the steam cycle. In order to exploit this advantage, the mass flow rates is increased in the steam cycle by a parametric factor of 1.25 from the original values. Thus, the coolant has a total mass flow rate of 72.5 kg/s as well as the bleedings have a mass flow rate of 10.125 kg/s and 3.5 kg/s for medium and low pressure, respectively.

3.3.4 Aspen Plus model for the electrolyser

The oxy-fuel combustion is achieved owing to an electrolysis unit, which supplies the required oxygen to the furnace. The electrolysis process is not comparable to any pre-modelled Aspen Plus library component. Therefore, the electrolyser is designed by creating a User Model block. The chosen User Model consists in User2 because it allows the user to connect up to 4 inlet as well as 4 outlet streams to the block, instead of one input and one output like User component. In addition, with respect to User and User3, heat and work streams can be directly linked with User2 block.

The proposed self-made electrolyser block simulates the essential working of a real electrolyser. This modelled block is known as "ELECTSIS" and it performs the mass and energy balance of a real electrolyser. The whole electrolysis system is not addressed in this model. This means that no electrolyte recirculation system or product filtration will be simulated. Furthermore, the electrolyser is considered without heat loss. As presented in Section 2.4, the electrolysis process consists in splitting water into oxygen and hydrogen, owing to an electrical power supply to the unit. The electrolysis process has a molar stoichiometric ratio between reactant and products of 1:1:0.5 (H_2O-H_2-O_2) by following the Equation 24. ELECTSIS block uses an excel file calculation to perform the mass balance of the reaction and it adopts a calculator block (Calculator, "POW") to achieve the energy balance.

Regarding to the mass balance, ELECTSIS block receives a supply of pure water and produces hydrogen and oxygen. This user block provides the mole flow rates of hydrogen and oxygen from a given mole flow rate of water. It is assumed that no separation process is

needed. Thus, the electrolysis modelled block directly produces two separate streams: one for hydrogen and the other for oxygen with a purity of 100%. In addition, the unit specifies a stream flash on the two products about temperature and pressure. The goal of this user block is to obtain a link between the inputs and outputs. Therefore, it needs to be parametrically stated that every 1 mol/s of input water should correspond to an hydrogen output of 1 mol/s and oxygen production of 0.5 mol/s. The electrolyser works at a pressure of 1 bar and a temperature of 75 °C, as discussed in Section 2.4.

The required Excel file contains the main calculation to emulate the electrolysis molar balance. The calculation file comprises six sheets: "Aspen_IntParams", "Aspen_RealParams", "Aspen_Input", "Aspen_INP_NC", "Aspen_OUT_NC", and "Aspen_Output". The first two sheets declare all the parameter that can be used to calculate the possible outputs inside Excel, which in this model are not needed. Aspen_Input collects the input stream by specifying its elemental content and thermodynamic state. The only input for this block is the water feed because the power supplied to the electrolyser is considered as a negative output. The molar flow rate of water is defined as a variable inside Excel, which will be used in the output calculation. Aspen_INP_NC and Aspen_OUT_NC refer to non-conventional components input-output calculation. Water, hydrogen and oxygen are conventional components, so these previous two sheets are not needed in the calculation. These are automatically created because the main model includes also non-conventional stream calculations. Aspen_Output states the output variables values, which will be retrieved by Aspen Plus and used in the simulation. This latter Excel sheet contains the two streams in output with their specification values. All declared elements as well as compounds in the main model are present in the output Excel sheet of the electrolyser sub-model. They have to be specified, even though they are not involved in the sub-model. Since the water inflow has been declared as a variable in Excel file, it is possible to state the stoichiometric balance. Regarding to the component "O2", the oxygen molar flow is equal to half of water molar flow. With respect to "H2" component, the hydrogen molar flow is equal to the molar flow of water. Other parameters in the output sheet are set to 0, thus meaning a 0 molar flow of the other elements/compound in the output flows. The temperature and pressure are parametrised like the molar flow rate. The pressure is constant in the process, thus neglecting any pressure loss in the cells. Regarding to the temperature, it is considered an increased in temperature of 2°C during the process, as reported in Section 2.4. Therefore in the Aspen_Output sheet the temperature of the two resulting streams is equal to the input one plus this temperature increase. The thermodynamic state of the output flows is automatically calculated owing to temperature and pressure flash option. The output oxygen flow is supplied directly to the combustion cycle, where is mixed with recirculated stream and fed to RGIBBS reactor. Examples of the most important Excel sheets are illustrated in Table A3 and in Table A4 in Appendix A.

Regarding to the power required by the electrolyser, POW calculator block firstly collects the mass flow rate value of the produced oxygen. Then, it calculates how much power is required by following Equation 37. For instance, every 1 kg/s of produced oxygen corresponds to 22.69 MW_{el} of requested electrical power. The work stream is connected between the electrolyser and the resulting work balance of the thermal power plant, thus achieving the net work produced or required by the whole MSW oxy-fuel power plant.

3.3.5 Flue gas treatment

The flue gas treatment system should produce an almost pure carbon dioxide as a by-product from the combustion flue gas. The oxy-fuel combustion exploits an electrolysis unit, which requires a constant supply of pure water to produce oxygen. Thus, it is possible to directly extract the required water for the electrolysis from the flue gas. The flue gas treatment system comprises a dehydration system as well as a carbon dioxide purification system. The Aspen Plus model is presented in Figure 13. The block used in the flowsheet are summed up in Appendix A in Table A5.

The hot flue gas is dehydrated owing to four stages of condensation and three of compression. The condensation task is performed through a heat exchanger (HeatX), which extracts the thermal power from the flue gas. This thermal power is provided to district heating network. As mentioned in Sub-section 3.3.2, it is assumed that district heating has an inlet and outlet temperature of 50 °C and 90 °C, respectively. Thus, the colder flue gas has an achievable realistic temperature not lower than 55°C. Consequently, the exchangers are set with an outlet hot temperature of 55 °C as design specification. After the condensation, the liquid water is separated from the flue gas by Flash2 unit at the same temperature and pressure of the incoming flue gas. The gaseous fraction proceeds in the dehydration system, where it encounters the first compression stage. After the compression, the flue gas is sent again to a condensation exchanger. The flue gas is compressed progressively to a pressure of 3.13 bar, 9.7 bar, and lastly to 30 bar by following typical values for dehydration from literature, as discusses in Section 2.2 [12]. The compressors have an assumed isentropic efficiency of 0.9 and a mechanical efficiency of 0.95. The four condensed fraction are mixed together after a lamination to 1 bar. The first condensed water stream has a pressure of 1 bar, so no lamination is needed.

The total condensed water is supplied to an deaerator unit, thus extracting the non-condensable contaminating gas from the stream. This subsystem comprises an additional water stream supply in case of lack of water from the flue gas condensation to the electrolyser. The additional water stream is assumed to have standard condition of pressure and temperature. Since the additional water supply has a temperature of 25°C, the stream is used to cooled down further the flue gas after the first flue gas condenser. The working point for the electrolyser is around 75 °C, as discussed in Section 2.4. Thus, the required water encounters a heat exchanger, which heats up the latter stream to a temperature of 75 °C. The thermal power is given by the flue gas after the steam cycle and before the flue gas treatment. The heated water is supplied to the electrolyser. The compressors work is linked to the work from the steam cycle, thus obtaining the balance of the whole plant work.

Through compression and condensation physical separation at temperatures of 55 °C, it is not possible to extract the whole water content in the flue gas [12][72]. The flue gas has reduced water content, but it has other combustion compound, such as sulphur oxides, as presented in Section 2.1. This compound is particularly harmful in P2X process for the catalyser, as discussed in Section 2.3. Therefore, the sulphur oxides are removed owing to Sep block. The model adopts fluidized gas desulphurisation, which has an assumed efficiency of 98 %, as reported in Section 2.1. The remaining water fraction in the flue gas after the desulphurisation is removed through a chemical separation process. The chemical dehydration removes completely the water content, which is modelled with a separation block (Sep) with 100% efficiency.

3.4 Summary

This chapter has introduced the model description of the studied reference case and its retrofitting into an oxy-fuel thermal power plant. In order to achieve oxy-fuel combustion, the main modifications refer to the flue gas treatment and the electrolysis unit with respect to the original thermal power plant. The next chapter will look at the results of the simulated model in Aspen Plus and it will discuss the main key findings in comparison to previous technologies.

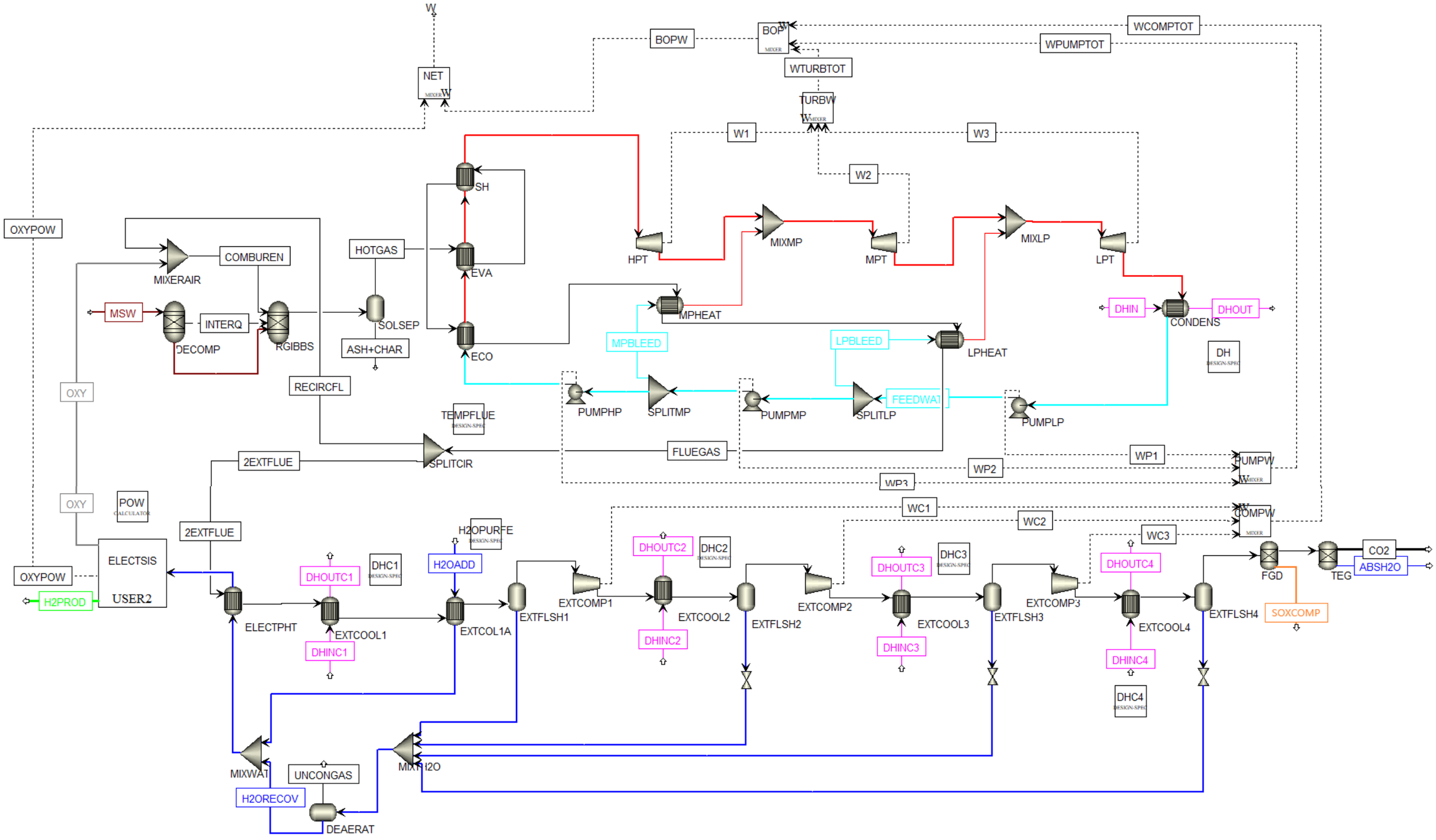

Figure 13: Oxy-fuel combustion with electrolysis system flowsheet in Aspen Plus.

4 Results and discussion

This chapter will present the results of the proposed model simulation. The results will include the comparison between Vantaan Energia thermal power plant and its Aspen Plus model outputs in order to validate the modelled system. The feasibility of the oxy-retrofitted simulated thermal power plant will be investigated by analysing its several outputs, such as net electrical and district heating power as well as its by-products including hydrogen and carbon dioxide. In addition, this chapter will cover a sensitivity analysis of the flue gas recirculation fraction.

This chapter is structured as follows. Section 4.1 presents the power outputs comparison and discussion between Vantaan Energia real case and the two simulated model in Aspen Plus: the reference model and the oxy-fuel thermal power plant with electrolysis. Section 4.2 investigates the product composition. Section 4.3 shows the sensitivity analysis of the model of the flue gas OFC recirculation fraction. Section 4.4 reports the LCOH (levelized cost of hydrogen) break-even cost for MSW OFC proposed in this thesis.

4.1 Power production

The modelled Vantaan Energia reference case produces an electrical power of 47.5 MW and a thermal one of 171 MW for district heating purpose. With respect to the real case, the model produces less electrical power and more district heating power. The simulated electrical power of the reference model has a relative error of 4.04% with respect to the real case. The thermal power extracted in the condenser unit is close to the Vantaan real case with a relative error of 3.94%. However, the district heating extracted from the flue gas condensation has a relative error of 56.7%. Lack of data may have resulted in the incorrectness of the proposed simulation reference Vantaan model with respect to the real reference case. The results comparison among the Vantaan Energia real case, the reference model and the proposed oxy-fuel system are summed up in Table 6.

The oxy-fuel thermal power plant produces a district heating thermal power of 191.3 MW, from which 158.3 MW are extracted in the condenser and 33 MW in the dehydration system. Furthermore, the simulated oxy-fuel plant produces a power balance of plant of 53.6 MW by

Table 6: Comparison among Vantaan real case, Vantaan model and oxy-fuel model main outputs.

	Vantaan real case	**Vantaan model**	**OFC model**
District heating [MW_{th}] (Condenser + flue gas condensation)	119.3 + 30	124.0 + 47	158.3 + 33
Balance of plant [MW_{el}]	49.5	47.5	53.6
Electrolysis supply [MW_{el}]	0	0	-419.1
Net work [MW_{el}]	49.5	47.5	-365.5
Hydrogen produced [kg/s]	0	0	2.34

considering the work produced by turbines in the steam cycle as well as the one requested by pumps and compressors of the dehydration system.

The electrolysis process demands for an electrical power supply of 419.1 MW. The total electrical power production in the oxy-fuel model is not enough to fulfil the request of the electrolyser. The production and demand for electrical power in the oxy-fuel system results in an unbalance of the system, thus requiring an additional supply of 365.5 MW_{el}. Thus, the proposed system is not electrically auto-sustainable. The power break-down of the system is illustrated in Figure 14. The hydrogen power is calculated through the hydrogen HHV equal to 33.3 kWh/kg [47].

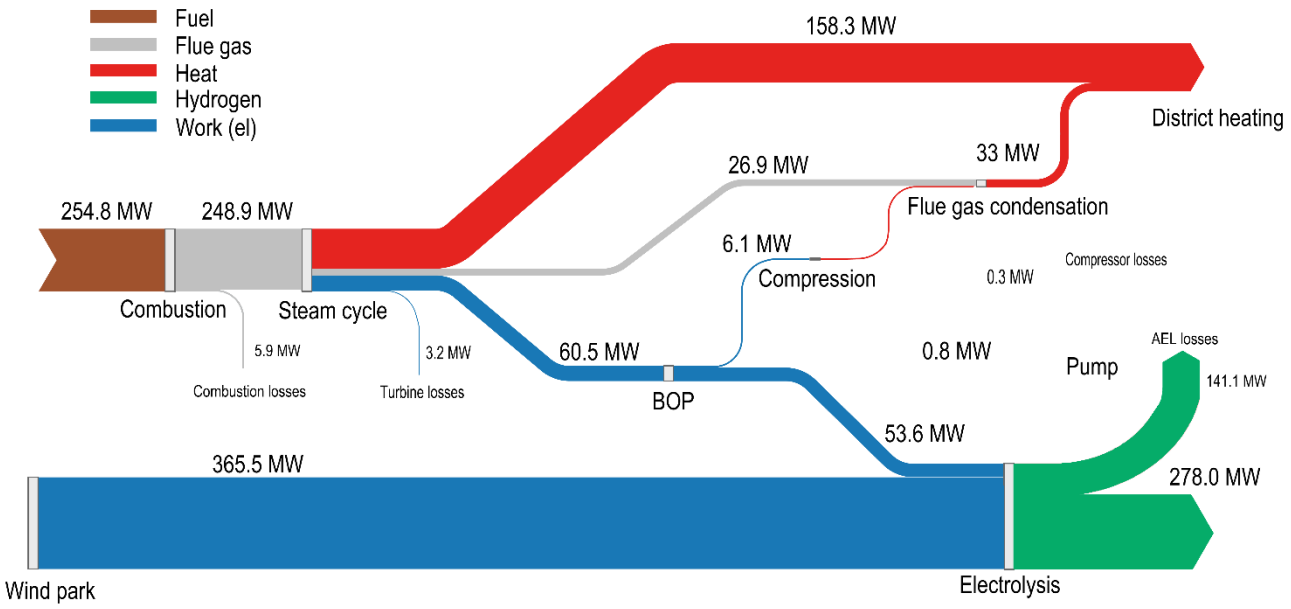

Figure 14: Sankey's diagram of power balance.

In order to cope with the electrically unbalanced system, one suitable solution consists of the exploitation of a wind park. In this case, the proposed system refers to a base load MSW thermal power plant. As discussed in Section 2.3, renewables energies experience sudden decrease or increase in the production out of forecasts. This characteristic cannot match with oxy-fuel combustion system, which should avoid unstable and steep transient functioning. Therefore, the inclusion of a wind park in the system requires the uncoupling of the system itself from the products of the electrolysis. This means that the system has to include an oxygen storage in order to uncouple electrical power from wind production and its usage in MSW OFC furnace. In addition, a possible design of a wind park should consider that the average power production has to be around the electrolysis power demand. The MSW OFC base load characteristic has an assumed capacity factor of 0.9, which means, that for 876 h the wind park is producing oxygen that will not be used by the system, thus filling up an oxygen tank, which will be used in case of lack or decrease of wind power production. The link between the installed nominal power and its actual energy production was evaluated in order to estimate the size of the wind park. This ratio is known as availability factor. In order to smooth any productions peaks by yearly exceptionalities, the availability factor is considered as an average factor from 2016 to 2020 referring to Finnish national overall wind production. Collected data is shown in Table 7 and the availability factor is calculated as

$$f_{av} = \frac{\sum E_{prod}}{\Delta t \cdot \sum W_{nom}} = 0.298 \quad , \tag{40}$$

where f_{av} is the availability factor of the wind park, E refers to the effective energy production, W to the nominal installed power and Δt a time interval of one year. Finnish wind energy production has an average availability factor of 0.298. The total energy required by the electrolyser and the nominal power designed wind park are calculated as follows

$$E_{electrolyser} = f_{c,OFC} \cdot W_{electrolyser} \cdot \Delta t = 0.9 \cdot 365.5 \cdot 8760 = 2882\ GWh \quad \text{and} \tag{41}$$

$$W_{nom,park} = \frac{E_{electrolyser}}{f_{av} \cdot \Delta t} = 1105\ MW \quad , \tag{42}$$

where $f_{c,OFC}$ is the capacity factory of the oxy-fuel plant, $E_{electrolyser}$ denotes the yearly energy requested by the electrolyser and $W_{nom,park}$ the nominal installed power of the wind park. In order to fulfil the energy and power requested by the electrolyser, the wind park should have a nominal installed power around 1105 MW.

Vantaan waste-to-energy thermal power plant reports the monthly energy obtained through combustion and the production of district heating as well as electricity, referring to 2019 [90]. Therefore, these efficiencies are calculated through the energies results instead of the power in order to compare the two simulations with Vantaan real case. The steam cycle efficiency of the three systems is calculated as follows

$$\eta_{steam\ cycle} = \frac{E_{elec} + E_{DH}}{E_{fuel\ input}} \cdot 100\% \quad , \tag{43}$$

where E_{elec} refers to the yearly produced net electrical energy of the system, $E_{fuel\ input}$ denotes the yearly energy fuel input. With respect to the two models, the real case uses as fuel also natural gas, which is included in the calculation. E_{DH} indicates the district heating thermal energy production. The power obtained from the two Aspen Plus simulations are multiplied by the availability factor of the plant and the yearly hours, thus obtaining comparable energy results. The efficiency as well as the energy involved in the calculations are reported

Table 7: Finnish wind installed power and its energy production. Data obtained from [42].

Year	Nominal installed power [MW]	Energy production [GWh]
2016	1533	3100
2017	2113	4800
2018	2041	5857
2019	2284	5987
2020	2586	7788

in Table 8. As discussed in Section 3.1, the two models have the same MSW yearly mass fuel input. However, the energy fuel input of the simulations are different. Vantaan Energia reports an average calorific value for MSW of 10.9 MJ/kg. Contrarily, the simulations retrieve the calorific value from Table 3, as no chemical characterization of the fuel was provided. Vantaan real case has a steam cycle efficiency of 95.65%, whereas its reference model has an efficiency of 87.75%. The highest efficiency is achieved by the OFC model, which is equal to 96.11%.

The OFC simulation produces district heating and hydrogen power as products by requiring MSW fuel as well as wind park electrical power input. Therefore, two efficiencies regarding only the oxy-fuel combustion model can be calculated through the following equations:

$$\eta_{OFC} = \frac{P_{DH} + P_{H_2}}{P_{MSW} + P_{wind,elec}} \cdot 100\% \quad \text{and} \tag{44}$$

$$\eta_{OFC,overall} = \frac{P_{DH} + P_{H_2}}{P_{MSW} + P_{wind,energy}} \cdot 100\% \quad . \tag{45}$$

Equation 44 refers to the efficiency of the oxy-fuel system with electrical power wind park supply η_{OFC}, whereas Equation 45 calculates the efficiency of the OFC system $\eta_{OFC,overall}$ by including the wind park efficiency owing to its capacity factor, previously obtained owing to Equation 40. In Equation 44 and 45, P_{DH} and P_{H_2} denote the power production district heating as well as hydrogen, respectively. The hydrogen power is calculated by considering a hydrogen LHV of 33.3 kWh/kg, which results in 118.8 MW/(kg/s) of produced power per mass flow of hydrogen. P_{MSW} refers to the input fuel power obtained by multiplying the MSW HHV from Table 3 for the MSW mass flow rate input in Equation 38. $P_{wind,elec}$ and $P_{wind,energy}$ indicate the wind power production of the wind park as well as the nominal installed power, respectively. The OFC system has an efficiency of 75.66%, whereas by including the capacity factor of the wind park, the proposed system results in an efficiency decrease to 26.21%. Nevertheless, the overall efficiency of the OFC system with electrolysis is higher than the one with CAS-ASU, which has simulated efficiency of 9.57% [12].

Table 8: Energy input-output and efficiency analysis. Data obtained from [90].

	Vantaan real case (2019)	**Vantaan model**	**OFC model**
$E_{fuel\ input}$ [GWh]	1222.3	2008.8	2008.8
E_{net} [GWh]	250.6	374.5	470.7
E_{DH} [GWh]	918.5	1348.1	1508.2
$\eta_{steam\ cycle}$ [%]	95.65	87.75	96.11

4.2 Products analysis

The oxy-fuel thermal power retrofit is the only strategy, which involves hydrogen production. The electrolysis produces as a by-product hydrogen with a mass flow rate of 2.34 kg/s.

The electrolysis model produces a 100% pure hydrogen stream. Furthermore, it has a temperature of 77 °C and a pressure of 1 bar.

Owing to the oxy-fuel retrofit of the reference model, the simulation shows different combustion values, such as the oxygen supply, the combustion temperature and the in-boiler flue gas mass flow rate. These values are compared for the two simulated models in Table 9. In the reference model the comburent consists in a molar fraction of 21%, which results in a demand for a total comburent mass flow rate of 108.0 kg/s of air. With respect to the reference case, the oxy-fuel simulation shows an oxygen supplied flow of 18.54 kg/s. The two different values are caused by the design specifications discussed in Section 3.3. By assumptions, the oxygen supply is designed to have a molar fraction of 5mol% in the flue gas. However, in order to obtain a purer carbon dioxide in the flue gas as well as a lower demand for electricity to the electrolyser, the design specification of the oxygen content in the flue gas after the combustion in the oxy-fuel case was modified to 0.05mol%. Therefore, the oxy-fuel case reports a lower oxygen supply.

Owing to a recirculated fraction of 83.39% the simulation achieves a combustion temperature of 1100 °C. The recirculation allows the simulation to obtain a combustion temperature closer to the Vantaan Energia real case, as presented in Section 3.2. The simulation converges to a total mass flow of the flue gas through the boiler of 179.8 kg/s.

The oxy-fuel combustion strategy results in a flue gas, which is mainly composed of carbon dioxide and water vapour, as reported in Section 2.2. Table B5 in Appendix B shows the flue gas composition comparison between the two simulations analysed in this thesis. After the combustion and ash removal stage, the highest content compounds in the flue gas consist in carbon dioxide with a molar fraction content in the stream of 49.9mol% and water vapour with a molar fraction of 49.7mol%. With respect to the reference conventional incineration Vantaan plant, the nitrogen fraction decreased from 72mol% to 0.228mol%. Furthermore, the flue gas increases its sulphur content from 0.0179mol% to 0.0790mol% in the oxy-fuel simulation. The flue gas is composed of carbon monoxide, hydrogen and nitrogen oxides, which have altogether a fraction less than 0.5%.

The oxy-fuel combustion produces a flue gas with high carbon dioxide and water vapour content. As the two proposed simulation have a different flue gas mass flow because of the comburent recirculation strategy, the flue gas composition is compared also for the singular mass flow compounds, summed up in Table B5 . The production of carbon dioxide and water is not changed. The oxy-fuel strategy results in a flue gas with a much higher concentration

Table 9: Comparison between Vantaan and oxy-fuel model about the combustion cycle.

	Vantaan model	**OFC model**
O_2 supply fraction [mol%]	21	100
Comburent mass flow [kg/s] (O_2)	108.0 (25.2)	18.41
Combustion temperature [°C]	1697	1100
Recirculated fraction [%]	0	83.39
Boiler flue gas mass flow [kg/s]	118.5	179.7

of CO_2 and H_2O. Molecular hydrogen is produced as a result of the incomplete MSW hydrogen content combustion.

The analysed results refer to the flue gas after combustion before any treatment. The pollutants concentration are summed up in Table 10. The oxy-fuel strategy affects consistently all main pollutants except for the sulphur dioxide. As discussed in Section 2.1, the nitrogen products are directly proportional to the nitrogen reactant concentration. The oxy-fuel combustion solutions consists in an absence of nitrogen in the comburent. However, nitrogen is still present in small quantities in the fuel, which results in reduction in concentration by three order of magnitude for NO and one for NO_2. In both simulations, the sulphur mass flow in the fuel is completely oxidised into SO_2. Table 10 reports an increase in the sulphur oxide concentration from the reference case to the oxy-fuel model. However, with respect to the oxy-fuel simulation, the reference Vantaan case simulation involves a higher comburent air to the furnace, which dilutes more the pollutants, especially sulphur oxides. The comparison of sulphur oxides production of the two simulation shows that the mass flow rate of this pollutant is the same, equal to 169.5 kg/h. Therefore, the oxy-fuel strategy does not affect the production of sulphur oxides, but its concentration in the flue gas. The same effect is obtained for water vapour and carbon dioxide.

Vantaan Energia reports annually the emission of the reference waste-to-energy thermal power plant taken for this case study [90]. In this analysis the report year refers to 2019. Table 11 shows the comparison of the annual emission for the three investigated cases. The emissions are analysed for carbon monoxide, nitrogen oxides and sulphur dioxide. The total emission are sampled after the flue gas treatment stage for all cases. However, as no data is possible to retrieve from Vantaan Energia about the denitrification system, the two simulations do not comprise any nitrogen oxides removal system. The OFC system produces almost the same annual quantity of carbon monoxide as the Vantaan real case. As discusses in Section 3.3, the products are the combustion are obtained by minimizing the Gibbs free energy of the system. Therefore, it is possible that in the real case combustion more stable products than carbon monoxide are formed, thus resulting in its lower production than the two simulations. Moreover, even though the real case comprises a denitrification unit, it produces two order of magnitude more than the OFC system. The reference model does not comprise any denitrification facility, which might decrease the nitrogen oxides emission by two orders of magnitude, thus obtaining a very close value to the real case. As previously discussed in this Section, the production of sulphur oxide does not change between the two

Table 10: Comparison between Vantaan model and oxy-fuel model about the main pollutants composition in the flue gas after the combustion.

	Vantaan model [ppmv]	**OFC model [ppmv]**
CO	512	3.81
H_2	116	1.89
NO	3490	5.33
NO_2	2.87	0.145
SO_2	179	786

models, which is slightly higher than the one provided by Vantaan Energia. The chemical characterization of the MSW fuel used in the two simulations, where the sulphur content is specified, could be different with respect to the Vantaan Energia fuel. Therefore, a different source of data for the MSW chemical analysis might have resulted in different emissions results for sulphur oxides between the real case and the proposed simulations.

Vantaan Energia also reports the pollutants concentration, which is compared with the two simulations in Table 12 [90]. Vantaan waste-to-energy power plant reports the concentration for each of the two MSW furnaces. These concentrations are obtained referring to a molar oxygen content in the dry flue gas of 11mol%, starting from the molar fraction of the pollutant [21]. The comparison with respect to the OFC simulation is referred to the CO_2 output stream. As for the total emission comparison, the Vantaa model result refers to a system without the denitrification unit, which results in a higher concentration of nitrogen oxides in the flue gas in comparison with the real case. The OFC system has the lowest concentrations in the flue gas except for sulphur oxide. The concentration of sulphur oxide is the highest as a result of the lower mass flow rate of the flue gas. In addition, the OFC strategy produces almost a flue gas with half water content. Therefore, when compared to the limit values referring to the dry flue gas, the concentration of the sulphur oxide increases consistently. All cases respect the limit values from the European Directive, except for the Vantaan model about NO_xs and the OFC model about SO_2. Nevertheless, the OFC strategy produces a CO_2 stream, which is not freely emitted into the environment, as it is supplied to other facilities, thus fulfilling the European pollutants concentration limit values.

The oxy-fuel proposed simulation shows a higher thermal power available in the boiler. Thus, the coolant in the steam cycle was increased by a factor 1.25 with respect to the Vantaan real and model cases, as shown in Table 13.

Table 11: Comparison of annual emissions among Vantaan real case (2019) and the two simulations. Data obtained from [90].

	Vantaan real case	**Vantaan model**	**OFC model**
CO [kg]	8007	$1.670 \cdot 10^6$	7658
NO_x [kg]	$4.563 \cdot 10^5$	$1.219 \cdot 10^7$	1841
SO_2 [kg]	6495	$2.674 \cdot 10^4$	$2.665 \cdot 10^4$

Table 12: Comparison of main pollutants concentration among Vantaan real case (2019), the two simulations and EU limit values. Data obtained from [21] and [90].

	Vantaan line 1	**Vantaan line 2**	**Vantaan model**	**OFC model**	**Limit value**
CO [mg/Nm^3]	3.23	3.04	4.24	2.51	50
NO_x [mg/Nm^3]	185.24	183.29	1943	83.8	200
SO_2 [mg/Nm^3]	3.19	2.28	3.27	72.1	50

Table 13: Comparison between Vantaan model and oxy-fuel model about the mass flows of the steam cycles.

	Vantaan real case	Vantaan model	OFC model
Total steam mass flow to the condenser [kg/s]	57	57	72.5
LPHEAT mass flow [kg/s]	2.8	2.8	3.5
MPHEAT mass flow [kg/s]	8.1	8.1	10.125

The flue gas dehydration system recovers a water mass flow rate of 8.28 kg/s form the flue gas, as summed up in Table B6. In addition, the dehydration system provides an additional district heating power of 32.9 MW_{th}. The compressors requires an electrical supply of 6.06 MW_{el}. The condensed water is used to supply the electrolyser. However, the simulation reports that the condensed water is not enough to fulfil the water demand for the electrolyser, which consists in 20.7 kg/s. An additional feedwater from outside the system of 12.4 kg/s needs to be considered. The condensation occurs in 4 consecutive stages. Table 14 shows pressure, condensation mass flow, efficiencies and district heating as well as compression power. The stage without compression condenses most of the water vapour content in the flue gas. Owing to compression and inter-condensation phase, the efficiencies of all stages are higher than 60%, which refers to the condensed fraction with respect to the water input of the stage. The compression work is decreasing in the consecutives stages because the consistent reduction of the flow to compress has a stronger effect than the increase of compression pressure. Without compression and inter-condensation stages the resulting flow would have a water content of 16.7wt% in the flue gas, thus highly contaminating the CO_2 output stream. The last stage of the dehydration system condensed 0.993% of the initial water flue gas content. The chemical adsorption completely removes the remaining 0.637% of vapour content after the gas desulphurisation. Before the chemical dehydration the carbon dioxide has purity of 98.8mol%, thus depending on the purity requirement as well as the water content tolerance, the system might not involve any chemical dehydration unit. The same discussion is applicable to the last stage of the physical condensation, as it removes less than 1mol% of the water contained in the flue gas after the combustion.

Table 14: Flue gas dehydration system results analysis stages.

	0^{th} stage	1^{st} stage	2^{nd} stage	3^{rd} stage
Pressure [bar]	1.00	3.13	9.7	30.0
Condensed mass flow [kg/s]	6.94	0.986	0.273	0.0828
Stage dehydration efficiency [%]	83.3	70.9	66.7	60.9
DH [MW_{th}]	23.3	4.58	2.66	2.34
Compression work [MW_{el}]	-	2.24	1.97	1.85

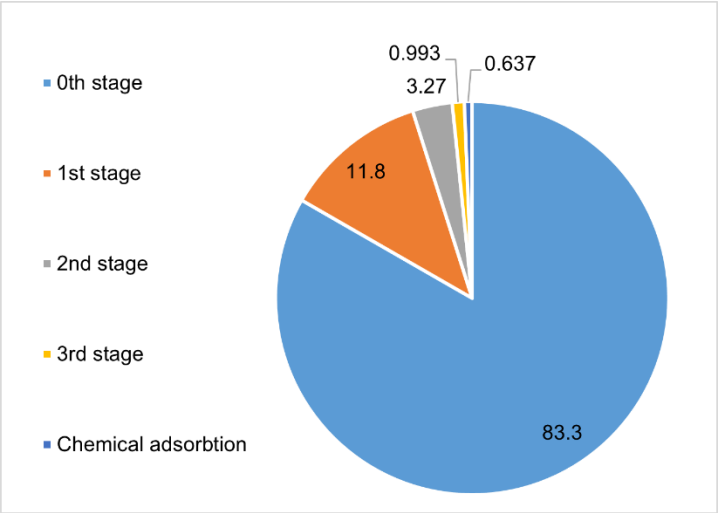

Figure 15: Flue gas dehydration water extraction percentage in each stage referring to the initial water flow.

The liquid condensed water from the dehydration system contains come gaseous impurities from the flue gas. The last stage because of the compression at high pressure results in a higher content of gaseous solution in the condensed water. The condensed water is purified by gaseous flash, thus reaching a purity of 99.994wt%. In addition, the supply of pure water to the system results in a dilution of the gaseous polluting fraction. Lastly, the liquid water has a purity of 99.998wt%, as reported in Table 15. The most contaminating gases dissolved in the electrolysis feed water are the carbon dioxide and sulphur dioxide, which have a weight fraction in the water of 0.17wt% and 0.051wt%, respectively. Other gaseous fraction are negligible.

After the flue gas dehydration the carbon dioxide has a purity of 98.7% mol. Owing to desulphurisation and chemical adsorption, the carbon dioxide achieves a purity of 99.4%.

Table 15: Electrolysis feed water composition analysis.

	Electrolysis feedwater [wt%]
CO	$7.8 \cdot 10^{-12}$
CO_2	$1.7 \cdot 10^{-3}$
H_2	$2.9 \cdot 10^{-12}$
H_2O	99.998
N_2	$1.2 \cdot 10^{-9}$
NO	$5.7 \cdot 10^{-11}$
NO_2	$6.2 \cdot 10^{-9}$
O_2	$7.8 \cdot 10^{-8}$
SO_2	$5.1 \cdot 10^{-4}$

As shown in Table B7, the nitrogen has a molar fraction of 0.454% and other compounds are negligible.

The carbon dioxide stream output has molar flow of rate of 0.464 kmol/sec. The hydrogen produced by electrolysis has a mole flow rate of 1.15 kmol/sec. Therefore, the hydrogen-carbon dioxide proposed simulation production has a molar ratio of 2.48. As discussed in Section 2.3, the carbon dioxide and hydrogen can be used in power-to-methanol processes, whose stoichiometric reactants ratio is close to 3. Regarding to power-to-methane, the hydrogen production is not sufficient, as it is should be close to 4. Thus, in order to fulfil the stoichiometric balance of any P2X reaction, part of the carbon dioxide production should be discharged or the hydrogen production increased. Increasing the hydrogen production will results in an enlargement of the wind park and the AEL, consequently affecting their cost. Besides, the unused carbon dioxide could be stored or sold to the steel industry and other sectors, as discussed in Section 2.5. With respect to hydrogen increasing capacity production, this latter option would not affect the cost, as no upgrades are needed in the system. The free emissions of this carbon dioxide quantity will result in a loss of a valuable resource, as this product has a very high purity as well as small but non-negligible price. Furthermore, the production of carbon dioxide can be regulated owing to the recirculation fraction to the furnace, which directly affects the mass flow of the flue gas to the flue gas treatment subsystem.

The oxy-fuel strategy produces 4 main outputs: carbon dioxide, hydrogen, water and oxygen, whose characteristic are summed up in Table 16.

Table 16: Oxy-fuel products comparison.

	CO_2	**H_2**	**H_2O (cond.)**	**O_2**
Mass flow [kg/s]	20.51	2.34	8.28	18.41
Temperature [°C]	55	77	75	77
Pressure [bar]	1	1	1	1
Purity [mol%]	99.44	100	99.999	100
End-use	Storage (P2X)	Storage (P2X)	Electrolysis	Furnace

The OFC proposed strategy achieves carbon neutrality target by avoiding any carbon dioxide emissions. The proposed system fits the future requirements about energy and emissions policies. As discussed in Section 2.5, Finland targets to achieve carbon neutrality by 2035. In this scenario, electricity and district heating emissions need to be reduced. Table 17 reports the average emission that power plants producing either district heating and electricity have to respect in order to achieve carbon neutrality. The emission should be reduced by 90% for electricity and 75% for district heating production [70]. Vantaan Energia provides data about CO_2 emission referring to 2019 [90], as presented in Table 18. Vantaan Energia MSW power plant has an energetic specific emission of 714.3 kg_{CO2}/MWh for electricity and 194.9 kg_{CO2}/MWh for district heating. The current specific energetic emissions are much higher with respect to planned average emission. The Vantaan Energia reference model specific emissions are calculated from simulation results about the power output and carbon dioxide production. However, in order to be comparable with Vantaan Energia real

case, the emission from turbine gas has to be included in the calculation. Therefore from Vantaan Energia emission report turbine gas power output and emission are retrieved and added to one from the reference model [90]. The oxy-fuel proposed system does not produce any electricity, because it is entirely supplied to the electrolysis. Nevertheless, district heating energy is available to be extracted and sold. The oxy-fuel strategy results in zero-emission carbon dioxide solution, which would perfectly fit Finland's carbon neutrality target, thus strongly reducing the overall average emission production.

Table 17: Finland carbon dioxide average emissions previsions from electricity and district heating energy production. Data obtained from [70].

	Reference	**Baseline scenario**		**Low-carbon scenario**	
Target year	2017	2035	2050	2035	2050
Electricity [kg_{CO2}/MWh]	131	14	1	10	1
District heating [kg_{CO2}/MWh]	148	38	6	34	6

Table 18: Comparison of kg_{co2}/MWh among Vantaan real case and the two simulations. Data obtained from [90].

	Electricity [kg_{CO2}/MWh]	**District heating [kg_{CO2}/MWh]**
Vantaan real case (2019)	736.2	194.1
Vantaan reference model	1484.9	438.8
Vantaan OFC retrofit model	-	0

4.3 Sensitivity analysis

The recirculated fraction of the flue gas to the furnace is an essential parameter, as it results in the flue gas thermodynamic state and chemical composition. Therefore, the flue gas recirculated fraction is the dependent parameter for the sensitivity analysis of the main outputs of the MSW OFC simulation. The recirculated fraction is varied from 5% to 95% of the produced flue gas. In order to be consistent among all cases, the steam mass flow rate is parameterized. The parametrization consists in obtaining the highest steam cycle coolant mass flow for every recirculation fraction value, thus extracting the highest power referring to the balance of plant and district heating production. A first sensitivity analysis is investigated with respect to the thermodynamics of the flue gas depending on the recirculated fraction. The investigation results are presented in Figure 16. The sensitivity of recirculated fraction analyses the combustion temperature in the furnace, the in-boiler flue gas mass flow and its temperature after the steam cycle. In addition, the parametrization of the steam mass flow is also investigated. Increasing the recirculated fraction results in a higher mass flow circulating through the boiler and a lower combustion temperature. A higher recirculated fraction results in a higher mass flow recirculated to the furnace, which is mixed with a constant mass flow of oxygen. Therefore, the boiler experiences an increase in the mass flow. On the contrary, the temperature decreases as the cold flue gas recirculated mass flow

increases to the furnace. The heat released by the combustion is constant, which means that if the mass flow of the flue gas is increased, consequently the temperature will decrease in order to obtain a constant thermal power delivered by the flue gas. The flue gas mass flow has an exponential behaviour depending on the recirculated fraction. The temperature of the flue gas after the steam cycle is almost constant and below 500 °C. Oscillations are present in the analysed parameters because the maximum steam mass flow rate was calculated through a nested sensitivity analysis for each split fraction. Therefore, the nested sensitivity interval refinement causes non-smoothness of the flue gas temperature. The thermal power extracted to the steam cycle from the flue gas is directly proportional to the difference of the boiler inlet and outlet temperature as well as the in-boiler circulating flue gas mass flow. The increase of the steam cycle mass flow demonstrates the higher possible extractable thermal power with increasing recirculated fraction. The steam mass flow is linearly increasing with a recirculated fraction less than 60%, evaluated in the normal scale. However, even though the thermal power is increasing, after 60% of flue gas recirculation fraction, the steam mass flow reaches a plateau, as the temperature is too cold to heat up the steam cycle coolant in order to achieve the set design specifications. The optimum point should consider the highest extractable thermal power as well as the lowest temperature in order to reduce heat stresses in the combustion chamber, as discussed in Section 2.2. Thus, a feasible operating point should consider a recirculated fraction of 80–90%, very close to the one set in this thesis.

Figure 17 shows the sensitivity analysis of the district heating and balance of plant power production of the proposed system. This second sensitivity analysis shows that the power production of district heating and balance of plant is dependent on the steam mass flow rate, which is consecutively dependent from the recirculated fraction, as discussed in the previous

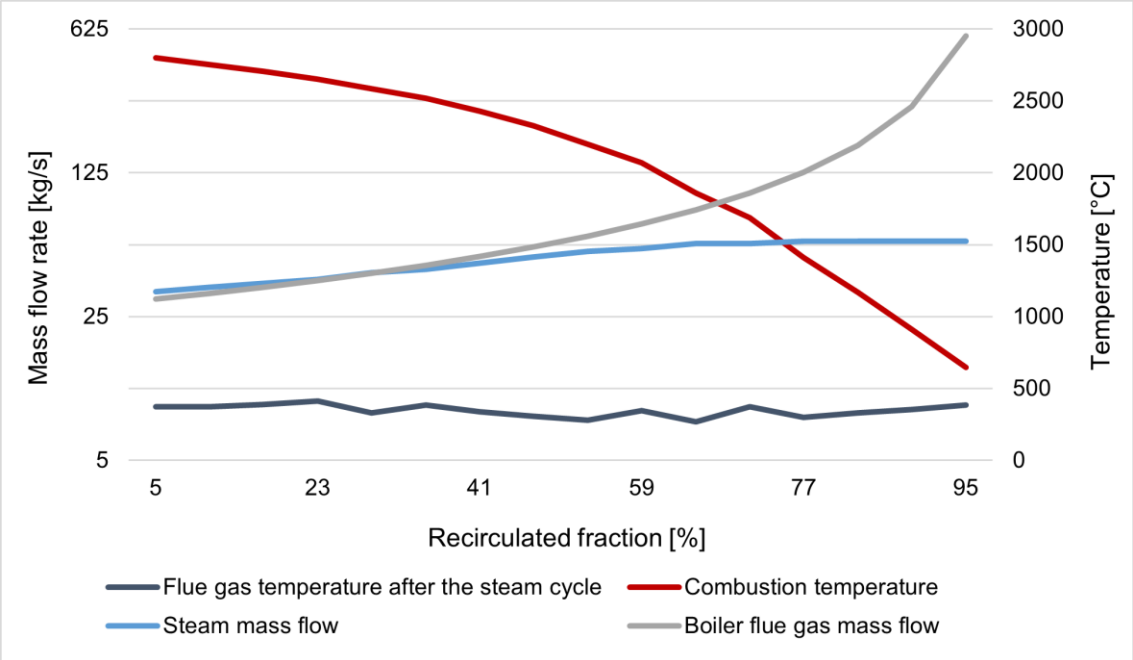

Figure 16: Sensitivity analysis of thermodynamic flue gas parameters dependent on the recirculated fraction.

sensitivity analysis. Since the highest steam mass flow rate was obtained with a nested sensitivity analysis for each split fraction, the behaviour of the steam mass flow rate is not smooth. However, the analysis reports two main behaviours. The first is quasi-linear with respect to a recirculated flue gas fraction from 5% to 60%. The remaining fraction results in a plateau of steam mass flow rate, which consequently affects the power production. The plateau is obtained because of the superposition of the increasing flue gas mass flow through the boiler and of the decreasing temperature with respect to the recirculation fraction increment. These two behaviours determine the maximum extractable thermal power to the steam cycle. Even though, the in-boiler flue gas mass flow increases, the temperature of the flue gas is too low in order to fulfil the design specification requirements, such as the temperature of the superheated steam after the boiler and the bleeding heaters. In this analysis district heating refers to the total thermal power for district heating, which comprises the extraction from the condenser and the flue gas dehydration. A low recirculation fraction produces a higher mass flow rate of flue gas to the flue gas treatment. Moreover, it reduces the maximum extractable thermal power to the steam cycle, which results in a lower power production from turbines as well as from the condenser. Nevertheless, this effect is slightly counterbalanced by a higher production of district heating in the dehydration system because of the higher mass flow rate of the non-recirculated flue gas. Besides, the higher flue gas mass flow rate to be treated demands for a higher power supply to the compressors, thus negatively affecting the net electrical output of the MSW OFC thermal power plant. Thus, the highest power production takes place between a recirculated fraction of 80% and 95%. The proposed MSW OFC model has a maximum thermal power for district heating of 193.8 MW and a balance of plant of 53.6 MW, which are very close to the results obtained from Vantaan Energia input parameters and some assumptions.

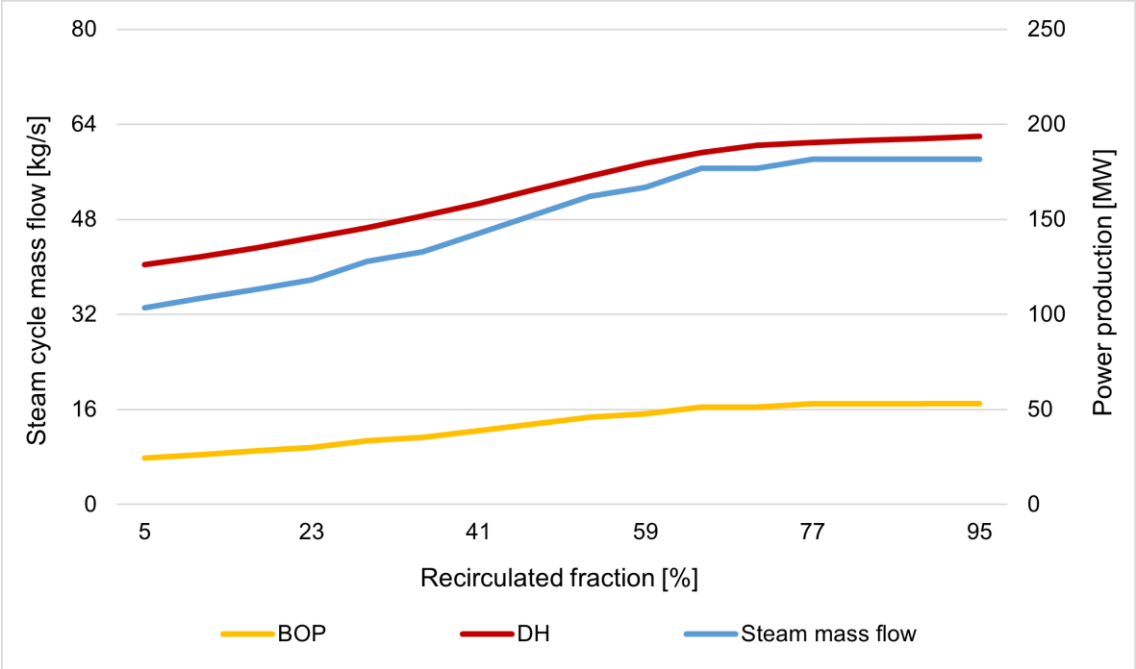

Figure 17: Sensitivity analysis of the power production dependent on the recirculated fraction.

A last sensitivity analysis investigates the production of the main compounds, such as hydrogen, carbon dioxide and condensed water as well as the purity of the carbon dioxide stream by varying the flue gas recirculation fraction. Since the oxygen demanded is proportional the fuel input, which is constant in this analysis, the electrolysis has the same working point. Therefore, the electrolysis does not produce more or less hydrogen. An increase in the recirculated fraction decreases the flue gas to the dehydration system. Nevertheless, the condense water mass flow rate experiences a slight increase. The phenomenon could be caused by the higher concentrated water content in the flue gas, as the condensation process is identified in the partial pressure of the gas with respect to the dew point. The oxygen concentration in the flue gas is lower at higher recirculated fraction, which supports the previous claim. The higher recirculation fractions produce carbon dioxide with a purity higher than 90mol%. Because of the impossibility to fulfil thermal exchange from the boiler to the steam cycle, carbon dioxide purity and condensed water experience a plateau similar to the previous analyses. A higher flue gas recirculated fraction than 77% achieves an almost pure carbon dioxide stream.

Thus, supported by the previous analyses, the optimum point of recirculated fraction is between 80% and 90%. In this interval all analysed parameters are almost constant by varying the recirculated fraction. The previous section reported that the OFC system has to discharge some of the carbon dioxide in order to fulfil the chemical ratio reactants requirement for power-to-methanol. This means that the recirculated fraction might be slightly increased, thus producing less carbon dioxide. However, any decrease of carbon dioxide would not be enough to achieve the wanted ratio. In addition, a recirculated split fraction close to 90% results in a lower mass flow of the flue gas through boiler, which requires larger piping as well as exchangers, increasing the cost of the retrofitting. Moreover, 80% of split fraction results in temperatures that are lower with respect to the reference model and close to the real case, thus meaning the same mechanical and thermal stress as for the original furnace.

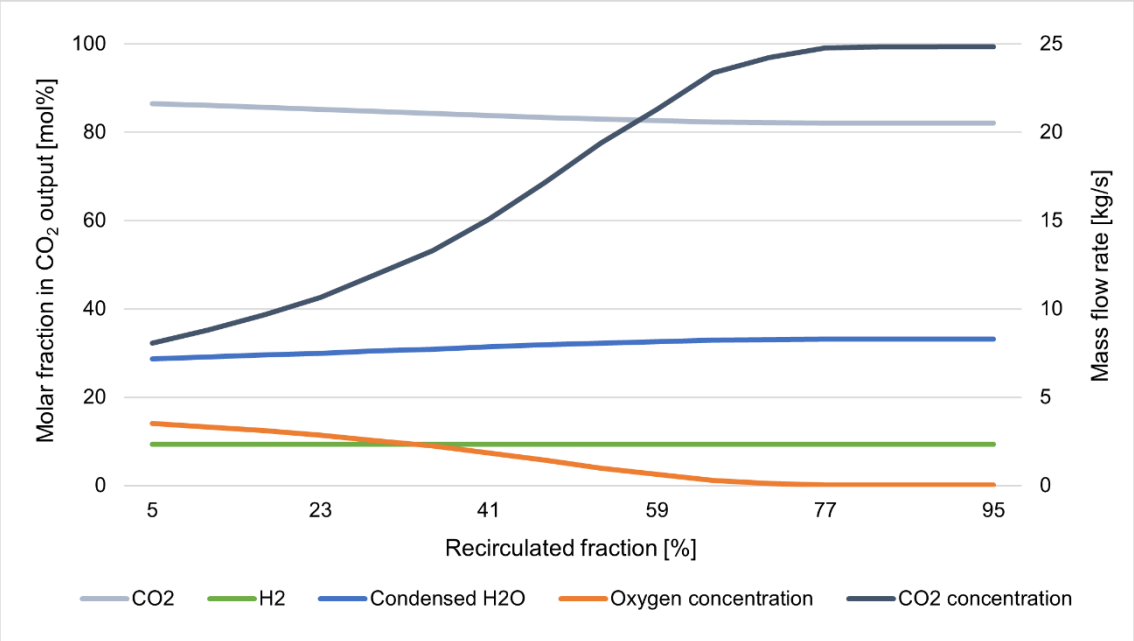

Figure 18: Sensitivity analysis of the main MSW OFC products dependent on the recirculated fraction.

Thus, a recirculated split fraction close but not less than 80% consists in a suitable option for the oxy-fuel combustion strategy.

4.4 LCOH analysis

The MSW OFC simulation produces 4 main products: district heating power, carbon dioxide, calcium sulphate and hydrogen. Other products from the combustion, such as water and oxygen are not considered in pricing analysis because they are directly exploited within the system. The revenue about the MSW OFC simulation products is summed in Table 19. The products pricing is evaluated in order to obtain a break-even hydrogen price. Thus, the actual expenditures of the system subtracted by the valuable sellable resources will determine the final cost of hydrogen. The LCOH cost analysis procedure is shown in Figure 19.

District heating thermal power is an increasing valuable resource, which in Finland is estimated to have an weighted average price of 80.85 EUR/MWh [13]. The reference real case is already providing district heating thermal power with a similar production. Therefore, no big improvement about district heating capacity is needed, which results in a lower retrofitting capital cost.

As discussed in Section 2.5, carbon dioxide can refer to allowing price market at 25 EUR/t, as any carbon dioxide market has been set yet. This means that this by-product can result in a revenue.

Calcium sulphate is obtained by the dry flue gas desulphurisation. This flue gas treatment unit is already present in the real case, which does not result in higher capital cost for retrofitting a pre-existent thermal power plant. Calcium sulphate has an industrial price of 5 EUR/kg, which is easily industrially sellable [49].

The system has an assumed life of the plant of 40 years and an availability factor of 0.9. This means that the production of these valuable commodities refers to 7884 h out of 8760 h every year. Instead, the capital cost and operating management cost is calculated for the whole year during the life of the plant.

The break-even cost of hydrogen is dependent on the expenditures of the MSW OFC system, such as CAPEX, OPEX, wind park, CaO and $Ca(OH)_2$. The cost for each quantity is summed up in Table 20. Firstly, this break-even levelized cost of hydrogen (LCOH) analysis will be calculated with wind park electrical energy supply. Then, LCOH will be calculated with other electrical energy sources, such as the national grid.

Table 19: Revenues MSW OFC products.

	Selling price	**Production**
District heating	80 EUR/MWh	191.1 MW
Carbon dioxide	25 EUR/t	20.5 kg/s
Calcium sulphate	5 EUR/kg	310.0 kg/h
Hydrogen	to be determined	2.34 kg/s

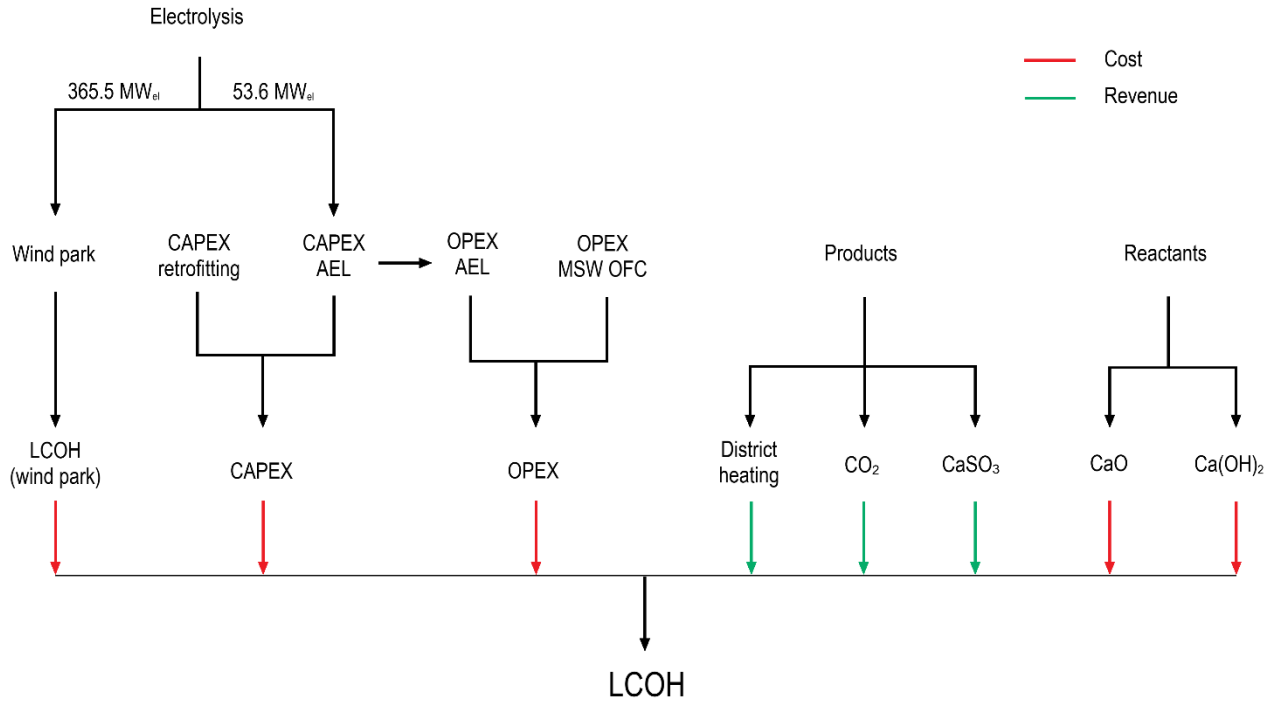

Figure 19: LCOH cost analysis scheme.

The capital cost refers to the purchase of the new equipment as well as the retrofitting of the real MSW power plant. As the analysis consists in retrofitting a pre-existent thermal power plant, the new components belong to the dehydration system and to the electrolyser. As discussed in Section 3.3, the dehydration system is composed of three compressors, five heat exchangers and five flash extraction units. The cost of these components is calculated inside Aspen Plus environment owing to Aspen Process Economic Analyzer, which provides an overall new equipment of cost of $29.2 \cdot 10^6$ EUR. In this thesis, the produced electricity from the steam cycle is fed to the electrolyser, which is proving a power of 53.6 MW_{el}. In the cost analysis it is useful to split the two different feeding electrolysis sources of electrical power: from the steam cycle and the wind park. As reported in Section 2.4, electrolysis cell has a CAPEX around 700 EUR/kW, which results in capital cost of $37.5 \cdot 10^6$ EUR only for the 53.6 MW_{el} fraction from the steam cycle. Regarding to the remaining 365.5 MW_{el}, the CAPEX of the electrolyser is included directly in the wind park expenditure, thus not affecting the CAPEX cost. The total CAPEX for Vantaan Energia real case retrofitting consists in $66.7 \cdot 10^6$ EUR.

The OPEX refers to the operating and management expenditures with respect to the whole system, which is calculated owing to Aspen Process Economic Analyzer. The MSW OFC thermal power plant has an OPEX of $6.80 \cdot 10^6$ EUR/y. Moreover, the electrolyser has an OPEX equal to 3% of the AEL CAPEX in EUR/y [60]. The electrolyser OPEX is calculated by considering only the fraction of the electrolyser, which receives electrical power supply from the MSW OFC. The remaining OPEX, similar to the AEL CAPEX, is included in the wind park cost.

The break-down cost of the wind park refers to the break-even cost of hydrogen for a system, which comprises a wind park and an electrolysis system. Therefore, the CAPEX and

Table 20: Main expenditures of MSW OFC system.

	Expenditures	Demand
CAPEX	66.7 10^6 EUR	-
OPEX	8.09 10^6 EUR/y	-
Wind park	60.4 EUR/MWh	365.5 MW_{el}
CaO	100 EUR/t	2686 t/y
$Ca(OH)_2$	500 EUR/t	1855 t/y

OPEX of an electrolyser, whose nominal power is 365.5 MW, is not included in the overall retrofitting CAPEX and OPEX expenditures. As presented in Section 2.5, the break-even cost of hydrogen, produced by wind park and electrolysis, consists in 3.05 EUR/kg. With some calculations the break-even cost of hydrogen from a wind park is converted into the energy specific cost of this sub-system, i.e. 60.4 EUR/MWh by referring to the energy of the electrolysis demand. Therefore, the cost of the required wind park and the electrolysis, whose size refers only to 365.5 MW, is not considered, as in the cost analysis it is sufficient to obtain the cost of hydrogen production from an electrical power supply of 365.5 MW. The MSW OFC plant produces hydrogen in parallel with the base load thermal power plant, i.e. 7884 h out of 8760 h every year.

The desulphurisation unit exploits calcium oxide and calcium hydroxide, as presented in Section 3.2. In order to accomplish this process, Vantaan Energia thermal power plant requires 2686 t/y of CaO as well as 1855 t/y of $Ca(OH)_2$ [90]. These two compounds have an average market price of 100 EUR/t and 500 EUR/t, respectively for CaO and $Ca(OH)_2$ [2].

The sum of all positive and negative contribution in the MSW OFC system results in a break-even LCOH of 0.851 EUR/kg, as illustrated in Figure 20. The break-down LCOH shows that the highest cost for the MSW OFC consists in the implementation of the wind park together with the electrolyser, which is almost less than 2.91 EUR/kg. Nevertheless, district heating power production revenue results in halving the cost of the wind park. The CAPEX retrofitting cost is negligible with respect to wind park and district heating contributions. Calcium oxide and calcium hydroxide reactants have the same weigh of the CAPEX with respect to the final break-even cost of hydrogen. Carbon dioxide and calcium sulphite counterbalance the other small negligible cost.

The calculated LCOH refers to the retrofitting of a pre-existent waste-to-energy thermal power plant. Table 21 presents LCOH results affected by some changes on the proposed MSW OFC coupled with wind park system. For instance, the LCOH is not consistently affected by considering a new-build for the same typology and size of the reference case. A new-build thermal power plant with 53.6 MW has a CAPEX of 174.1 $\cdot 10^6$ EUR by taking as reference a biogas thermal power plant of 50 MW, which has a specific CAPEX cost of 3482 EUR/kW [88]. By summing the retrofitting previously calculated CAPEX, the hydrogen production has a break-even cost of 0.916 EUR/kg.

The wind park possible solution is particularly convenient with respect to national grid as the electrolysis power source. Finland has an industrial electricity price of 70 EUR/MWh,

Figure 20: Levelized cost of hydrogen break-down.

which results in a LCOH of 1.31 EUR/kg [79]. The break-even cost of hydrogen in that case has a lower cost with respect to other hydrogen production technologies because of district heating selling.

As reported in Section 2.4 and 2.5, the AEL CAPEX is decreasing and ETS price is increasing. By 2035 it can be estimated that AEL could have a CAPEX of 350 EUR/kw [24] and ETS price of 100 EUR/t. Furthermore, the wind parks are becoming each year less expansive with break-even LCOE reduction from 90 EUR/MWh to 50 EUR/MWh [8]. Thus, the hydrogen cost will be consistently affected by decreasing the major expenditures and increasing the revenue about carbon dioxide. In this 2035 scenario the hydrogen would have a negative break-even LCOH of -1.11 EUR/kg. Thus, without selling any hydrogen, the system would still have a revenue.

The biggest advantage consists in the usage of MSW, which in Finland is free-tax fuel and zero-cost. The comparison between MSW and hard coal reports that hard would results in a higher LCOH by 0.886 EUR/kg, i.e. +104.4%. The hard coal calculation has a price of 30 EUR/MWh and it has to provide the same thermal power as the MSW in order to be comparable [79]. The hard-coal OFC would have a LCOH of 1.74 EUR/kg.

Table 22 reports the comparison between the cheapest LCOH for each available current technology, as was presented in Section 2.5 in Table 2, and the LCOH calculated in this thesis. With respect to other technologies, the MSW OFC has zero-cost fuel and produces district heating, which results in the cheapest technology to produce hydrogen. The LCOH with the production of district heating and the exploitation of MSW reduces on average the break-even price by 61.8%.

Table 21: LCOH comparison among different scenarios with respect to the reference MSW OFC result.

	LCOH [EUR/kg]
OFC reference retrofitted plant	0.851
New MSW OFC plant	0.916
Electrical national grid supply	1.31
2035-scenario	-1.11
Coal-run OFC retrofitted plant	1.74

Table 22: Comparison between resulting MSW OFC LCOH calculated in this thesis and the cheapest LCOH for each current hydrogen production technology.

	LCOH [EUR/kg]	Reference
MSW OFC (wind park)	0.851	Calculated in this thesis
Electrolysis (smart grid)	2	[33]
Electrolysis (mix renewables)	2.71	[71]
Steam methane reforming	1.8	[47]

As discussed in Section 4.2, the MSW OFC produces two streams: hydrogen and carbon dioxide, which have a molar ratio of 2.48 (H_2-CO_2). These products can be directly supplied to a power-to-methanol facility, as the required reactant molar ratio is 3. The MEOH plant is not economically feasible because of the high impact of hydrogen cost in the break-even analysis [69]. The main expenditures of the power-to-methane are summed up in Table 23. Since the hydrogen results in the highest cost for the MEOH plant and the MSW OFC has LCOH cheaper than current technologies, the exploitation of MSW OFC hydrogen reduces consistently the break-even cost of MEOH from 852.4 EUR/t (699.9 EUR/t with oxygen selling) to 221.1 EUR/t. Furthermore, this low MEOH price is supported by a zero-cost carbon dioxide supply, as the proposed OFC plant produces carbon dioxide as a by-product. Methanol has an average price of 410 EUR/t referring to July 2021 for the European market [63]. Therefore, the low-cost MSW OFC hydrogen results in the economic feasibility of a MEOH plant, as the break-even cost of MEOH is almost half the price of the current market.

4.5 Summary

This chapter has introduced the results of the simulation in Aspen Plus of the MSW OFC model and the comparison with the reference model as well as the real Vantaan Energia waste-to-energy thermal power plant. The MSW OFC proposed system does not produce enough electrical power to produce through AEL its demand for oxygen. The MSW OFC electrolysis requires an additional supply of 365.5 MW_{el}. One possible solution consists in combining the MSW OFC plant with a wind park, which should have a nominal installed

power of 1.1 GW_{el} in order to fulfil the oxygen yearly demand for the furnace. The retrofitted power plant produces a higher thermal power for district heating of 191.1 MW_{th} with respect to the real case. The OFC system has an overall efficiency of 26.21%. The flue dehydration system demands for 10% of the power produced in the steam cycle and it condenses a mass flow rate, which covers less than half of the electrolysis water demand. Furthermore, after the flue gas dehydration, carbon dioxide is produced as a by-product with a purity of 99.4mol% with a sulphur dioxide content of 786 ppmv. The hydrogen produced by the electrolysis has a mass flow rate of 2.34 kg/s, which can be used for power-to-methanol processes, as the molar ratio H_2-CO_2 is 2.48:1. The sensitivity analysis reports that the best flue gas recirculated fraction refers to 80–90% interval. The production of district heating results in the economic feasibility of the MSW OFC proposed system, which is counterbalanced by the higher cost of the wind park. The produced hydrogen has a LCOH of 0.851 EUR/kg. This low-cost hydrogen consecutively results in the feasibility of a methanol plant, which could exploit the carbon dioxide and the hydrogen produced in the MSW OFC plant. The produced MEOH has a break-even cost of 0.221 EUR/kg, half price of the current MEOH market.

Table 23: MEOH plant expenditures. Data obtained from [69].

	Expenditures	**Demand/supply**
CAPEX	$382 \cdot 10^6$ EUR	-
OPEX (no CO_2 and H_2 included)	$30 \cdot 10^6$ EUR/y	-
CO_2	25 EUR/t	6985 t/d
Original supply H_2	4100 EUR/t	960 t/d
MSW OFC supply H_2	832 EUR/t	960 t/d

5 Summary and conclusions

This thesis has proposed the design of a municipal solid waste oxy-fuel combustion (MSW OFC) thermal power plant. This non-conventional system promotes not only circular economy by exploiting municipal solid waste as energy recovery solution but also carbon neutrality, as oxy-fuel combustion produces no carbon dioxide emissions. The proposed design involves the usage of electrolysis in order to provide the required oxygen for oxy-fuel combustion. Thus, the OFC design would also produce hydrogen for replacing fossil fuels in the transport sector.

The MSW OFC thermal power plant was modelled using Aspen Plus simulation software. The oxy-fuel combustion model was retrofitted starting from the existing Vantaan Energia MSW thermal power plant. Firstly, the real Vantaan Energia case was modelled in order to compare and then validate its Aspen Plus simulation with respect to the real case. The oxy-fuel strategy involved an electrolysis unit and flue gas dehydration.

The oxy-fuel combustion simulation demonstrates that the MSW oxy-fuel system is not electrically auto-sustainable, as it requires additional electrical power of 365.5 MW_{el} compared to the net electrical power produced by the thermal power plant. One possible solution consists in combining the proposed oxy-fuel strategy together with a wind park in order to provide the remaining required electrical power. Nevertheless, the simulation produces a thermal power for district heating of 191.3 MW_{th}. The OFC system has an efficiency of 75.66% without considering the efficiency of the wind park. The low capacity factor of the wind park results in a decrease of the overall efficiency of the OFC system to 25.61%. The sensitivity analysis shows that the recirculated fraction of the flue gas to the furnace could be further decreased to 80% fraction without affecting the district heating and electrical power production as well as carbon dioxide output mass flow. The valuable production of thermal power for district heating purpose affects consistently the break-even price of the generated hydrogen, thus resulting in an hydrogen price of 0.851 EUR/kg. The low price of hydrogen is favoured by the combustion of MSW, as in Finland it refers to zero-cost free-taxation fuel. Furthermore, the oxy-fuel model produces carbon dioxide with a purity of 99.94mol%, which can be used in P2X purposes. The simulation reports a stoichiometric ratio H_2-CO_2 of 2.48:1. One suitable P2X process could be power-to-methanol, as this technology has a stoichiometric ratio between hydrogen and carbon dioxide of 3:1. The cheaper cost of hydrogen results in the economic feasibility of a MEOH plant by reducing its break-even cost, thus obtaining a MEOH production with half selling price compared to the current market. The remaining carbon dioxide can be sold for other purposes.

The proposed MSW OFC system produces no electrical output. Moreover, it requires a consistent demand for electrical power, which could lead to a severe unbalance of the national electrical grid. In the proposed design, retrofitting the existing thermal power plant would not involve the current gas turbine of the Vantaa power plant, which would result in a loss of revenue by eliminating it from the system. Nevertheless, the current turbine gas could still be used to produce electrical power and hot flue gas, thus providing more thermal power to the steam cycle.

One limitation of the Aspen Plus software is that the model is calculated by considering 0^{th} dimensional balance on system components in steady state. This prevents any calculation or regulation of transients, which is essential for the system, as MSW is a highly aleatory calorific fuel.

The model proposed in this thesis consists of retrofitting a MSW OFC thermal power plant with hydrogen production. However, the model does not comprise any P2X facilities, which could be directly coupled with the proposed system. Thus, in the future, the Aspen Plus model could include a power-to-methanol facility, and the electrolyser-wind park electrical power coupling could be further optimized. This would enable the demand for electrical power by the electrolysis unit to follow energy market fluctuations by purchasing electrical power directly from the grid during intra-day low-price intervals. Contrarily, the wind park could sell its production to the national grid during high-price intervals. This market strategy should reduce even more the LCOH, thus increasing the revenue of the MSW OFC concept.

References

[1] O. Y. Abdelaziz., W. M. Hosny, M. A. Gadalla, F. H. Ashour, I. A. Ashour, C. P. Hulteberga, “Novel process technologies for conversion of carbon dioxide from industrial flue gas streams into methanol”, J. of CO_2 Utilization, vol. 21, pp. 52–63, Oct. 2017, doi: 10.1016/j.jcou.2017.06.018

[2] Alibaba, alibaba.com https://www.alibaba.com/countrysearch/CN/industrial-calcium-oxide.html (accessed Jul. 1 2021)

[3] Aspen Plus. (V11). Aspen One.

[4] I. Boumanchar, Y. Chhiti, F. Ezzahrae M'hamdi Alaoui, M. Elkhouakhi, A. Sahibeddine, F. Bentiss, C. Jama, M. Bensitel, “Investigation of (co)-combustion kinetics of biomass, coal and municipal solid wastes”, Waste Manage., vol. 97, pp. 10–18, Sep. 2019, doi: 10.1016/j.wasman.2019.07.033

[5] J. Brauns, T. Turek, “Alkaline Water Electrolysis Powered by Renewable Energy: A Review”, Processes 2020, vol. 8(2), n. 248, Feb. 2020, doi: 10.3390/pr8020248

[6] Power plant operating method, involves expanding combustion exhaust gas from afterburner, and discharging oxygen removed from combustion exhaust gas from pre-burner by sweep gas that is inert gas, by D. Dr. Brücker, (2014, Apr. 6), DE102005042176A1. [Online]. Available: https://patents.google.com/patent/DE102005042176A1/en

[7] A. Buttler, H. Spliethoff, “Current status of water electrolysis for energy storage, grid balancing and sector coupling via power-to-gas and power to liquids: A review”, Renewable and Sustainable Energy Rev., vol. 82, no. 3, pp. 2440–2454, Feb.2018. [Online]. Available: https://www.sciencedirect.com/science/article/abs/pii/S136403211731242X

[8] G. Calado, R. Catro, “Hydrogen Production from Offshore Wind Parks: Current Situation and Future Perspectives”, Appl. Sci., 11, 5561, Jun. 2021, doi: 10.3390/app11125561

[9] D. Campbell-Lendrum, A. Pruss-Ustun, “Climate change, air pollution and noncommunicable diseases”, who.int https://www.who.int/bulletin/volumes/97/2/18-224295/en/

[10] L. Chen, Y. Liao, X. Ma, S. Lu , “Heavy metals chemical speciation and environmental risk of bottom slag during co-combustion of municipal solid waste and sewage sludge”, J. of Cleaner Prod., vol. 262, 121318, Jul. 2020, doi: 10.1016/j.jclepro.2020.121318

[11] P. Costamagna, “Three-pipeline gas grid: A new concept for power-to-gas associated with complete carbon capture and utilization”, Energy Conv. and Manage., vol. 229, n. 113739, Feb. 2021, doi: 10.1016/j.enconman.2020.113739

[12] G. Ding, B. He, Y. Cao, C. Wang, L. Su, Z. Duang, J. Song, W. Tong, X. Li, “Process simulation and optimization of municipal solid waste fired power plant with oxygen/carbon dioxide combustion for near zero carbon dioxide emission”, Energy Convers. and Manage., vol. 157, pp. 157–168, Feb. 2018. [Online] Available: https://www.sciencedirect.com/science/article/abs/pii/S0196890417311482

[13] Energiateollisuus, “District heating in Finland 2019”, Finnish Energy, FI, Rep. ISSN 0786-4809, 2020. Accessed: Jun. 29, 2021. [Online]. Available: https://energia.fi/en/newsroom/publications/district_heating_statistics.html#material-view
[14] European Commission, “A European Green Deal”, ec.europa.eu https://ec.europa.eu/info/strategy/priorities-2019-2024/european-green-deal_en (accessed Mar. 21 2021)
[15] European Commission, “A hydrogen strategy for a climate-neutral Europe”, Brussels, Belgium, COM(2020) 301 final, Jul. 8 2020. [Online]. Available: https://www.google.com/url?sa=t&rct=j&q=&esrc=s&source=web&cd=&cad=rja&uact=8&ved=2ahUKEwih0ODQipfwAhV0AxAIHYsHAWYQFnoECAMQAA&url=https%3A%2F%2Fec.europa.eu%2Fenergy%2Fsites%2Fener%2Ffiles%2Fhydrogen_strategy.pdf&usg=AOvVaw2iwcGeqPYL2Pv0qpM26cdq
[16] European Commission, “EU ETS Handbook”, 2015. [Online]. Available: https://www.google.com/url?sa=t&rct=j&q=&esrc=s&source=web&cd=&cad=rja&uact=8&ved=2ahUKEwiU9PWZn8zxAhVx-yoKHekoDEsQFnoECAQQAA&url=https%3A%2F%2Fec.europa.eu%2Fclima%2Fsites%2Fclima%2Ffiles%2Fdocs%2Fets_handbook_en.pdf&usg=AOvVaw2O_RFMs1aQhFbopRDpG6cX
[17] European Commission, “EU Emissions Trading System (EU ETS)”, ec.europa.eu. https://ec.europa.eu/clima/policies/ets_en (accessed Apr. 26 2021)
[18] European Commission, “Paris Agreement”, ec.europa.eu. https://ec.europa.eu/clima/policies/international/negotiations/paris_en (accessed Mar. 21 2021)
[19] European Commission, “2050 long-term strategy”, ec.europa.eu https://ec.europa.eu/clima/policies/strategies/2050_en (accessed Mar. 21 2021)
[20] European Environmental Agency, “Managing municipal solid waste – a review of achievements in 32 European countries”, Publications Office of the European Union, Luxembourg, 2013, [Online]. Available: https://www.eea.europa.eu/publications/managing-municipal-solid-waste
[21] European Parliament and of the council. (24 Nov. 2010). Directive 2010/75/EU on industrial emissions (integrated pollution prevention and control). [Online]. Available: https://eur-lex.europa.eu/legal-content/EN/TXT/?uri=CELEX%3A02010L0075-20110106
[22] Eurostat, “Municipal waste statistics”, ec.europa.eu/eurostat. https://ec.europa.eu/eurostat/statistics-explained/index.php/Municipal_waste_statistics#Municipal_waste_generation (accessed Mar. 1 2021)
[23] Eurostat, “Treatment of waste by waste category, hazardousness and waste management operations”, ec.europa.eu/eurostat. https://ec.europa.eu/eurostat/databrowser/view/env_wastrt/default/table?lang=en (accessed Mar. 1 2021)
[24] D. Ferrero, M. Gamba, A. Lanzini, M. Santarelli, “Power-to-Gas Hydrogen: Techno-economic Assessment of Processes towards a Multi-purpose Energy Carrier”, Energy Procedia, vol. 101, pp. 50–57, Nov. 2016, doi: 10.1016/j.egypro.2016.11.007
[25] Finnish Energy, “Almost 15,000 km of district heating networks”, energia.fi https://energia.fi/en/energy_sector_in_finland/energy_networks/district_heating_networks (accessed Jun. 10 2021)

[26] Finnish Energy, “District heating in Finland 2018”,Helsinki, FI, ISSN 0786-4809, 2019. [Online]. Available: https://www.google.com/url?sa=t&rct=j&q=&esrc=s&source=web&cd=&cad=rja&uact=8&ved=2ahUKEwiU8pHArpTxAhXV_ioKHeZqCd0QFjACegQIAxAD&url=https%3A%2F%2Fenergia.fi%2Ffiles%2F4092%2FDistrict_heating_in_Finland_2018.pdf&usg=AOvVaw0yQoEGoTVkSnj5E5OJmsCZ
[27] Finnish Government, “Finland has an excellent opportunity to rebuild itself in line with the principles of sustainable development”, valtioneuvosto.fi. https://valtioneuvosto.fi/en/marin/government-programme/carbon-neutral-finland-that-protects-biodiversity
[28] Energy supply system and operating procedures, by V. Dipl.-Ing. Frick, B. Hahn, M. Dr. Specht, M. Dipl.-Ing. M.Sc. Sterner, B. Dipl.-Ing. Stürmer (FH), (2010, Oct. 14), DE102009018126A1. [Online]. Available: https://patents.google.com/patent/DE102009018126A1/en
[29] Z.Fu, S. Zhang, X. Li, J. Shao, K. Wang, H. Chen, “MSW oxy-enriched incineration technology applied in China: Combustion temperature, flue gas loss and economic considerations”, Waste Manage., vol. 38, pp. 149–156, Apr. 2015, doi: 10.1016/j.wasman.2014.12.026
[30] C. Gaber, C. Schluckner, P. Wachter, M. Demuth, C. Hochenauer, “Experimental study on the influence of the nitrogen concentration in the oxidizer on NO_x and CO emissions during the oxy-fuel combustion of natural gas”, Energy, vol. 214, 118905, Jan. 2021, doi: 10.1016/j.energy.2020.118905
[31] V. Giaretto, *Lezioni di termodinamica applicata e trasmissione del calore*, 2nd ed. Turin, Italy: C.L.U.T, 2017.
[32] D. O. Glushkov, K. K. Paushkina, D. P. Shabardin, “Co-combustion of coal processing waste, oil refining waste and municipal solid waste: Mechanism, characteristics, emissions”, Chemosphere, vol. 240, 124892, Feb. 2020, doi: 10.1016/j.chemosphere.2019.124892
[33] F. Grüger, O.Hoch, J.Hartmann, M.Robinius, D.Stolten, “Optimized electrolyzer operation: Employing forecasts of wind energy availability, hydrogen demand, and electricity prices”, Int. J. of Hydrogen Energy, vol. 44, n. 9, pp. 4387–4397, Feb. 2019, doi: 10.1016/j.ijhydene.2018.07.165
[34] Oxyfuel boiler and a method of controlling the same, by Y. Hayashi, A. Yamada, T. Shibata, (2013, Apr. 9), US8413596B2. [Online]. Available: https://patents.google.com/patent/US8413596B2/en
[35] Operating steam plant for producing electrical energy by combustion process, comprises operating electrolysis unit to provide hydrogen and oxygen, and operating methanation unit under consumption of hydrogen and carbon dioxide, by O. Hein, H, Kliemke, D. Razowski, A. Waruschewski, (2013, Oct. 24), DE 10 2012 214 907 A1. [Online]. Available: https://patents.google.com/patent/DE102012214907A1/en
[36] Steam power plant for generating electrical energy according to the oxyfuel process, by O. Hein, H. Kliemke, D. Razowski, A. Waruschewski, (2015, Mar. 21), DE102012214907B4. [Online]. Available: https://patents.google.com/patent/DE102012214907B4/en
[37] Helsinki Region Environmental Services Authority, “”, HSY, Finland, 2019. [Online]. Available: https://julkaisu.hsy.fi/paakaupunkiseudun-sekajatteen-koostumus-2018.pdf

[38] S. C. Hill, L. Douglas Smoot, “Modelling of nitrogen oxides formation and destruction in combustion systems”, Progress in Energy and Combustion Sci., vol. 26, no. 4–6, pp. 417–458, Aug. 2000, doi: 10.1016/S0360-1285(00)00011-3
[39] J. Horák, L. Kuboňová, S. Bajer, M. Dej, F. Hopan, K. Krpec, T. Ochodek, “Composition of ashes from the combustion of solid fuels and municipal waste in households”, J. of Environmental Manage., vol. 248, 109269, Oct. 2019, doi: 10.1016/j.jenvman.2019.109269
[40] M.Hupponen, K.Grönman, M.Horttanainen, “How should greenhouse gas emissions be taken into account in the decision making of municipal solid waste management procurements? A case study of the South Karelia region, Finland”, Waste Manage., vol. 42, pp. 196–207, Aug. 2015, doi: 10.1016/j.wasman.2015.03.040
[41] International Energy Agency, “Data and statistics”, iea.org. https://www.iea.org/data-and-statistics?country=WORLD&fuel=Energy%20supply&indicator=TPESbySource (accessed Feb. 27 2021)
[42] International Energy Agency, “Data and statistics”, iea.org. https://www.iea.org/data-and-statistics?country=FINLAND&fuel=Electricity%20and%20heat&indicator=ElecGenByFuel (accessed Apr. 10 2021)
[43] International Energy Agency, “The future of Hydrogen”, iea.org. https://www.iea.org/reports/the-future-of-hydrogen (accessed Apr. 24 2021)
[44] N. Kezibri, C. Bouallou, “Conceptual design and modelling of an industrial scale power to gas-oxy-combustion power plant”, Int. J. of Hydrogen Energy, vol. 42 , no. 30, pp. 19411–19419, Jul. 2017. [Online]. Available: https://www.sciencedirect.com/science/article/abs/pii/S0360319917320414?via%3Dihub
[45] N. Khallaghi, D. P. Hanak, V. Manovic, “Techno-economic evaluation of near-zero CO2 emission gas-fired power generation technologies: A review”, J. of Natural Gas Sci. and Eng., vol. 74, n. 103095, Feb. 2020, doi: 10.1016/j.jngse.2019.103095
[46] Method and fuel generation assembly for the carbon dioxide-neutral compensation of energy peaks and troughs in the generation of electrical energy and/or for producing a fuel containing hydrocarbons, by K. Knop, L. Zoellner, (2012, Mar. 7), EP2426236A1. [Online]. Available: https://patents.google.com/patent/EP2426236A1/en
[47] J. Koponen, “Review of water electrolysis technologies and design of renewable hydrogen production systems”, M.S. thesis, Dept. Elect. Eng., Lappeenranta Univ. of Technol., Lappeenranta, Finland, 2015.
[48] Procedure for the production of electricity, heat and hydrogen and/or methanol, comprises coupling an oxyfuel-steam power plant with a modular high temperature reactor power plant, by B. Krieg, (2008, Dec. 11), DE102007026570A1. [Online]. Available: https://patents.google.com/patent/DE102007026570A1/en
[49] Laboratoriumdiscounter, “Calcium sulfate dihydrate”, laboratoriumdiscounter.nl. https://www.laboratoriumdiscounter.nl/en/calcium-sulfate-dihydrate-food-grade-e516.html?gclid=EAIaIQobChMIw-HK9-S88QIV5EeRBR3yVQ3uEAYYASABEgJ2f_D_BwE (Accessed Jul. 1 2021)
[50] C. Lamy, P. Millet, “A critical review on the definitions used to calculate the energy efficiency coefficients of water electrolysis cells working under near ambient temperature conditions”, J. of Power Sources, vol. 447, n. 227350, Jan. 2020, doi: 10.1016/j.jpowsour.2019.227350

[51] J. Laurikko, J. Ihonen, J. Kiviaho, O. Himanen, R. Weiss, V. Saarinen, J. Kärki, M. Hurskainen, “National hydrogen roadmap for Finland”, Business Finland, Nov. 2020. [Online]. Available: https://www.businessfinland.fi/4abb35/globalassets/finnish-customers/02-build-your-network/bioeconomy--cleantech/alykas-energia/bf_national_hydrogen_roadmap_2020.pdf
[52] B. Leckner, F. Lind, “Combustion of municipal solid waste in fluidized bed or on grate – A comparison”, Waste Manage., vol. 109, pp. 94–108, May 2020, doi: 10.1016/j.wasman.2020.04.050
[53] D. Li, C. Gao, T. Chen, X. Guo, S. Han, “Planning strategies of power-to-gas based on cooperative game and symbiosis cooperation”, App. Energy, vol. 288, n. 116639, Apr. 2021, doi: 10.1016/j.apenergy.2021.116639
[54] Z. Li, H. Zhang, H. Xu, J. Xuan, “Advancing the multiscale understanding on solid oxide electrolysis cells via modelling approaches: A review”, Renewable and Sustain. Energy Reviews, n. 110863, vol. 141, May 2021, doi: 10.1016/j.rser.2021.110863
[55] C. Liu, S. Shih, T. Huang, “Effect of SO2 on the Reaction of Calcium Hydroxide with CO2 at Low Temperatures”, Ind. Eng. Chem. Res., vol. 49, n. 19, pp. 9052–9057, Aug 2010, doi: 10.1021/ie100924z
[56] X. Liu, T. Asim, G. Zhu, R. Mishra, “Theoretical and experimental investigations on the combustion characteristics of three components mixed municipal solid waste”, Fuel, vol. 267, 117183, May 2020, doi: 10.1016/j.fuel.2020.117183
[57] E. J. Lopes, N. Queiroz, C. Itsuo Yamamoto, P. Ramos da Costa Neto, “Evaluating the emissions from the gasification processing of municipal solid waste followed by combustion”, Waste Manage., vol. 73, pp. 504–510, Mar. 2018, doi: 10.1016/j.wasman.2017.12.019
[58] D. Kim, W. Yang, K. Y. Huh, Y. Lee, “Demonstration of 0.1 MWth pilot-scale pressurized oxy-fuel combustion for unpurified natural gas without CO2 dilution”, Energy, vol. 223, 120021, May 2021, doi: 10.1016/j.energy.2021.120021
[59] C. Ma, B. Li, D. Chen, T. Wenga, W. Ma, F. Lin, G. Chen “An investigation of an oxygen-enriched combustion of municipal solid waste on flue gas emission and combustion performance at a 8 MWth waste-to-energy plant”, Waste Manage., vol. 96, pp. 47–56, Aug. 2019, doi: 10.1016/j.wasman.2019.07.017
[60] G. Matute, J. M. Yusta, L. C. Correas, “Techno-economic modelling of water electrolysers in the range of several MW to provide grid services while generating hydrogen for different applications: A case study in Spain applied to mobility with FCEVs”, Int. J. of Hydrogen Energy, vol. 44, n. 33, pp. 17431–17442, Jul. 2019,doi: 10.1016/j.ijhydene.2019.05.092
[61] Process to convert and store geothermal energy and/or regenerative energy e.g. hydroelectricity by conversion into chemical energy, by G. Mayer (2006, Jan. 19), DE 10 2004030717A1. [Online]. Available: https://patents.google.com/patent/DE102004030717A1/en
[62] A. Mayyas, M. Wei, G. Levis, “Hydrogen as a long-term, large-scale energy storage solution when coupled with renewable energy sources or grids with dynamic electricity pricing schemes”, Int. J. of Hydrogen Energy, vol. 45, n. 33, pp. 16311–16325, Jun. 2020, doi: 10.1016/j.ijhydene.2020.04.163
[63] Methanex, “Methanex posts regional contract methanol prices for North America, Europe and Asia”, methanex.com https://www.methanex.com/our-business/pricing (accessed Jul. 1 2021)

[64] M. Minutillo, A. Perna, A. Forcina, S. Di Micco, E. Jannelli, “Analyzing the levelized cost of hydrogen in refueling stations with on-site hydrogen production via water electrolysis in the Italian scenario”, Int. J. of Hydrogen Energy, vol. 46, n. 26, pp. 13667–13677, Apr. 2021, doi: 10.1016/j.ijhydene.2020.11.110
[65] P. Moçoteguy, A. Brisse, “A review and comprehensive analysis of degradation mechanisms of solid oxide electrolysis cells”, Int. J. of Hydrogen Energy, pp. 15887–15902, n. 36, vol. 38, Dec. 2013, doi: 10.1016/j.ijhydene.2013.09.045
[66] M. Momeni, M. Soltani, M. Hosseinpour, J. Nathwani, “A comprehensive analysis of a power-to-gas energy storage unit utilizing captured carbon dioxide as a raw material in a large-scale power plant”, Energy Convers. and Manage., vol. 227, n. 113613, Jan. 2021, doi: 10.1016/j.enconman.2020.113613
[67] L. E. Monroy Sarmiento, K. A. Clavier, T. G. Townsend, “Trace element release from combustion ash co-disposed with municipal solid waste”, Chemosphere, vol. 252, 126436, Aug. 2020, doi: 10.1016/j.chemosphere.2020.126436
[68] M. Nasrullah, “Material and energy balance of solid recovered fuel production”, Ph.D. dissertation, Dep. of Biotechnology and Chem. Technol., Aalto Univ., Espoo, Finland, 2015.
[69] J. Nyári, M. Magdeldin, M. Larmi, M. Järvinen, A. Santasalo-Aarnio, “Techno-economic barriers of an industrial-scale methanol CCU-plant”, J. of CO_2 Utilization, vol. 39, n. 101166, Jul. 2020, doi: 10.1016/j.jcou.2020.101166
[70] M. Paloneva, S. Takamäki, “Summary of sector-specific low carbon roadmaps”, Ministry of Economic Affairs and Employment 2021:9, Helsinki, Finland, Feb. 2021. [Online]. Available: https://julkaisut.valtioneuvosto.fi/handle/10024/162851
[71] G. Pan, W. Gu, H. Qiu, Y. Lu, S. Zhou, Z. Wu, “Bi-level mixed-integer planning for electricity-hydrogen integrated energy system considering levelized cost of hydrogen”, Appl. Energy, vol. 270, n. 115176, Jul. 2020, doi: 10.1016/j.apenergy.2020.115176
[72] N. Pedroni. (2019). Impatto ambientale nei sistemi energetici. [PowerPoint slides].
[73] E. Portillo, B. Alonso-Fariñas, F. Vega, M. Cano, B. Navarrete, “Alternatives for oxygen-selective membrane systems and their integration into the oxy-fuel combustion process: A review”, Separation and Purification Technol., vol. 229, 115708, Dec. 2019, doi: 10.1016/j.seppur.2019.115708
[74] Pöyry, “Vantaan Energy Finland Waste-to-energy”. [Online]. Available: https://www.poyry.com/sites/default/files/media/related_material/poyry_Vantaan_energy_technical_leaflet_2.pdf
[75] A. Ríos, A. J. Picazo-Tadeo, “Measuring environmental performance in the treatment of municipal solid waste: The case of the European Union-28”, Ecological Indicators, vol. 123, 107328, Apr. 2021, doi: 10.1016/j.ecolind.2020.107328
[76] M. Sánchez, E. Amores, D. Abad, L. Rodríguez, C. Clemente-Jul, “Aspen Plus model of an alkaline electrolysis system for hydrogen production”, Int. J. of Hydrogen Energy, vol. 45, n. 7, pp. 3916–3929, Feb. 2020, doi: 10.1016/j.ijhydene.2019.12.027
[77] G. Scheffknecht, L. Al-Makhadmeh, U. Schnell, J. Maier, “Oxy-fuel coal combustion - A review of the current state-of-the-art”, Int. J. of Greenhouse Gas Control, vol. 5, supp. 1, pp. 16–35, Jul. 2011, doi: 10.1016/j.ijggc.2011.05.020
[78] S. Shih, C. Ho, Y. Song, J. Lin, “Kinetics of the Reaction of Ca(OH)2 with CO2 at Low Temperature”, Ind. Eng. Chem. Res., vol. 38, n. 4, pp. 1316–1322, Mar 1999, doi: 10.1021/ie980508z

[79] Statista, “Prices of electricity for industry in Finland from 1995 to 2020”, statista.com
https://www.statista.com/statistics/595853/electricity-industry-price-finland/ (accessed Jul. 1 2021)
[80] Statistics Finland, “Energy prices rose in the first quarter”, stat.fi
https://www.stat.fi/til/ehi/2021/01/ehi_2021_01_2021-06-10_tie_001_en.html (accessed Jul. 1 2021)
[81] Y. T. Tang, X. Q. Ma, Z. Y. Lai, Y. Chen, “Energy analysis and environmental impacts of a MSW oxy-fuel incineration power plant in China”, Energy Policy, vol. 60, pp. 132–141, Sep. 2013, doi: 10.1016/j.enpol.2013.04.073
[82] M. Thema, F. Bauer, M. Sterner, “Power-to-Gas: Electrolysis and methanation status review”, Renewable and Sustain. Energy Rev., vol. 112, pp. 775–787, Sep. 2019, doi: 10.1016/j.rser.2019.06.030
[83] D. Thiel, “A pricing-based location model for deploying a hydrogen fueling station network”, Int. J. of Hydrogen Energy, vol. 45, n.6, pp. 24174–24189, Sep. 2020, doi: 10.1016/j.ijhydene.2020.06.178
[84] Trinomics, “Finland. Opportunities for hydrogen energy technologies, considering the national energy & climate plans”, 2020. [Online]. Available: https://www.fch.europa.eu/sites/default/files/file_attach/Brochure%20FCH%20Finland%20%28ID%209473037%29.pdf
[85] United Nations, “Population Division – World Population Prospect 2019”, population.un.org.
https://population.un.org/wpp/ (accessed Feb. 27 2021)
[86] United Nations, “The 17 goals”, sdgs.un.org.
https://sdgs.un.org/goals (accessed Feb. 27 2021)
[87] Uusi Vantaannkoski, “Vantaann Energia Oy”, uusiVantaannkoski.fi
https://www.uusiVantaannkoski.fi/11124 (accessed Jun. 10 2021)
[88] U.S. Department of Energy, Independent Statistics & Analysis, (Feb. 2020), “Capital Cost and Performance Characteristic Estimates for Utility Scale Electric Power Generating Technologies”. [Online]. Available: https://www.eia.gov/analysis/studies/powerplants/capitalcost/
[89] Vantaan Energia, “Waste-to-energy gives a new life for rubbish”, Vantaannenergia.fi.
https://www.Vantaannenergia.fi/en/waste-to-energy-gives-a-new-life-for-rubbish/ (accessed Mar. 21 2021)
[90] Vantaann Energia Oy, “Jätevoimala Vuosirapporti 2018”, Vantaann Energia Oy, Vantaan, Finland, Feb. 2020. Accessed: Jun. 29 2021. [Online]. Available: https://www.google.com/url?sa=t&rct=j&q=&esrc=s&source=web&cd=&cad=rja&uact=8&ved=2ahUKEwi5vvHKw7zxAhWp-yoKHQjvAh4QFnoECAUQAA&url=https%3A%2F%2Fwww.ymparisto.fi%2Fdownload%2Fnoname%2F%257B1BCE8419-77F6-4CB1-8F64-90C09FEA9E02%257D%2F146167&usg=AOvVaw3y3aJiQqOO7HeMCLYztfBU
[91] U. F. Vogt, M. Schlupp, D. Burnat, A. Züttel, “Novel Developments in Alkaline Water Electrolysis”, presented at 8th International Symposium Hydrogen & Energy, Zhaoquing, China, Feb. 16–21 2014.

[92] Method and device for using emissions of a power station, by M. Waidhas, D. Wegener, (2011, Aug. 25), WO2011101209A2. [Online]. Available: https://patents.google.com/patent/WO2011101209A2/en
[93] Wärtsilä Corporation, “Finland's largest Power-to-Gas plant - Wärtsilä and Vantaa Energy to continue planning towards an investment decision”, wartsila.com. https://www.wartsila.com/media/news/15-06-2021-finland-s-largest-power-to-gas-plant---wartsila-and-vantaa-energy-to-continue-planning-towards-an-investment-decision-2931814?utm_source=linkedin&utm_medium=social-org&utm_term=energy&utm_content=pressrelease&utm_campaign=2021pressreleases (accessed Jul. 5 2021)
[94] P. Wienchol, A. Szlęk, M. Ditaranto, “Waste-to-energy technology integrated with carbon capture – Challenges and opportunities”, Energy, vol. 198, 117352, May 2020, doi: 10.1016/j.energy.2020.117352
[95] World Bank, “Purchasing Power Parities and the Size of World Economies: Results from the 2017 International Comparison Program”, Washington, DC: World Bank, US, 2020, doi: 10.1596/978-1-4648-1530-0
[96] F. Wu, M. D. Argyle, P. A. Dellenback, F. Maohong, “Progress in O2 separation for oxy-fuel combustion–A promising way for cost-effective CO2 capture: A review”, Prog. in Energy and Combustion Sci., vol. 67, pp. 188–205, Jul. 2018, doi: 10.1016/j.pecs.2018.01.004
[97] B. Xiong, J. Predel, P. C. del Granado, R. Egging-Bratseth, “Spatial flexibility in redispatch: Supporting low carbon energy systems with Power-to-Gas”, App. Energy, vol. 283, n. 116201, Feb. 2021, doi: 10.1016/j.apenergy.2020.116201
[98] G. Zang, P. Sun, A. A. Elgowainy, A. Bafana, M. Wang, “Performance and cost analysis of liquid fuel production from H_2 and CO_2 based on the Fischer-Tropsch process”, J. of CO_2 Utilization, vol. 46, n. 101459, Apr. 2021, doi: 10.1016/j.jcou.2021.101459
[99] S. Zhang, X. Lin, Z. Chen, X. Li, X. Jiang, J. Yan, “Influence on gaseous pollutants emissions and fly ash characteristics from co-combustion of municipal solid waste and coal by a drop tube furnace”, Waste Manage., vol. 81, pp. 33–40, Nov. 2018, doi: 10.1016/j.wasman.2018.09.048

A. Modelling

Appendix A reports a more detailed analysis about the Aspen Plus model. Firstly, the Fortran code is explicitly written down for YIELD block. Furthermore, Appendix A presents the most useful Excel sheets for the Electrolysis user-made model. Then, every block in the MSW OFC Aspen Plus model is listed and its functioning explained.

Fortran code for YIELD block:

```
FACT = (100-WATER)/100

H20 = WATER/100

ASH = ULT(1)/100 * FACT

C = ULT(2)/100 * FACT

H = ULT(3)/100 * FACT

N = ULT(4)/100 * FACT

S = ULT(5)/100 * FACT

O = ULT(6)/100 * FACT
```

In the decomposition Fortran script, FACT refers to the factor needed to obtain the wet basis analysis from Ultanal of MSW feed stream. The script provides the elements fraction on wet basis of the resulting stream, such as ash, carbonium, hydrogen, nitrogen, sulphur, and oxygen (ASH, C, H, N, S, O).

Table A1: Combustion system blocks Aspen Plus reference.

Aspen Plus block type	Block ID	Description
Flash2	SOLSEP	Separator – it separates the non-conventional ash fraction from the flue gas after the combustion
HeatX	AIRPRH	Heat exchanger – it heats up the incoming air comburent by cooling down the flue gas after the steam cycle (LPHT)
	ECO	Heat exchanger – it heats up the feedwater to its saturated liquid state by cooling down the flue gas coming from the SH
	EVA	Heat exchanger – it heats up the saturated liquid water to the dry steam condition by cooling down the flue gas coming from RGIBBS
	LPHEAT	Heat exchanger – it heats up a fraction of the feedwater to a super-heated steam condition by cooling down the flue gas coming from the MPHT
	MPHEAT	Heat exchanger – it heats up a fraction of the feedwater to a super-heated steam condition by cooling down the flue gas coming from the boiler (ECO)
	SH	Heat exchanger – it heats up the dry steam to superheated condi-tion by cooling down the flue gas coming from the EVA
RGIBBS	RGIBBS	Gibbs free energy reactor – it simulates the combustion
RYIELD	DECOMP	Yield reactor – it converts the non-conventional stream MSW into usable conventional components

Table A2: Steam cycle blocks Aspen Plus reference.

Aspen Plus block type	Block ID	Description
Compr (turbine)	HPT	Turbine – it expands the steam from high pressure to a medium pressure state
	LPT	Turbine – it expands the steam from medium pressure to a low pressure state
	MPT	Turbine – it expands the steam from low pressure to the condenser working pressure
FSplit	SPLITLP	Stream splitter – it splits the low pressure feedwater into two streams: to the boiler and the LPHEAT
	SPLITMP	Stream splitter – it splits the medium pressure feedwater into two streams: to the boiler and to the MPHEAT
HeatX	CONDENS	Heat exchanger – it condenses the wet steam coming from LPT and it provides thermal power to district heating network
Mixer	MIXLP	Stream mixer – it combines the low pressure bleeding from the feed-water line and the steam from the MPT
	MIXMP	Stream mixer – it combines the medium pressure bleeding from the feed-water line and the steam from the HPT
Pump	PUMPHP	Pump – it compresses the feedwater to high pressure
	PUMPLP	Pump – it compresses the feedwater to low pressure from the condenser
	PUMPMP	Pump – it compresses the feedwater to medium pressure

Table A3: Excel Aspen_Input sheet for the electrolyser model.

OUTPUT	H2PROD	HEATAIR	units
H2O	0	0	kmol/s
C	0	0	kmol/s
O2	0	=H2OFEED/2	kmol/s
H2	=H2OFEED	0	kmol/s
CO2	0	0	kmol/s
CO	0	0	kmol/s
NO2	0	0	kmol/s
NO	0	0	kmol/s
N2	0	0	kmol/s
SULFUR	0	0	kmol/s
SO2	0	0	kmol/s
TOTFLOW	=H2OFEED	=H2OFEED/2	kmol/s
TEMP	=TEMPFEED+2	=TEMPFEED+2	K
PRES	=PRESFEED	=PRESFEED	N/m^2
ENTHALPY	0	0	J/kg
VAP FRAC	0	0	molar
LIQ FRAC	0	0	molar
ENTROPY	0	0	J/kg-K
DENSITY	0	0	kg/m^3
MOLE WT	0	0	kg/kmol

Table A4: Excel Aspen_Output sheet for the electrolyser model.

INPUT	H2OFEED	units	defined as
H2O	0	kmol/s	H2OFEED
C	0	kmol/s	
O2	0	kmol/s	
H2	0	kmol/s	
CO2	0	kmol/s	
CO	0	kmol/s	
NO2	0	kmol/s	
NO	0	kmol/s	
N2	0	kmol/s	
SULFUR	0	kmol/s	
SO2	0	kmol/s	
TOTFLOW	0	kmol/s	TOTFEED
TEMP	0	K	TEMPFEED
PRES	0	N/m^2	PRESFEED
ENTHALPY	0	J/kg	
VAP FRAC	0	molar	
LIQ FRAC	0	molar	
ENTROPY	0	J/kg-K	
DENSITY	0	kg/m^3	
MOLE WT	0	kg/kmol	

Table A5: Flue gas treatment system blocks Aspen Plus reference.

Aspen Plus block type	Block ID	Description
Compr (compressor)	EXTCOMP1	Compressor – it compress the flue gas to a low pressure as the first stage of compression
	EXTCOMP2	Compressor – it compress the flue gas to a medium pressure as the second stage of compression
	EXTCOMP3	Compressor – it compress the flue gas to a high pressure as the third stage of compression
Flash2	DEAERAT	Separator – it extracts the gaseous contaminating fraction from flue gas condensed water
	EXTFLSH1	Separator – it extracts the liquid condensed fraction from flue gas as the first stage of condensation and separation
	EXTFLSH2	Separator – it extracts the liquid condensed fraction from flue gas as the second stage of condensation and separation
	EXTFLSH3	Separator – it extracts the liquid condensed fraction from flue gas as the third stage of condensation and separation
	EXTFLSH4	Separator – it extracts the liquid condensed fraction from flue gas as the final stage of condensation and separation
HeatX	ELECTPHT	Heat exchanger – it heats up the feedwater to the electrolyser up to its working optimal point and it cools down the flue gas from the combustion cycle
	EXTCOOL1	Heat exchanger – it cools down the flue gas to condense its water content and it gives thermal power to district heating network
	EXTCOOL1A	Heat exchanger – it cools down the flue gas to condense its water content and heats up the additional water supply for the electrolyser
	EXTCOOL2	Heat exchanger – it cools down the flue gas to condense its water content and it gives thermal power to district heating network
	EXTCOOL3	Heat exchanger – it cools down the flue gas to condense its water content and it gives thermal power to district heating network
	EXTCOOL4	Heat exchanger – it cools down the flue gas to condense its water content and it gives thermal power to district heating network

Aspen Plus block type	Block ID	Description
Mixer	MIXH2O	Stream mixer – it combines together the condensed water streams from all liquid extraction units
	MIXWAT	Stream mixer – it combines the purified condensed water with the additional pre-heated water supply
Sep	FGD	Separator – it simulates the functioning of a fluidized gas desulphurisation unit
	TEG	Separator – it simulates the chemical adsorption through triethyleneglycol (TEG) of the remaining water content in the flue gas
Valve	EXTLAM1	Lamination valve – it laminates the pressurized extracted condensed water to room pressure
	EXTLAM2	Lamination valve – it laminates the pressurized extracted condensed water to room pressure
	EXTLAM3	Lamination valve – it laminates the pressurized extracted condensed water to room pressure

B. **Results**

Appendix B reports a more detailed presentation of results from the Aspen Plus MSW OFC simulation. The reference Aspen Plus flowsheet for the MSW OFC model is illustrated in Figure B1 in Appendix B.

Table B1: Vantaan Energia waste-to-energy thermal power plant reference model results of the combustion cycle.

Stream	**p [bar]**	**T [°C]**	$\dot{m}$ **[kg/s]**
AIR	1	25.0	108
COMBUREN	1	250	108
MSW	1	25	13
ASHGAS	1	1697	121
ASH+CHAR	1	1697	2.52
HOTGAS	1	1697	118.5
FLUE1	1	1300	118.5
FLUE2	1	1123	118.5
FLUE3	1	795	118.5
FLUE4	1	638	118.5
FLUEGAS	1	590	118.3
FLUEDH	1	414	118.5
STACK	1	55	118.5

Table B2: Vantaan Energia waste-to-energy thermal power plant reference model results of the steam cycle.

Stream	**p [bar]**	**T [°C]**	**v [%]**	$\dot{m}$ **[kg/s]**
PUMPIN	2.7	95	0	57
FEEDWAT	5.5	95	0 (sc.)	57
LPCOLD	5.5	95	0 (sc.)	54.2
MPCOLD	38	95	0 (sc.)	54.2
HPCOLD	38	95	0 (sc.)	46.1
BOILERIN	91	96	0 (sc.)	46.1
BOILER1	91	303	0	46.1
BOILER2	91	303	100	46.1
HPTIN	87	535	100 (sh.)	46.1
HPTOUT	38	396	100 (sh.)	46.1

Stream	p [bar]	T [°C]	v [%]	$\dot{m}$ [kg/s]
MPBLEED	38	95	0 (sc.)	8.1
MPHOT	38	400	100 (sh.)	8.1
MPTIN	38	397	100 (sh.)	54.2
MPTOUT	5.5	168	100 (sh.)	54.2
LPBLEED	5.5	95	0 (sc.)	2.8
LPHOT	5.5	157	100 (sh.)	2.8
LPTIN	5.5	168	100 (sh.)	57
INCOND	0.8	95	92.5	57
DHIN	4	50	0	684.1
DHOUT	4	90	0	684.1
DH2IN	4	50	0	260.9
DH2OUT	4	90	0	260.9

sc. subcooled, sh. superheated

Table B3: MSW OFC thermal power plant model results of the combustion cycle.

Stream	p [bar]	T [°C]	$\dot{m}$ [kg/s]
OXY	1	77	18.4
COMBUREN	1	271	169.2
MSW	1	25	13
ASHGAS	1	1100	182.2
ASH+CHAR	1	1100	2.52
HOTGAS	1	1100	179.7
FLUE1	1	815	179.7
FLUE2	1	685	179.7
FLUE3	1	442	179.7
FLUE4	1	324	179.7
FLUEGAS	1	288	179.7
2EXTFLUE	1	288	28.9
RECIRCFL	1	288	150.8

Table B4: MSW OFC thermal power plant model results of the steam cycle.

Stream	p [bar]	T [°C]	$\dot{m}$ [kg/s]
EXT0	1	231	28.9
EXT1	1	55	28.9
EXT1A	1	49	28.9

Stream	p [bar]	T [°C]	$\dot{m}$ [kg/s]
EXTH2O1	1	55	6.94
EXT2	1	55	22.0
EXT3	3.13	154	22.0
EXT4	3.13	55	22.0
EXTH2O2	1	55	0.987
EXT5	1	55	21.0
EXT6	9.7	153	21.0
EXT7	9.7	55	21.0
EXTH2O3	1	55	0.273
EXT8	9.7	55	20.7
EXT9	30	155	20.7
EXT10	30	55	20.7
EXTH2O4	1	56	0.0828
FLWTFREE	30	55	20.6
SOXCOMP	30	55	0.0461
ABSH2O	30	55	0.0533
CO2	30	55	20.52
EXTH2OTT	1	55	8.28
UNCONGAS	1	55	0.000333
H2ORECOV	1	55	8.284
H2OADD	1	25	12.4
H2OADDHT	1	50	12.4
PUREH2O	1	52	20.7
H2OFEED	1	75	20.7
DHINC1	4	50	128
DHOUTC1	4	90	128
DHINC2	4	50	25.3
DHOUTC2	4	90	25.3
DHINC3	4	50	14.7
DHOUTC3	4	90	14.7
DHINC4	4	50	12.9
DHOUTC4	4	90	12.9

Table B5: Comparison between Vantaan model and oxy-fuel model about the flue gas composition after the combustion.

	Vantaan model		**Oxy-fuel model**	
	[mol%]	**[kg/s]**	**[mol%]**	**[kg/s]**
CO	0.0512	0.0588	$1.36\ 10^{-3}$	0.000355
CO_2	11.3	20.3	49.9	20.4
H_2	$1.16\ 10^{-2}$	0.000960	$6.67\ 10^{-4}$	$1.25\ 10^{-5}$
H_2O	11.3	8.33	49.7	8.34
N_2	72	82.7	0.228	0.0593
NO	0.349	0.429	$1.76\ 10^{-4}$	$4.92\ 10^{-5}$
NO_2	$2.87\ 10^{-4}$	0.000542	$6.67\ 10^{-8}$	$2.86\ 10^{-8}$
O_2	5.01	6.57	0.0495	0.0147
SO_2	0.0179	0.0471	0.0790	0.0471

Table B6: Flue gas dehydration system results.

	Oxy-fuel model
District heating [MW_{th}]	32.9
Compression work [MW_{el}]	-6.06
Condensed water [kg/s]	8.28
Requested water by electrolyser [kg/s]	20.7
Water to supply into the system [kg/s]	12.4

Table B7: Chemical composition of the flue gas after each phase.

	Combustion	**Dehydration**	**Desulphurisation**	**Chemical adsorption**
CO [mol%]	$1.36\ 10^{-3}$	$2.70\ 10^{-3}$	$2.70\ 10^{-3}$	$2.70\ 10^{-3}$
CO_2 [mol%]	49.9	98.7	98.8	99.4
H_2 [mol%]	$6.67\ 10^{-4}$	$1.32\ 10^{-3}$	$1.32\ 10^{-3}$	$1.33\ 10^{-3}$
H_2O [mol%]	49.7	0.628	0.629	0.0
N_2 [mol%]	0.228	0.450	0.451	0.454
NO [mol%]	$1.76\ 10^{-4}$	$3.49\ 10^{-4}$	$3.49\ 10^{-4}$	$3.51\ 10^{-4}$
NO_2 [mol%]	$6.67\ 10^{-8}$	$1.26\ 10^{-7}$	$1.26\ 10^{-7}$	$1.27\ 10^{-7}$
O_2 [mol%]	0.0495	0.0979	0.0981	0.0987
SO_2 [mol%]	0.0790	0.156	$3.12\ 10^{-3}$	$3.14\ 10^{-3}$

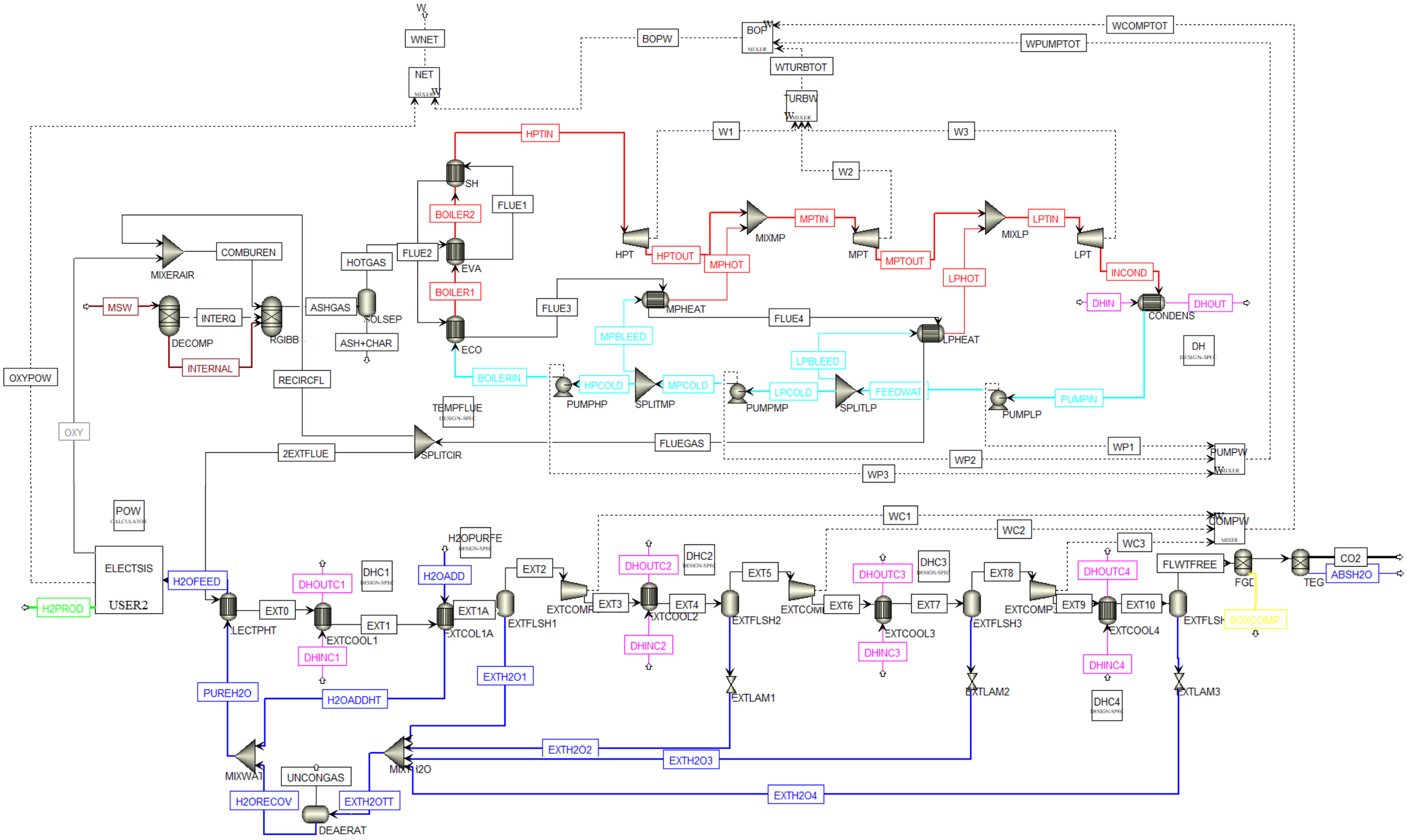

Figure B1: Aspen Plus flowsheet of MSW OFC model with all nickname streams.